UNIVERSIDADE
BEIRA INTERIOR

Preliminary Design of a Four-Stroke Axial Engine Prototype
(versão final após defesa)

José Pedro da Silva Atilano

Dissertação para obtenção do Grau de Mestre em
Engenharia Aeronáutica
(Mestrado Integrado)

Orientador: Prof. Doutor Miguel Ângelo Rodrigues Silvestre

Setembro de 2024

Folha em branco

Declaração de Integridade

Eu, José Pedro da Silva Atilano, que abaixo assino, estudante com o número de inscrição 38501 de Mestrado Integrado em Engenharia Aeronáutica da Faculdade de Engenharia, declaro ter desenvolvido o presente trabalho e elaborado o presente texto em total consonância com o **Código de Integridades da Universidade da Beira Interior**.

Mais concretamente afirmo não ter incorrido em qualquer das variedades de Fraude Académica, e que aqui declaro conhecer, que em particular atendi à exigida referenciação de frases, extratos, imagens e outras formas de trabalho intelectual, e assumindo assim na íntegra as responsabilidades da autoria.

Universidade da Beira Interior, Covilhã 02 /09 /2024

José Pedro da Silva Atilano

(assinatura conforme Cartão de Cidadão ou preferencialmente
assinatura digital no documento original se naquele mesmo formato)

Acknowledgments

I would like to thank to the people that directly help me through the completion of this dissertation for the crucial teachings and suggestions, my supervisor Professor Miguel Ângelo Silvestre and to Professor André Vieira for the explanations in mechanical engineering.

A huge tank to all my friends in Vizela and the course, that help me on this journey and made part of it.

Obviously, and most important, a special thanks to my family, specially, my parents for the immeasurable support, financially and emotionally.

Resumo

Esta dissertação teve como objetivo realizar o projeto preliminar de um motor axial e de pistões opostos a quatro tempos. O trabalho focou-se principalmente no movimento da cambota/placa oscilante/biela/pistão selecionado e no novo mecanismo do sistema de distribuição a quatro tempos.

Para começar, os parâmetros iniciais do motor foram selecionados, juntamente com um pistão pré-fabricado e em seguida estimou-se a carga máxima nos principais componentes do motor devido à pressão resultante da combustão. Foi feita a análise cinemática e definidas as equações do movimento cambota/placa oscilante/biela/pistão usando folhas de cálculo Excel sendo posteriormente calculado as forças atuantes nos rolamentos que ligam a cambota à placa oscilante, e na própria cambota. Foi feito o desenho e dimensionamento de algumas das peças do mecanismo mais concretamente a cambota, rolamentos, biela e acoplamento das cambotas em CATIA V5 tendo em conta o processo de montagem e desmontagem do motor. Como a cambota é de geometria irregular, foi necessário dimensioná-la através de uma análise estrutural realizada em CATIA V5. Essa análise proporcionou uma otimização no dimensionamento e desenho da cambota tendo em conta o posicionamento dos rolamentos que ligam a cambota à placa oscilante.

O mecanismo do sistema de distribuição a quatro tempos foi pensado e desenhado usando uma came cilíndrica com uma "ranhura" que se interseta a si própria fazendo com que o percurso da ranhura demore duas revoluções da cambota a ser percorrido. Nessa came cilíndrica está um "rolo de leva" que translaciona dentro da ranhura. Esse rolo de leva está conectado a um braço "seguidor" que atua nas válvulas abrindo-as. O sistema de mola encontrado em qualquer motor convencional foi usado para fazer com que as válvulas fechem de novo depois de serem abertas pelo braço "seguidor". Este sistema faz com que cada válvula se abra uma vez a cada duas revoluções da cambota criando um sistema de distribuição a quatro tempos.

Após terem sido desenhados todos os componentes do motor em CATIA V5, a montagem e simulação do modelo virtual completo do motor foi realizada também em CATIA V5. A simulação demonstrou que o mecanismo funciona como esperado, no entanto há uma falha que a simulação não demonstra. O mecanismo é incompleto porque necessita de uma peça ou mecanismo que garanta que o rolo de leva permaneça no percurso correto durante a interseção da ranhura. A posterior simulação de uma solução envolvendo dois rolos de leva em fila demonstrou não ser viável.

Esta dissertação foi concluída não sendo encontrada uma solução possível para resolver esse problema.

Palavras-chave

Motor, Design Preliminar, Axial, Pistões-opostos, Quatro-tempos

Folha em branco

Abstract

This dissertation had the objective of developing a preliminary design of a four-stroke axial opposed-piston engine. The design was mainly focused in the type of movement of the crankshaft/wobble plate/connecting rod/piston selected and the new mechanism for a four-stroke distribution system.

To begin, the initial parameters of the engine were selected including a pre-fabricated piston following the estimative of the maximum force acting on the piston resultant of the pressure inside the combustion chamber as it is with this force that the whole engine is dimensioned. The kinematic analysis and the movement equations of the crankshaft/wobble plate/connecting rod/piston were implemented using Excel sheets being posteriorly also calculated the reactions acting on the bearings that connect the crankshaft to the wobble plate, and in the crankshaft itself. The design and sizing of the most important engine components were conducted in CATIA V5, more specifically the crankshaft, the rolling bearings, the connecting rod and the shaft coupling having in consideration the process of assembly and disassembly of the engine. Because the crankshaft is designed with an irregular geometry, its structural sizing was conducted using a structural analysis in CATIA V5. This analysis allowed an optimization in the dimensioning and design of the crankshaft depending on the rolling bearings positioning.

The four-stroke distribution system mechanism was thought and designed using a cylindrical cam with a self-reversing and intersecting groove with the objective of the groove path be concluded in two revolutions of the crankshaft. Inside the groove of the cylindrical cam translates a cam follower. The cam follower is connected to a follower that opens the valves. The spring mechanism found in any conventional engine was used to close the valves once opened. This system allows the valves to be opened only once per two revolutions of the crankshaft turning it into a four-stroke system.

The assembly and simulation of the engine was conducted once all the components of the engine were designed in 3D using CATIA V5. The simulation showed the mechanism performing as expected, however there is a flaw in the mechanism not shown in the simulation. The mechanism is incomplete because it requires an extra piece to ensure that the cam follower stays in the correct path inside the groove during its passage thought the intersection of the groove. The posterior simulation of possible solution using two cam followers instead of one proved not possible.

This dissertation was concluded without being possible to find a solution for that problem.

Keywords

Engine, Preliminary Design, Axial, Opposed-piston, Four-stroke

Folha em branco

Contents

Folha em branco

List of figures

Folha em branco

List of Tables

Folha em branco

Acronyms

GRP	Gabinete de Relações Públicas
UBI	Universidade da Beira Interior
VAS	Variable Angle Shift
VCR	Variable Compression Ratio
VPA	Variable Port Area
TDC	Top Dead Center
BDC	Bottom Dead Center
VVT	Variable Valve Timing
VVL	Variable Valve Lift
CAD	Computer-Aided Design
S/B	Stroke to Bore ratio
WOT	Wide-Open Throttle

Nomenclature

Roman Symbols

r_c	Compression Ratio
$V_d[mm^3]$	Swept/Displace Volume
$V_c[mm^3]$	Clearance Volume
$F_{max}[N]$	Combustion Maximum Force
$d_{pin}[mm]$	Gudgeon Pin Outer Diameter
$l_{pin}[mm]$	Connecting Rod Small End Supported Length
$p_{bp}[MPa]$	Maximum Allowable Journal Lubrification Bearing Pressure
$p_{max}[MPa]$	Combustion Maximum Pressure
$D_{piston}[mm]$	Piston Diameter
$F_{cr}[N]$	Connecting Rod Maximum Force
$E[MPa]$	Elasticity Modulus
$I[kg.m^2]$	Moment of Inertia
$L[mm]$	Connecting Rod Length
$L_e[mm]$	Connecting Rod Equivalent Length
$d_{cr}[mm]$	Connecting Rod Circular Section Diameter
$F_{\mathrm{q}}[N]$	Resultant Force
$w_{secr}[mm]$	Connecting Rod Small End Width
$d_{pp}[mm]$	Piston Gudgeon Pin Outside Diameter
$d_{i_{secr}}[mm]$	Connecting Rod Small End Inside Diameter
$d_{o_{secr}}[mm]$	Connecting Rod Small End Outside Diameter
$r_{lecr}[mm]$	Connecting Rod Socket and Ball Joint Radius
$S[mm]$	Engine Stroke
$B[mm]$	Engine Bore
$F_{q_x}[N]$	Resultant Force x-component
$F_{q_y}[N]$	Resultant Force y-component
$r[mm]$	Vertical Distance Variation between Connecting Rod and Cylinder Center Axis
$Z[mm]$	Wobble Plate Arm Length
$x_E[mm]$	Point E x-component
$y_E[mm]$	Point E y-component
$X[mm]$	Crankshaft Arm Length
$M[mm]$	Diagonal Crankshaft Half Length
$H[mm]$	Horizontal Crankshaft Half Length
$Q[mm]$	Horizontal Crankshaft Half Length of M
$T[mm]$	Vertical Crankshaft Half Length
$N_A[mm]$	Distance between Bearing A and Crankshaft Center
$N_B[mm]$	Distance between Bearing B and Crankshaft Center
$V_A[mm]$	Vertical Distance between Bearing A and Crankshaft Center

$V_B[mm]$	Vertical Distance between Bearing B and Crankshaft Center
$P_A[mm]$	Horizontal Distance between Bearing A and Crankshaft Center
$P_B[mm]$	Horizontal Distance between Bearing B and Crankshaft Center
$T_{crankshaft}[N.mm]$	Crankshaft Torque
$C_x[mm]$	Distance between Bearing C and Crankshaft Center
$D_x[mm]$	Distance between Bearing D and Crankshaft Center
$R_{arc_{A;C}}[mm]$	Crankshaft Corner Radius between Bearings A and C
$L_{wall_A}[mm]$	Crankshaft Wall Width to Support Bearing A
$L_{brg_A}[mm]$	Bearing A Width
$D_{arc;nut}[mm]$	Distance between Bearing B Nut and Crankshaft Corner
$L_{wall_C}[mm]$	Crankshaft Wall Width to Support Bearing C
$L_{wall_D}[mm]$	Crankshaft Wall Width to Support Bearing D
$L_{brg_C}[mm]$	Bearing C Width
$L_{brg_D}[mm]$	Bearing D Width
$D_{arc;wall\ D}[mm]$	Distance between Crankshaft End Corner between Bearings B and D and Backrest of Bearing D
$D_{arc_{A;C}}[mm]$	Distance between Crankshaft End Corner between Bearings A and C and Crankshaft Arm
$D_{arc_{B;D}}[mm]$	Distance between Crankshaft End Corner between Bearings B and D and Crankshaft Arm
$R_{arc_{A;C}}[mm]$	Crankshaft Corner Radius between Bearings A and C
$R_{arc_{B;D}}[mm]$	Crankshaft Corner Radius between Bearings B and D
$F_{max_{brg}}[N]$	Bearings Maximum Force
$F_{lf}[N]$	Bearings Maximum Force with Safety Factor
$F_m[N]$	Average Bearings Force
$R^{´´}[N]$	Bearings Life Force
s_f	Crankshaft Safety Factor
$P_s[N]$	Shaft Coupling Total Screws Force
$d_{coupling}[mm]$	Shaft Coupling Inner Diameter
$p_{coupling}[MPa]$	Shaft Coupling Projected Area Pressure
$L_{coupling}[mm]$	Shaft Coupling Length
n_{screw}	Shaft Coupling Screws Number
$P_p[N]$	Shaft Coupling Screw Force
$S_p[mm^2]$	Screw Thread Section Area
$d_{screw}[mm]$	Screw Thread Internal Diameter
$p_{adm}\ [MPa]$	Shaft Coupling Material Permissible Maximum Pressure
$Q_p[m^3/s]$	Gas Flow Rate thought Ports
$v[m/s]$	Mean Piston Velocity through Ports
$N[rpm]$	Engine Speed
$d_p[m]$	Port Diameter
$w[m]$	Valve Seat Width
$d_{iv}[mm]$	Intake Valve Head Diameter

$d_{ev}[mm]$	Exhaust Valve Head Diameter
$d_{ip}mm]$	Inlet Port Dimeter
$d_{ep}[mm]$	Exhaust Port Diameter
$w_i[mm]$	Intake Valve Seat Width
$w_e[mm]$	Exhaust Valve Seat Width
$Q_v[m^3/s]$	Gas Flow Rate thought Valves
$l[mm]$	Valve Lift
$a[m/s^2]$	Simple Harmonic Motion Maximum Acceleration
$t[s]$	Opening Valve Time
$F_a[N]$	Inertia Force of Valvetrain Components
$m[kg]$	Valvetrain Components Mass that Translate
$m_{valve}[kg]$	Intake Valve Mass
$m_{retainer}[kg]$	Valve Retainer Mass
$m_{lock}[kg]$	Valve Lock Mass
$m_{spring}[kg]$	Valve Spring Mass
$d[mm]$	Spring Wire Diameter
$D[mm]$	Spring Mean Coil Diameter
$F_{max_{spring}}[N]$	Valve Spring Maximum Force
C	Spring Index
$F_{min_{spring}}[N]$	Valve Spring Seat Pressure Minimum Force
$k[N/mm]$	Spring Stiffness
$G_{spring}[MPa]$	“ASTM A232” Carbon Steel Rigidity Modulus
K	Wahl´s Correction Factor
$D_O[mm]$	Spring Outer Diameter
$D_I[mm]$	Spring Inner Diameter
N	Spring Active Number of Turns
N_t	Spring Total Number of Turns
$L_s[mm]$	Spring Solid Length
$L_{max\ lift}[mm]$	Spring Maximum Lift
$L_I[mm]$	Spring Installation Length
$L_F[mm]$	Spring Free Length
$f_{n_{minimum}}[Hz]$	Valve Spring Minimum Natural Frequency
$f_n[Hz]$	Valve Spring Actual Frequency
$F_{ls_{camfollower}}[N]$	Cam Follower Maximum Force
$F_g[N]$	Exhaust Gas Flow Force
$p_g[MPa]$	Pressure Variation During Exhaust Stroke and Ambient Pressure
$F_{cs_{camfollower}}[N]$	Crossing Section Acceleration Force
$m_{camfollower}[kg]$	Cam Follower and Assembly Components Mass
$r_{cs}[mm]$	Crossing Section Maximum Curvature Radius
$v_{camfollower}[m/s]$	Cam Follower Velocity
$l_{groove}[mm]$	Cylindrical Cam Groove Profile Full Length
$rpm_{max_{crankshaft}}[rpm]$	Crankshaft Maximum Rotational Speed
$P_{camfollower}[mm]$	Cam Follower Perimeter
$d_{camfollower}[mm]$	Cam Follower Diameter

$F_{m_{camfollower}}[N]$	Cam Follower Average Force
$F_{ss_{camfollower}}[N]$	Static Section Force
t_{ls}	Lift Section Duration Time Fraction
t_{cs}	Crossing Section Duration Time Fraction
t_{ss}	Static Section Duration Time Fraction
$L_{10_{camfollower}}[rpm]$	Cam Follower Nominal Life
f_w	Cam Follower Load Factor
C	Cam Follower Basic Dynamic Load
$L_{h_{camfollower}}[h]$	Service Bearing Life
$rpm_{camfollower}[rpm]$	Cam Follower Velocity
$F_{key}[N]$	Key Force
$r_{crankshaft}[mm]$	Crankshaft Radius
$t_{key}[mm]$	Key Width
$L_{key}[mm]$	Key Length
$t_{cylinder}[mm]$	Cylinder Wall Thickness

Greek Symbols

$\tau_{cr}[MPa]$	Connecting Rod Material Safe Tensile Stress
$\gamma[deg]$	Wobble Plate Angular Range
$\theta[deg]$	Connecting Rod Angle with Cylinder Center Axis
$\beta[deg]$	Angle between Wobble Plate Arm and y-axis in the Plane Oxy
$\Phi[deg]$	Crankshaft Rotation Angle
$\alpha[deg]$	Crankshaft Rotation Angle in relation to Plane Oxz
$\sigma_{máx_{cranksahft}}[MPa]$	Crankshaft Maximum Stress
$\sigma_{4340}[MPa]$	"AISI 4340" steel Yield Strength
$\delta[mm]$	Maximum Allowable Crankshaft Deflection
μ	Friction Coefficient between Shaft Coupling and Shaft
$\sigma_{adm}[MPa]$	Screw Permissible Tension
$v_g[m/s]$	Mean Gas Velocity
$v_{g_v}[m/s]$	Mean Gas Velocity through Valves
$\omega[rad/s]$	Simple Harmonic Motion Angular Velocity
$\lambda[deg]$	Opening Valve Duration
$\rho[kg/mm^3]$	Material Spring Density
$\tau_{spring}[MPa]$	"ASTM A232" Carbon Steel Maximum Shear Stress
$\rho_{spring}[kg/mm^3]$	"ASTM A232" Carbon Steel Density
$\tau_{key}[MPa]$	Key Maximum Shear Stress
$\sigma_{key}[MPa]$	Key Yield Strength
$\sigma_h[MPa]$	Cylinder Permissible Circumferential Stress

Chapter 1

1 Introduction

1.1. Motivation

The greenhouse gas emissions such as the carbon dioxide are a primary cause of global warming and climate change, an environmental problem that has been negatively affecting the planet and the world population. The combustion of fossil fuels in internal combustion engines are a significant contributor to the issue.

As concerns about the environmental impact those carbon emissions intensify, people start to defend the utter transition of internal combustion engines to electrical engines while others intensify their interest and emphasis in research and development of alternative/improved technologies for conventional internal combustion engines to enhance engine efficiency. Such technologies, like synthetic fuels or new mechanical upgrades like the VCR (Variable Compression Ratio), VVL (Variable Valve Lift) and VVT (Variable Valve Timing) are more recent. Others are old concepts that gained renewed attention due to their potential for improved efficiency like the axial/barrel and the opposed piston engine configuration.

A recent surge in development around those unconventional engines has shown various successful prototype designs being built and tested with excellent results in overall efficiency and higher power to weight ratios among other advantages. Of course, there are also disadvantages which some, with the new research and development, are being somewhat easily fixed. The main issue may not be in the mechanical or in the thermodynamic fronts but instead in the economic front. All those engines use a variety of configurations and mechanical cycles like, per example:

- The Achates Power engine is a two-stroke opposed piston engine *[1]*.
- The Duke engine is a four-stroke axial/barrel engine *[2]*.
- The PAMAR engine and the Covaxe engine are a two-stroke axial opposed piston engine *[3] [4]*.
- The Pinnacle engine is a four-stroke opposed piston engine *[5]*.

The present work has the objective of initiating the development of an internal combustion engine with both axial and opposed piston concepts while using a four-

stroke cycle and spark ignition as any other modern engines. The distribution system design will be using poppet valves and an innovative drive mechanism.

The engine parts will be virtually built and simulated in CATIA V5. In addition, some engine parts that affect the design the most, in terms of volume, mass and viability will be dimensioned such as the crankshaft, pistons, bearings, and main components of the distribution system.

1.2. Thesis Structure

This thesis is divided into five main chapters:

- Chapter 1 provides the introduction and the objective of this work and its organization.

- Chapter 2 provides a section with a summary of engine theory fundamentals necessary to understand the engine operation. A posterior section reviews, firstly, axial and opposed-piston engines old concepts, designs, and respective patents following more modern and in development ones.

- Chapter 3 provides the methodology on how to design the engine mechanism, including dimensioning, theoretical motion analysis and explanation of assembly and disassembly of the mechanism.

- Chapter 4 provides the results of the dimensioned components and their 3D design in CATIA V5. Posteriorly, its assembly and simulation images are also provided.

- Chapter 5 provides the conclusion and discussion of the engine mechanism movement and suggestions for improvement and future work.

Chapter 2

2 Literature Review

2.1. Fundamentals

2.1.1. Thermodynamic Cycles

The combustion of the mixture fuel/air increases the pressure and temperature of gas inside the combustion chamber of an internal combustion engine. It is that pressure that forces the piston to reciprocate. A thermodynamic cycle represents the transformations and changes of energy inside the combustion chamber.

An internal combustion engine operates on a mechanical cycle rather than a thermodynamic cycle. Although it is convenient to compare the performance of an engine with thermal efficiencies of hypothetical cycles due to the similarity of both *[6]*. This thermodynamic cycle is then studied by agglomerating the transformations undergone by the fluid in ideal thermodynamic processes. These processes, being theoretical, do not exactly represent the actual physical process of the engine being used. Several simplifications happen such as:

- The combustion process is replaced by a heat addition from an external source.
- The exhaust stroke is replaced for a heat rejection to the environment and the fluid returns to the initial parameters.
- Air behaves as a perfect gas with constant specific heat at environment temperature.
- No induction or exhaust processes, but a fixed quantity of air and no leakage.

The most famous engines, working with gasoline and diesel follow, respectively, the thermodynamic cycle of Otto and Diesel and their difference is in the heat addition. In the Otto cycle, the heat addiction is made at constant volume while in the Diesel cycle is made at constant pressure.

First presented in 1876 by Nicholaus Otto, the ideal Otto cycle at WOT is represented by six thermodynamic processes as shown in the *Figure 2.1*.

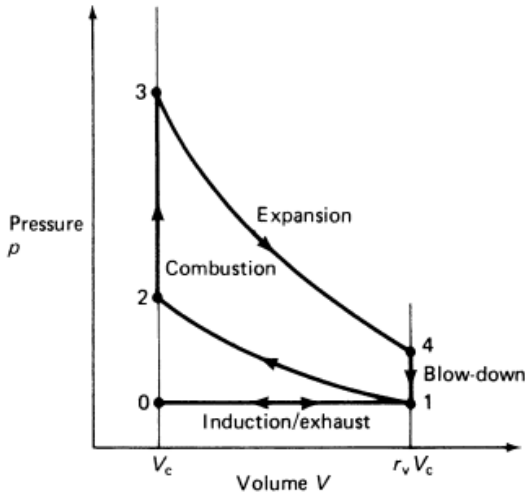

Figure 2.1 - Otto thermodynamic cycle [6]

- 0-1: **isobaric admission** (air/fuel mixture are drawn to the chamber at constant pressure)
- 1-2: **isentropic compression** (with no heat losses)
- 2-3: **isochoric combustion** (heat addition at constant volume)
- 3-4: **isentropic expansion** (with no heat losses)
- 4-1: **isochoric expansion** (heat release at constant volume as the exhaust valve opens)
- 1-0: **isobaric exhaust** (burned gases exit the chamber at constant pressure)

It is worth mentioning that the equivalent area of the graphic represents the useful work produced by the engine. As the exhaust stroke and intake stroke occur at the same pressure, the work produced and lost for those processes is equivalent to zero.

As mentioned above, the Otto thermodynamic cycle and the mechanical cycle of an engine/Otto mechanical cycle have some differences as the simplifications presented above do not really occur. The mechanical cycle is presented in the *Figure 2.2*.

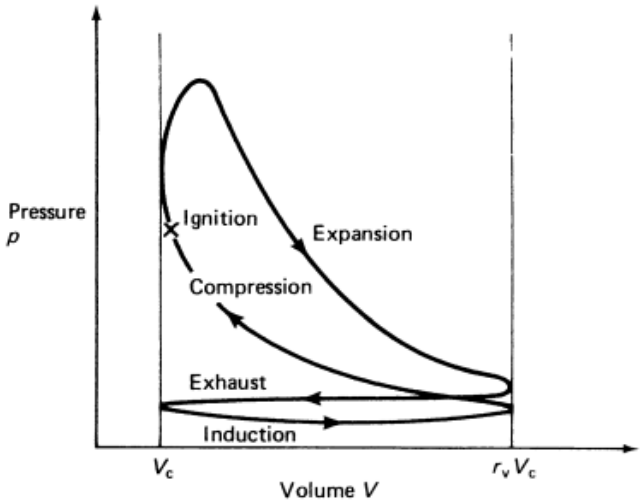

Figure 2.2 - Otto mechanical cycle [6]

When comparing both figures for equivalent engine parameters (ambient pressure, V_c, r_v and heat transfer), it is possible to conclude that the area of the graphic of the Otto thermodynamic cycle is larger than the Otto mechanical cycle which means that the useful work is also larger *[7]*.

- The intake and exhaust strokes are not isobaric, and they do not happen at the same pressure. While in an ideal cycle, the intake and exhaust strokes happen at ambient pressure, in a real engine the intake pressure is slightly lower, and the exhaust stroke is higher because not all the gases are expelled due to inefficiency and thus the pressure in the chamber is slightly higher than the ambient atmospheric pressure. This results in a loss of useful work.
- The compression and expansion strokes are not isentropic. That means the existence of heat losses through the cylinder walls to the environment. That loss is even greater due to the necessity to cool down the cylinder to not overheat.
- The combustion is not isochoric neither instantaneous meaning that in a real engine, ignition does not occur exactly at the Top Dead Center (TDC). Rather it happens slightly below TDC, and the peak pressure is not in point 3 as in the ideal cycle but slightly after. If the combustion happened in the TDC, the combustion would not have time to occur fully near the TDC and the value of the pressure peak would be lower resulting in greater losses of useful work.
- The exhaust valve is not opened exactly in the Bottom Dead Center (BDC) but before. This results in the loss of useful work. However, if the exhaust valve was opened exactly when the piston reached the BDC the losses of useful work would be greater.

2.1.2. Four Stroke Spark Ignition Engine Cycle

An engine working cycle is the sequence of processes suffered by the fluid (air/fuel mixture) inside the combustion chamber. Those processes are periodic and happen repeatedly for the engine to work. Those processes can happen in two strokes or in four strokes. A stroke represents an upward or downward movement, respectively, from BDC to TDC and vice versa, made by the piston inside the cylinder. TDC is the maximum point of the piston during its movement inside the cylinder while BDC is the lowest.

The engine working with four strokes per cycle by spark ignition (Otto Cycle) and by compression ignition (Diesel Cycle) are the most common engines. Both have the same movement but with different combustion and parameters.

Figure 2.3 demonstrates the four-stroke working cycle of an engine that consists in admission, compression, expansion, and exhaust strokes. It takes two full revolutions of the crankshaft to be complete, each stroke happening in half a crankshaft revolution.

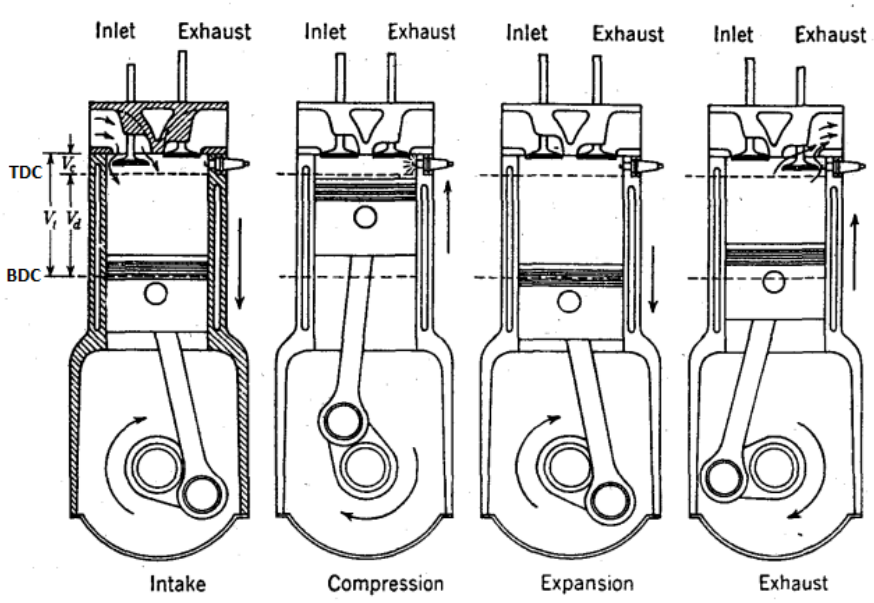

Figure 2.3 - Four stroke engine cycle [8]

The intake/admission stroke begins when the piston is at TDC. At this point the intake valve is already open as it was opened slightly before the piston reaches TDC. As the piston moves downward by the rotation of the crankshaft, a depression is created due to the difference of pressures inside the cylinder and outside, sucking the mixture air/fuel inside the cylinder *[9]*. Theoretically, when the piston reaches the BDC, the intake valve closes, and the admission stroke is finished however the intake valve closes

slightly after the piston reaches BDC to take advantage of the inertia of the charge mass flowing to the cylinder.

When the admission stroke is over, the piston starts its movement upward from the BDC and the compression stroke begins. Doing this, the piston compresses the air/fuel mixture inside the cylinder reducing its volume to its minimum and homogenizing the mixture. The pressure and temperature rise as the piston reaches TDC. It's worth mentioning that the temperature and pressure are very high but not enough to cause self-ignition. After the piston reaches TDC, the compression stroke is over.

The expansion stroke begins when the compressed air/fuel mixture is ignited by a spark created by a component inside the combustion chamber called spark plug. The combustion of the mixture is fast creating a peak pressure and combustion products gas that push the piston downwards. When the piston reaches BDC, the expansion stroke is over. This stroke is the only in the cycle that generates work while all others consume.

The exhaust stroke begins when the piston reaches the BDC. Theoretically, in this point, the exhaust valve opens, however in a real engine the exhaust valve is set to open slightly before the piston reaches BDC during the expansion stroke such that when the piston starts the upward exhaust motion, the pressure could drop to near ambient. As the piston initiates its movement upward, the gases originated from the air/fuel mixture combustion are expelled. When the piston reaches TDC, the exhaust valve closes and almost all the gases of the combustion are expelled being left only small remnants. That marks the end of the exhaust stroke and the full cycle. Again, the exhaust valve only closes, for best performance, slightly after TDC.

After the exhaust stroke, the cycle repeats beginning again the admission stroke.

2.2. Opposed Piston Engines

An opposed-piston engine is an engine configuration where two pistons are arranged in the same cylinder and reciprocate opposite to each other. This configuration is used for both four stroke operation as well as two stroke operation, but in general, the most significant advantages of opposed-piston engines are:

- Lack of cylinder head: The lack of a cylinder head and instead another piston reciprocating in the same cylinder means that the outside surrounding area of the combustion chamber where heat is lost to cooling and to outside is lower compared to a conventional engine with the same displacement and number of pistons. This increases the thermal efficiency of the engine *[5]*.

- High stroke-to-bore (S/B) ratio: As two pistons reciprocate opposite to each other in the same cylinder, the stroke to bore ratio is the double compared to a conventional engine without increasing the mean piston speed. A high stroke to bore ratio can lead to an improvement in thermal efficiency *[3]*.
- Better performance parameters: Higher power to bulk volume ratio, higher specific torque, higher power density and higher specific output as well as a superior fuel efficiency compared to conventional four stroke engines *[10]*.
- Lower material costs compared to equivalent power four stroke conventional engines *[10]*.

A two-stroke opposed-piston engine also has the additional advantages of:

- High reliability and low maintenance as fewer parts like cylinder head and poppet valves are not required meaning a possibility of potential failures is lower *[5]*.
- Possibility of uniflow scavenging where fresh gases enter the combustion chamber thought one side while the exhaust gases leave through the other side creating an uniflow inside the combustion chamber where fresh air and exhaust gases do not mix *[5]*.

Despite many advantages, a two-stroke opposed-piston engine have still the same issues identified in traditional two stroke engines like oil losses and lubrication issues specially in the small-end bushes or piston-pin bosses. Also, piston ring wear is more present due to local bending and distortion caused when the piston reciprocates through the piston ports *[10]*. The thermal load is also significantly higher because there are no additional two strokes to exchange the gases inside the combustion chamber which has the effect of cooling the engine *[3]*.

A four-stroke opposed-piston engine though, has lesser disadvantages. One of the two main issues is caused by the lack of a cylinder head which means the fuel must be injected perpendicular to the piston motion. If a L-chamber is used, then the injection can happen parallel to the piston motion but not directly and symmetrical from above like a conventional four-stroke engine. Either way, the intake charge does not have a uniform fuel distribution into the combustion chamber which can lead to an inefficient combustion *[5]*.

The other issue, affecting both the four and the two stroke opposed piston engines is to change linear motion into rotary motion. In a conventional engine, the linear motion is converted to rotary motion with one shaft, however, in an opposed-piston engine, it's a challenge to unite the power of the two pistons and put it in one shaft as they reciprocate opposite to one another *[5]*. Many mechanical solutions exist but

almost none has sufficient in-depth analysis as research and development of those mechanisms restarted in the early 21st century. One of those solutions is to use an opposed-piston engine configuration together with an axial engine configuration. Because an axial engine has its pistons reciprocating parallel to the crankshaft instead of perpendicular, a single shaft may be enough to unite the power of the two pistons reciprocating opposite to each other in an opposed-piston configuration.

2.3. Axial/Barrel Engines

The axial engine is an engine configuration in which the pistons reciprocate parallel to the crankshaft instead of perpendicular like in a conventional engine. Depending on the engine design and specifications of the pistons, those engines can have multiple cylinders and pistons arranged circumferentially about the crankshaft axle *[11]*.

In an axial engine, the mechanisms in which the linear motion of the pistons convert into rotary motion of the crankshaft are diverse. Between early 20th century until pre-World War II, various mechanisms were developed and despite some minor differences between them, almost all use mechanisms with some type of bevel gears, cams, swash plates and wobble plates. *Figure 2.4* represents a classification of the mechanisms used in barrel engines according to Pawel Mazuro in his PhD thesis *[12]* on how they transform linear motion into rotary motion and in the case of the wobble plate mechanism, how the plate movement is constraint.

Posteriorly, in the same work, a piston side thrust force analysis of each axial engine mechanism through the entire engine revolution range was conducted and compared to a classic crankshaft mechanism as, according to *[13]*, the dominant source of engine rubbing friction is the piston assembly. The results are presented in the graphic of the *Figure 2.5*.

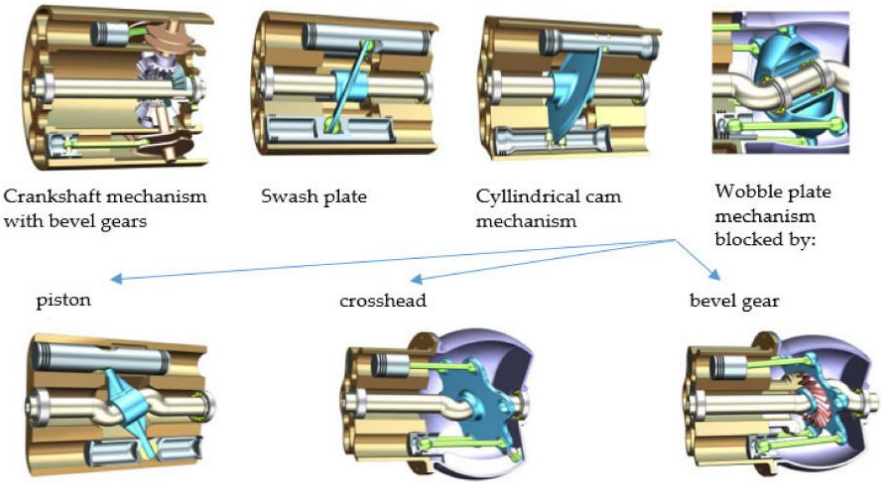

Figure 2.4 - Axial engine mechanisms classification [12]

The crankshaft mechanism with bevel gears consists of multiple conventionally crankshafts, one to each cylinder, with bevel gears at the inner end of each shaft ganged and geared to a central gear on the central output shaft *[14]*. The advantage of this mechanism is the ability to reduce the output shaft rotational speed to half the speed of the conventional crankshafts and other reciprocating components. The problem with this mechanism tough, is that the bevel gears mechanism proved to be overly complex, heavy, and costly to maintain or repair. None of the engines that were developed using this mechanism were successful and consequently, it was abandoned.

In the swashplate mechanism, the plate is angled compared to the engine horizontal axis, fixed to a straight crankshaft, and rotates with it. This makes impossible to fix the connecting rod to the plate with a spherical plain bearing, per example, unless the engine block or "barrel" also rotates. Instead, rollers or slipper pads are used to transfer the linear motion of the assembly connecting rod/piston to the swashplate and crankshaft. This mechanism is characterized to create a "nutation" motion of the plate. According to the piston side force mechanical analysis, this mechanism presents the biggest value among all mechanisms represented in the *Figure 2.5* and that may be the reason why there are no modern engine designs with this mechanism configuration. While not ideal for an engine, this mechanism seems to be very useful in air conditioning compressors, helicopter swashplates, etc.

The cylindrical cam mechanism is very similar to the swashplate mechanism. The main difference is that the plate is substituted by a cylindrical cam surface with a sinusoidal contour but is equally fixed and rotates with the crankshaft as in a swashplate mechanism. Normally in these engines, the cylindrical cam is placed in the middle of the crankshaft and connected to a double ended piston which reciprocate opposed to one another in double headed cylinders. Between the piston and the cylindrical cam surface,

two rollers are placed, one in each side of the cylindrical cam surface, to transfer the linear motion of the piston to the cylindrical cam surface and crankshaft. The cylindrical cam surface has the advantage of being programmable, allowing tailoring of velocity, acceleration, and extent of piston travel *[15]*. The result is a more efficient mechanical motion compared to the swashplate as the "nutation" motion is eliminated and the transfer of linear motion into rotary motion is smoother but even then, as depicted in *Figure 2.5*, the mechanical efficiency is far inferior to a conventional crank mechanism.

The wobble plate mechanism is characterized, as the name suggests, to create a "wobble" motion of the plate. In this mechanism, the crankshaft has a form of a Z-shape that creates an angle with its central axis. One or two bearings are used to connect the plate perpendicular to the Z-shape zone of the crankshaft. In this way, the plate does not go round together with the crankshaft and instead only goes back and forward with the assembly connecting rod/piston not in a perfect linear motion but with a wobbling motion. Because of that wobbling motion, spherical bearings are used to the joints plate/connecting rod and connecting rod/piston to grant the degrees of freedom required for their motion. The friction between the rotating crankshaft and the stationary plate causes a tendency for the rotation of the plate in turn of the horizontal axis of the crankshaft which is something not desired as it upsets its alignment with the pistons *[14]*. To prevent this phenomenon, the wobble plate rotation must be blocked which can be done by three major mechanisms:

- Blocked by piston: The rotation of the wobble plate can be stopped using the piston movement against the cylinder block/barrel. When that happens however, the motion of the mechanism starts to behave like a swashplate mechanism rather than a wobble plate mechanism. It is not coincidence that when Mazuro analysed the mechanism in his doctoral dissertation *[12]*, the side piston force of the wobble plate mechanism blocked by piston was equal to the swashplate mechanism through the entire engine revolution. For that reason, this mechanism did not present a good mechanical efficiency and was abandoned.
- Blocked by bevel gear: In this mechanism the wobble plate is fitted with a gear that engages with another gear fixed to the block engine around the crankshaft. The stationary gear has its horizontal axis perfectly aligned with the crankshaft horizontal axis and thus, the rotation of the wobble plate in that axis is prevented.
- Blocked by crosshead: A wobble mechanism blocked by crosshead is generally characterized to an extra "arm" of the wobble plate which is constrained to a boss present on the engine block. In that way the "arm" and the plate can not rotate together with the crankshaft and bearings. There are slight variations of this mechanism such as the mechanism used in the Bristol axial engine that uses a pair of helical gears instead of the boss to block the rotation of the wobble

plate. Although the same motion restriction is achieved in both mechanisms, the pair of helical gears mechanism is by far more complicated and requires more mechanical components. For that reason, the boss mechanism is preferred. In terms of mechanical efficiency, both mechanisms, together with the mechanism blocked by bevel gear explained above shows the best mechanical efficiency of all axial engine mechanisms presenting as much as 50% lower piston side force than a conventional crank mechanism *[13]*.

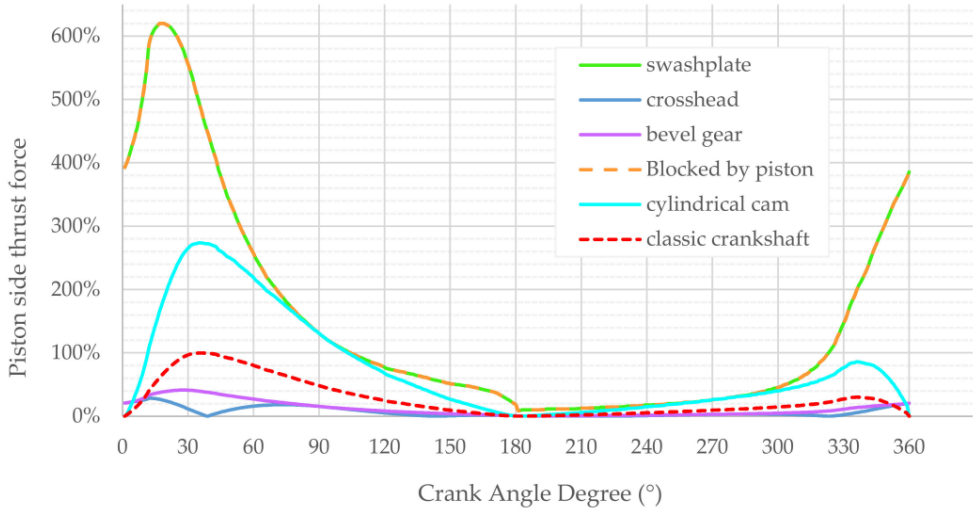

Figure 2.5 - Piston side force of axial engine mechanisms compared to a classic crankshaft [12]

In conclusion and according to Mazuro *[12]*, the wobble plate mechanisms blocked by bevel gear and crosshead presents the best mechanical efficiency as these mechanisms have the lesser piston side thrust force. An article from 1986 from Z. Yu and Ting W. Lee *[11]* also analysed the kinematics of the wobble plate/connecting rod/piston motion and agrees with this conclusion even adding that a five-link type (five connecting rods/pistons connected to the wobble plate) is the best of the wobble plate mechanisms blocked by crosshead.

2.3.1. Advantages and disadvantages

The advantages and disadvantages of axial engines can look a bit contradictory.

Many of the mechanical disadvantages of barrel engines, especially with wobble plate mechanisms, are considered historical and not factual because many were noted during the early 20th century development boom in different barrel engine mechanisms and in that time, the available technology was not yet capable to address those disadvantages. The goal was to test the different mechanisms and patented it for future

profits the fastest possible. The result was a severe lack of in-depth analysis as the technology was recent and the information regarding axial engines was mainly from patents and journal articles. With time and investment, surely, progress would be made to optimize and fix the issues encountered in the prototypes tests, however, as *[15]* mentions, the development and research of the axial engine seemed to lost momentum after World war II despite several tested design prototypes that shown promising results. This may be explained due to the development of bigger radial engines and the invention of turbine and jet engines. Per example, the Almen wobble plate engine had already five prototype designs when the investment was cancelled *[13]*.

The fact is that with the cut in investment, some disadvantages remained associated with axial engines wrongly. According to *[13]*, ongoing research and the current state of technology are already capable of address some of the challenges associated with this engine configuration and potentially unlock further advantages in the future.

Main historical disadvantages of axial engines fixed:

- Mechanical failures of wobble plate and piston joints: The mechanical failures observed in the early models of axial engines were due to two main factors: lack of precise kinematics analysis and lack of parts development. Per example, the wobble plate mechanism requires the use of spherical plain bearings as joints uniting the wobble plate/connecting rod/piston mechanism *[13]*. The lack of research and development of spherical bearings when the initial axial engine prototypes were developed caused them to fail and the belief that those bearings were not suited for engine applications just grew. As advancements were made in the innovation of those bearings, *[16]* affirms the problems leading it to mechanical failure were fixed and the spherical bearings became far more reliable even showing advantages and a better performance than conventional slide bearings and piston pins engine mechanisms.
- High friction losses: According to *[13]*, high friction losses are indeed a disadvantage of some of the mechanisms shown in *Figure 2.4* and may have caused the popular belief of mechanical inefficiency of barrel engines. However, *[12]* has proven that mechanisms using wobble plate blocked by crosshead and wobble plate blocked by bevel gear produce a significant lower piston side force compared to conventional crankshaft engines. Furthermore, the use of spherical bearings as joints such as socket and ball joints uniting the wobble plate/connecting rod/piston can be more efficient in reducing friction than slide bearings and piston pins joints.

Lubrication issues and cooling issues were also observed in some historical designs although modern axial engines development studies do not mention those issues when testing their prototype engines.

It is not in the performance aspect that the axial engine has disadvantages but rather in the financial aspect and it's here where these engines may have some difficulty in progressing. Despite worse in general, a conventional engine is reliable and extensively researched compared to an axial engine. As *[13]* mentions, the fact that an axial engine is a completely new mechanism with many different components necessary for its assembly, makes it very risky for a manufacturer to invest in, as switching production lines of conventional engine components for axial engine components is expensive. Also, unexpected issues may appear during prototype phase as the technology is not heavily researched as the conventional engine. If successful thought and the engine enters in production phase, the manufacturing costs can be lower due to a significant reduction in components compared to a conventional engine and a simpler design. Together with an opposed-piston layout, an axial engine has the capability of achieving a full engine symmetry and thus reducing further the costs of components manufacturing *[5]*.

The advantages of an axial engine are significant specially when restricted volume and weight is a strong requirement like in an aircraft. The following advantages are focused on a wobble plate mechanism because it is the best mechanism to use in an axial engine.

Advantages of a wobble plate mechanism *[13] [11]*:

- Longer service life of the piston-cylinder pair as the ratio of side pressure to normal pressure on pistons is lower than a conventional engine as proven in *Figure 2.5*.
- Lower vibration and mechanical noise level and smoother operation as modern kinematic and dynamic theory is capable of completely balancing the wobble-plate mechanism. Also, the piston motion on an axial engine is exactly or approximate to a harmonic motion which is a desirable advantage in all engines and heavily contributes to a smoother operation.
- More uniform output shaft-torque
- Compact design with less volume: axial/barrel engines have a cylindrical shape that allows for a compact and space-efficient layout. This can be beneficial in applications where size is a critical factor such as in aircrafts.
- High power-to-weight ratio: The barrel engine´s radial configuration has the possibility to offer a high power-to-weight ratio. This means that it can provide significant power output relative to its weight, which can be advantageous in applications that require high performance and low weight is a critical factor such as in aircraft engines.

- Potential for Improved efficiency: barrel engines have the potential to achieve good thermodynamic efficiency due to their compact design, reduced heat losses and low lateral piston side force. Also, the integration of additional engine control systems like VCR and VVT is relatively simple in axial engines.
- Large number of symmetrical parts and reduction of engine components can be a good financial advantage.
- Axial symmetry can enable the same filling, lubrication, and cooling conditions for all cylinders.

2.3.2. Axial engines evolution

The barrel engine configuration had a rapid boom in development of new mechanisms and different designs. Since the first in the early 20th century until World War II constant designs were being patented. Few engines saw prototypes being built and tested and even fewer were used in service. After World War II thought, the configuration practically disappeared and only a few continued being developed. An online museum for barrel engines *[14]* put in excellently into timeline a good number of engines developed with patents and prototype sketches.

2.3.2.1. Smallbone Axial Engine

The first appearance of an axial engine patent was in 1906 when Harry Eales Smallbone patented a four-cylinder four stroke wobble plate blocked by crosshead gas engine with a static barrel type and water cooled *[14]*. Despite being a wobble plate, this mechanism is different from any mechanism classified by Mazuro *[12]*. As observed in the patent sketch, the engine used plain spherical bearings to assembly the pistons/connecting rod/wobble plate but also as a mechanism to transform the linear motion of the wobble plate in rotary motion of the crankshaft. There is an unusual shaft with a spherical plain bearing at one extremity. The spherical plain bearing has the function to withstand the force of the wobble plate against the engine block where it is fixed. The other extremity of the shaft is connected to the crankshaft with an angle. The middle part of the shaft is connected to the wobble plate with a roller bearing. When the wobble plate moves back and forward, the shaft rotates working like a “hand crank” forcing the crankshaft to also rotate. It is worth noticing that the spherical plain bearing in the extremity of the shaft does not have any translation movement.

It is unknown if the engine was ever built.

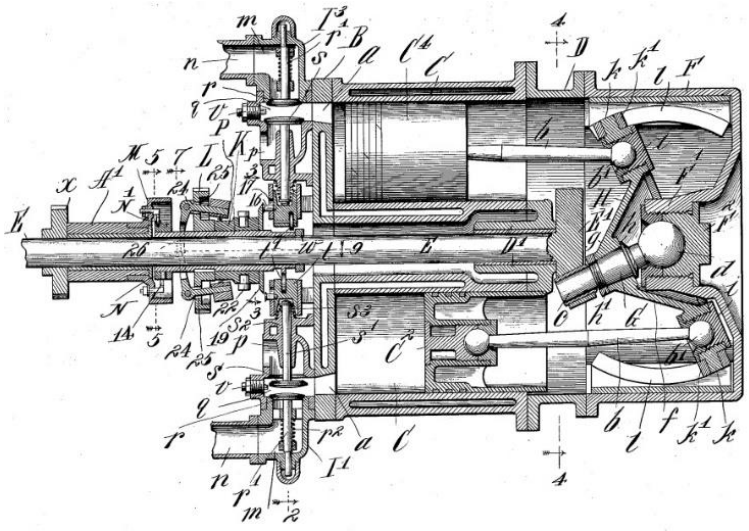

Figure 2.6 - Smallbone axial engine [17]

2.3.2.2. Macomber Axial Engine

The Macomber engine was the first known patented, built and used axial engine. Designed in 1911 by Walter G. Macomber, it was a four stroke, air-cooled rotating-barrel wobble plate engine with two versions with five and seven cylinders. The engine possessed the capability of varying the angle of the wobble plate, thereby effecting a change in the length of the stroke and the compression ratio *[18]*. The engine was first tested on a successful aircraft flight but only was commercialized for the automobile industry.

In 1918 the company and the engine disappeared *[14]*.

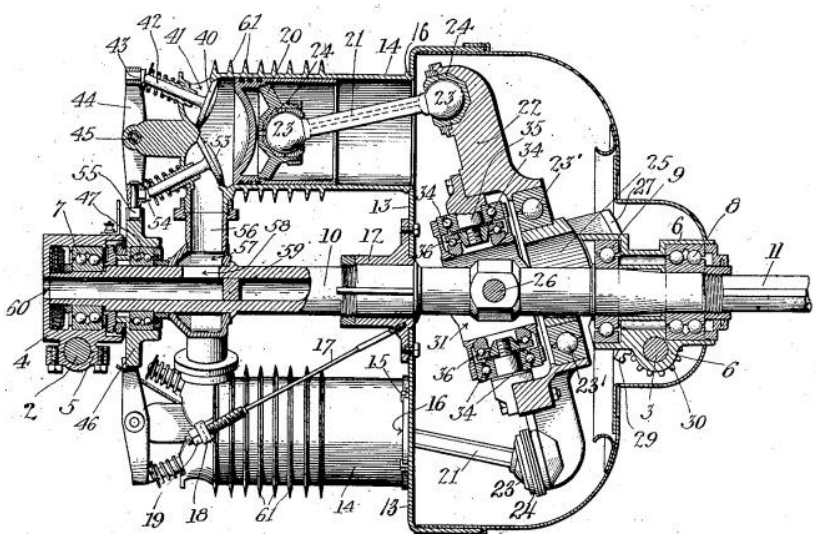

Figure 2.7 - Macomber axial engine [19]

2.3.2.3. Trebert Axial Engine

Despite only being patented in 1917, the Trebert engine was designed in 1912. It was the first between the few axial engines incorporating a crankshaft mechanism with bevel gears. This engine was an air-cooled four stroke six cylinders rotary engine with rotary sleeve valves *[18]* that produced $44.7kW$ with a mass of $104kg$. The interesting fact about this engine is that the whole engine went round except with the output shaft and its central gear, and the fixed terminal at the extreme left and at the extreme right which remained stationary during the engine movement. The power output was in fact taken from the rotary crankcase end in the right side instead of the central shaft like in any engine.

In *[14]*, there is a very good CAD simulation showing how the engine worked.

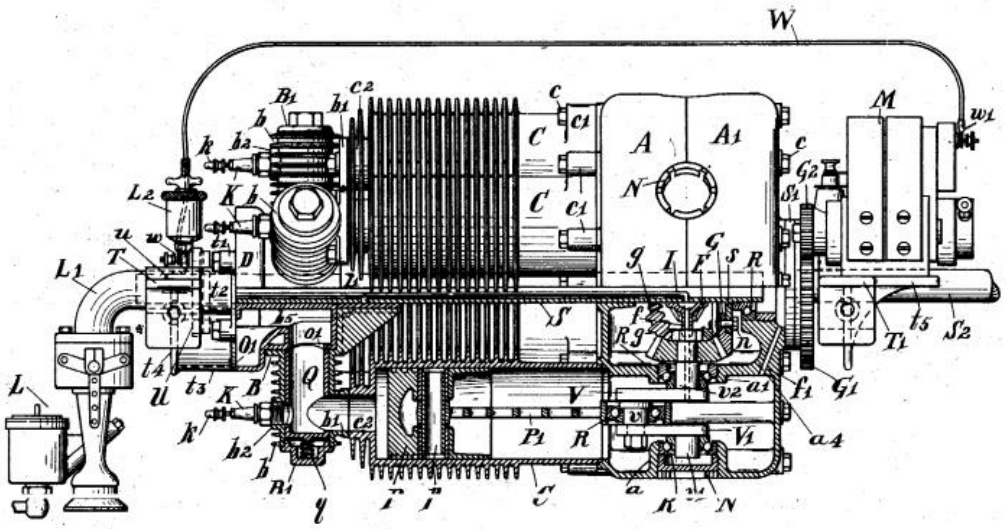

Figure 2.8 - Trebert axial engine [20]

2.3.2.4. Salmson Axial Engine

The Salmson was a French engineering company that developed aero and automobile engines. The aero engines developed were mainly radial however in 1908 until 1912, Salmson started to develop barrel type engines. The first barrel engines designed were 7-cylinder stationary opposed piston, water-cooled and with rotary valves with different specifications varying between 37.3 to $44.7kW$. Posteriorly Salmson started to make 9-cylinder stationary opposed-piston, water-cooled but with a distribution mechanism using poppet valves with an output of $56kW$ *[21]*. An

interesting fact about this engine is that it was the first axial engine using a high S/B ratio. The 7-cylinder version with an output of 44.7 had a S/B ratio of almost 3.5 *[14]*.

No patents of this engine were found but there are images available of multiple versions shown in the Paris air show of 1911 and 1913.

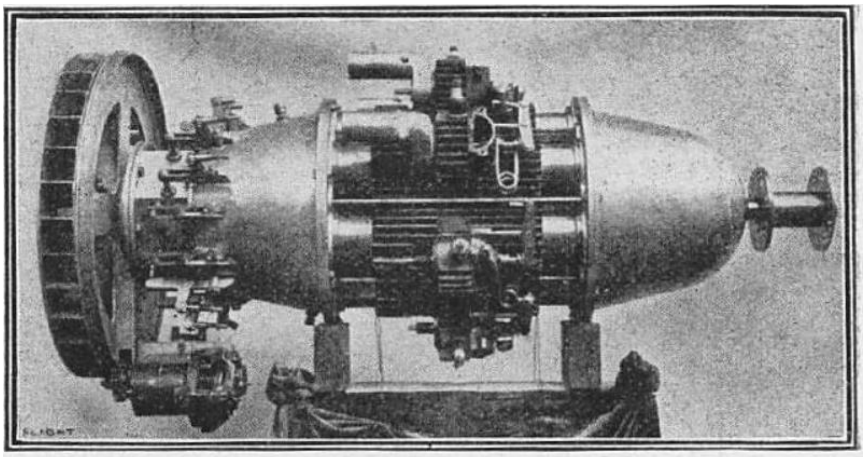

The 60-h.p. double 7-cyl. Salmson motor at the Paris Aero Salon.

Figure 2.9 - Salmson 7-cylinder axial opposed-piston engine [14]

2.3.2.5. Almen Aero Engine

John O. Almen was an American engine inventor that developed axial wobble plate engines blocked by bevel gear for the US army. In total four engine versions were developed between 1917 and 1921. The last version, the Almen A-4 was an eighteen horizontally opposed cylinder engine, four-stroke, water-cooled stationary axial engine. It had a central wobble plate blocked by bevel gear that connected to double ended pistons. At each end of the engine, a single rotary sleeve valve fed three cylinders at once through the intake and exhaust passages. Each cylinder had two spark plugs. The engine was successfully tested with impressive results. Its output was $317kW$ at $2000rpm$ with a mass of approximately $340kg$. Its frontal area was also very small compared to same output radial engines with only half a meter in diameter.

Despite successfully tested with impressive results, the funding was cut due to the US army increased preference for air-cooled radial engines *[14]*.

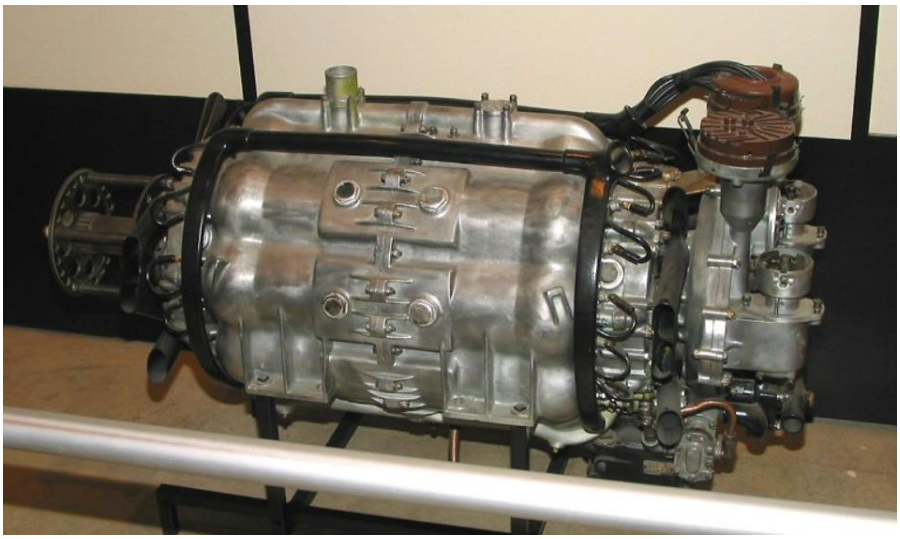

Figure 2.10 - Almen A-4 axial opposed-piston engine [14]

An initial version of the engine had a different design with a single wobble plate at one end, blocked by bevel gear and using spherical plain bearings (ball and socket joints) in the connecting rod (*Figure 2.11*). The interesting fact about this engine version is that it had another set of bevel gears used to control the rotary valve that fed the engine. So, the wobble plate had two bevel gears, one geared to a bevel gear in the engine block to stop the rotation of the plate and other geared to a bevel gear with a different gear ratio connected to the rotary vale to make it rotate at one tenth of the main shaft *[14]*.

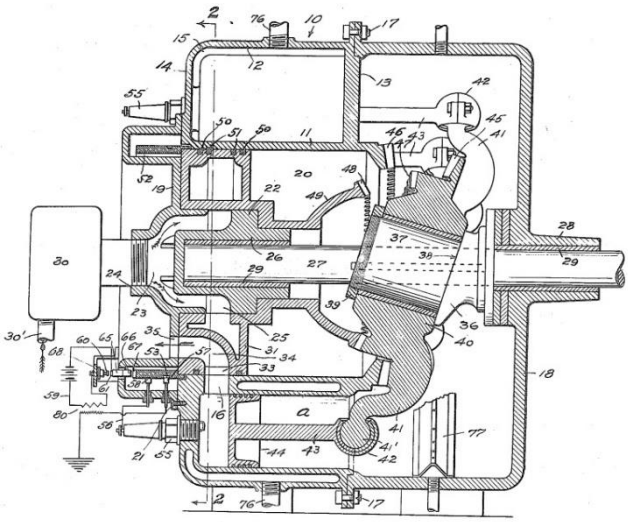

Figure 2.11 - Almen axial engine [22]

2.3.2.6. Bristol Axial Engine

The Bristol axial engine is not named after the inventor but rather the company that hired the inventor. Charles Redrup was an engine enthusiast with a long history of inventing new engines. Before being hired to create an engine in 1931 to the Bristol Tramways and Carriage Company, Charles created its own version of wobble plate barrel engine and even an axial engine with a cylindrical cam mechanism. However, it is the Bristol engine its famous work probably because a private company invested in it. The Bristol engine saw four versions being built and tested to use in the buses company. One of the versions of the engine was a 7-litre, four stroke nine-cylinder static barrel with a wobble plate mechanism blocked by crosshead using gears and rotary valves (*Figure 2.12*) that produced $108.2kW$ at $2900rpm$. This is the engine, mentioned previously, that used a pair of helical gears instead of the boss to prevent the rotation of the wobble plate. There is a CAD mechanism in *[14]* showing the engine motion.

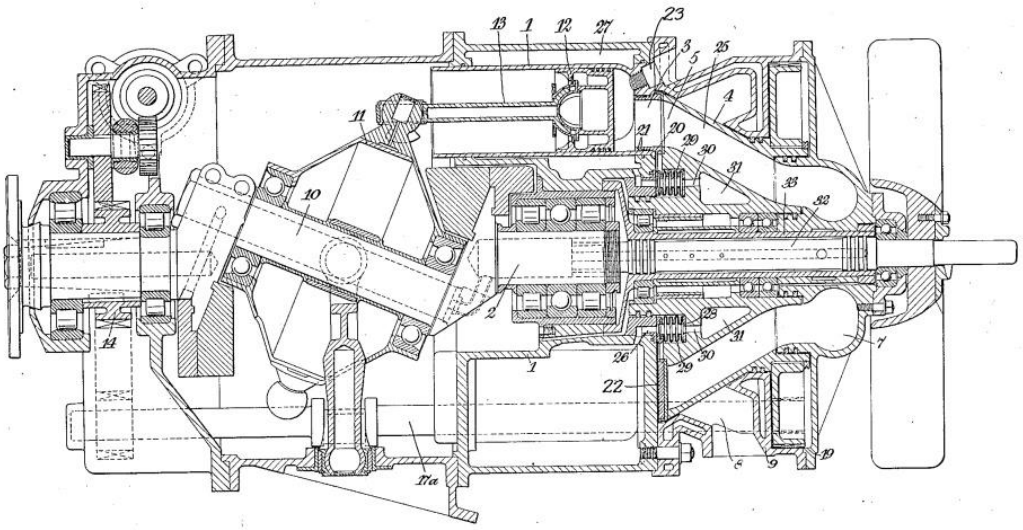

Figure 2.12 - Bristol axial engine [23]

According to *[14]*, the development of the Bristol engine stopped in October 1936 due to change in the management of the Bristol Tramways, however at least two patents inclusive a version of the Bristol engine with an opposed-piston configuration were filled after October 1936 (*Figure 2.13*) in the name of Charles Redrup and Bristol Tramways company.

According to the patent *[24]*, the engine is an improvement of the Bristol engine adding an opposed-piston configuration and an alternative rotary valve mechanism.

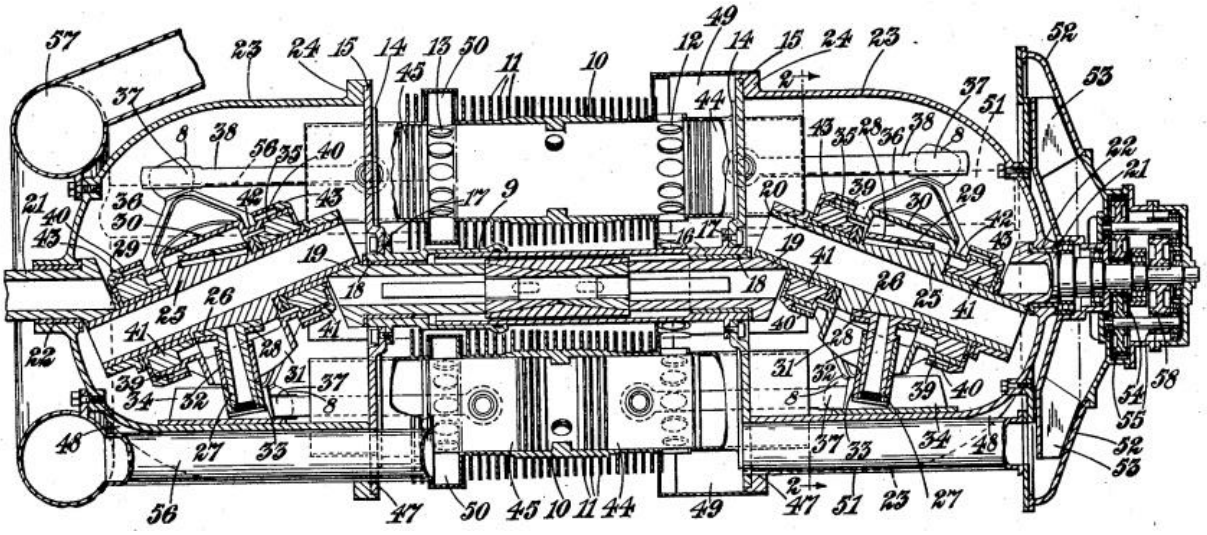

Figure 2.13 - Bristol axial opposed-piston engine [24]

2.3.2.7. Alfaro Axial Engine

In 1935, Heraclio Alfaro started to develop an axial engine under contract to the Civil Aeronautics Board in Boston Massachusetts *[15]*. The Alfaro engine was a two-stroke, 4-cylinder axial engine using a swashplate mechanism together with an opposed-piston configuration. Two plates were used, one at each end with two rollers to connect each connecting rod to the plate. The distribution system used was typical from a two-stroke engine. Exhaust ports at one side of the cylinder wall and intake ports in the other. The pistons closed and opened the ports purely with its reciprocating movement. There were no rotary valves or any timed system. When the pistons were close to the BDC unobstructed the ports and mixture came in through the intake port and exhaust gases exited thought the exhaust port. When the pistons moved towards TDC, its side walls obstructed the ports again.

Under tests, the engine outputted $115.6kW$ with a mass of $122kg$.

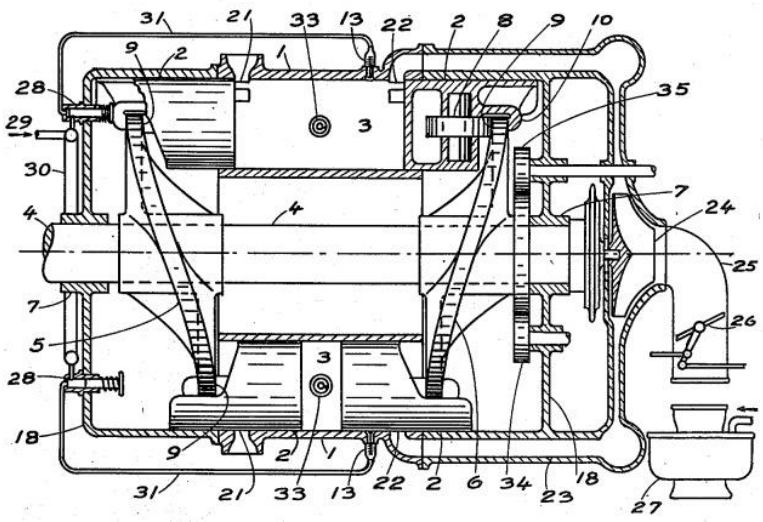

Figure 2.14 - Alfaro axial opposed-piston engine [25]

2.3.2.8. Dyna-Cam Axial Engine

In 1941, Karl Herrmann patented the Dyna-Cam axial engine with the US Patent 2,237,989. That engine was a two-stroke axial engine using a cylindrical mechanism together with an opposed-piston configuration, water cooled and a static barrel type. The sinusoidal cylindrical cam is in the centre of the output shaft with double-ended pistons reciprocating in six cylinders. Two rollers are placed between the double ended pistons and the cylindrical cam. Another cylindrical cam with a different configuration is also used to actuate the valves system using poppet valves.

The mechanism is surprisingly simple with very few pieces and a YouTube video [26] uses a real Dyna-Cam engine to explain in detail how the engine works. The engine has very good advantages which make it the only engine that saw continuous development even after World War II and until today.

In 1961 the engine and its patents were sold to Dennis Palmer which developed and optimized the engine even further getting a FAA Type certificate E-293 in 1981 that allowed it to be used in possible type certified aircrafts. In 1987 the engine was flown in a Piper Arrow and showed better performance than the conventional engine of the aircraft. This test can be also seen in the YouTube video [26]. Things seemed promising and the company “Piper Aircraft” was ready to use the Dyna-Cam engine in their aircrafts, until in went bankrupt in 1991 and the investment disappeared.

In 2003, the engine assets were sold to another company called Axial Vector Engine Corporation. This new company changed most of the design and implemented new technologies to the engine but updates on the engine stage are unknow as the company website is down.

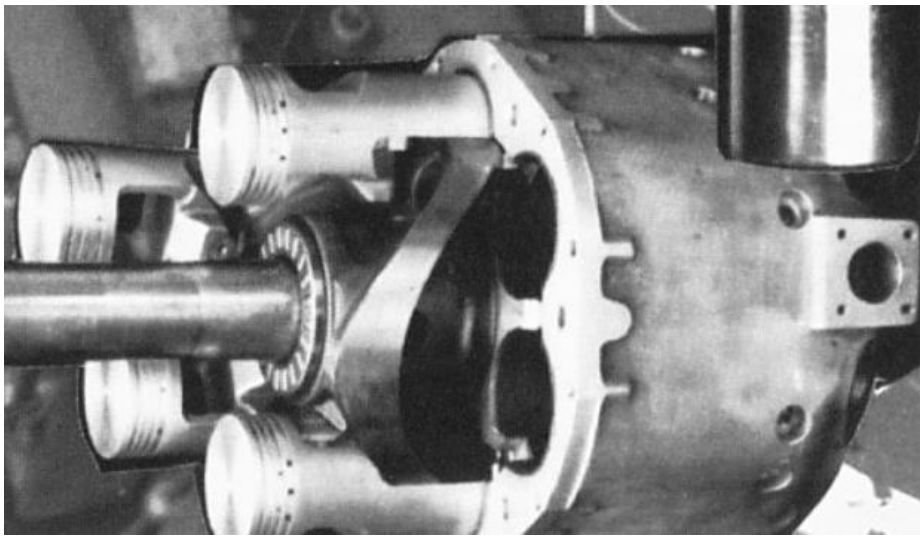

Figure 2.15 - Dyna-Cam engine [14]

2.4. State of the Art

Slightly after World War II, the boom in new axial engines stopped and only in the beginning of the 21st century when some companies start to look for new alternatives to the conventional internal combustion engine and alternative technologies to improve the efficiency of the internal combustion engine, the interest of the axial engine configuration re-emerged. There are now three major engine designs using an axial configuration not counting with the Dyna-Cam engine. The Duke engine, the Covaxe engine and the PAMAR engines.

2.4.1. Duke Engine

The Duke engine is a four-stroke spark plug axial engine being developed by Duke Engines company since 1993. Despite the similarity to the Smallbone engine wobble plate mechanism, the axial mechanism of the Duke engine is a new version of a swash plate mechanism as the movement of the plate is a nutation *[2]*.

The engine has three versions, with the last one using a rotating barrel with five cylinders and 3-litres. The distribution system is a rotary valve type where the cylinder head is stationary. Instead of the usual poppet valve system, the rotating cylinder barrel slides past ports that are mounted in the stationary cylinder head. As the cylinder slides past the ports, the mixture or exhaust gases are let through. Only three combustion chambers are necessary for the five cylinders, each one with an inlet and exhaust port,

spark plug and fuel injector. In their website *[2]*, there are multiple videos explaining in detail the engine movement.

With this configuration the company claims many advantages typical of axial engines such as less weight and smaller dimensions, higher power density and smoother operation compared to a conventional engine with similar performance. In fact, in their website, the company demonstrates the engine running with nearly free vibration *[2]*. The engine can also run on multiple fuels. The main applications for the Duke engine are motorcycles but also light aircrafts and unmanned aircrafts.

The engine seems to be in a very advance state and ready for production as it is trying to attract investors.

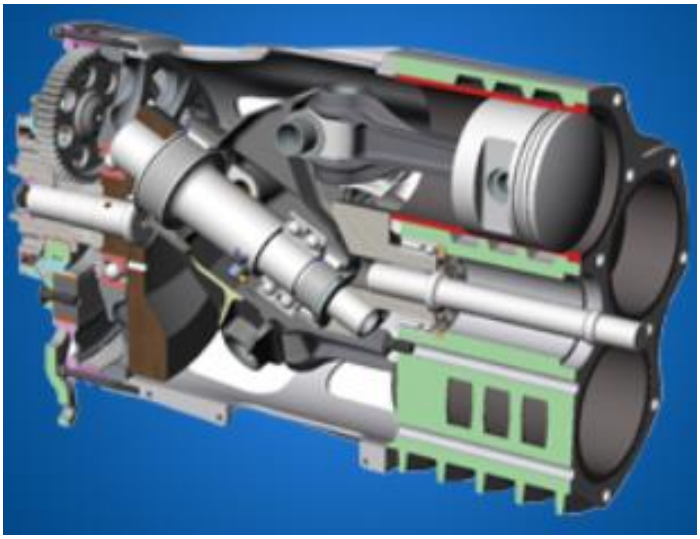

Figure 2.16 - V3 (3-litre) Duke engine [2]

2.4.2. Covaxe Engine

Covaxe engine is a diesel two-stroke axial and opposed piston engine being developed by Covaxe Limited in UK. It uses a cylindrical mechanism like the Dyna-Cam engine. The difference is that it uses two cylindrical cams, one in each end of the output shaft instead of a central one and so it only has one combustion chamber per cylinder. Double-ended pistons are used with two rollers between the cylindrical cam and the piston. The information about the distribution system mechanism is not abundant but it looks like the engine uses ports in the cylinder blocked and unblocked by the piston like in the Alfaro axial engine.

A CAD simulation of the cylindrical cam mechanism is shown in their website *[4]* together with some additional information about the engine.

Figure 2.17 - Covaxe engine [4]

2.4.3. PAMAR Engines

The PAMAR engines are a two-stroke opposed piston axial engines being developed at Warsaw University of Technology by a team lead by Pawel Mazuro. There are four versions already built and a fifth is being complete. The fourth version is still being tested and the results are shown in *[3]* and *[13]*. The fourth and most recent version uses a wobble plate mechanism blocked by crosshead while the third version uses a wobble plate mechanism blocked by bevel gear. Both versions use two wobble plates, one at each end of the output shaft. The third version has six cylinders while the fourth version has only two. Both versions seem to use ports in the cylinder blocked and unblocked by the pistons in the distribution system like the Alfaro engine.

The article *[13]* has more detailed information about the whole PAMAR project including the engine versions and the additional systems implemented such as the VCR, Variable Port Area (VPA) and the Variable Angle Shift (VAS) of the wobble plate. All those mechanisms help significantly in improving the efficiency of the engine and varying the engine specifications according to the application.

This is the present day project with more relevance and similarity with the present work as the goal is to build a similar engine but with a four-stroke cycle.

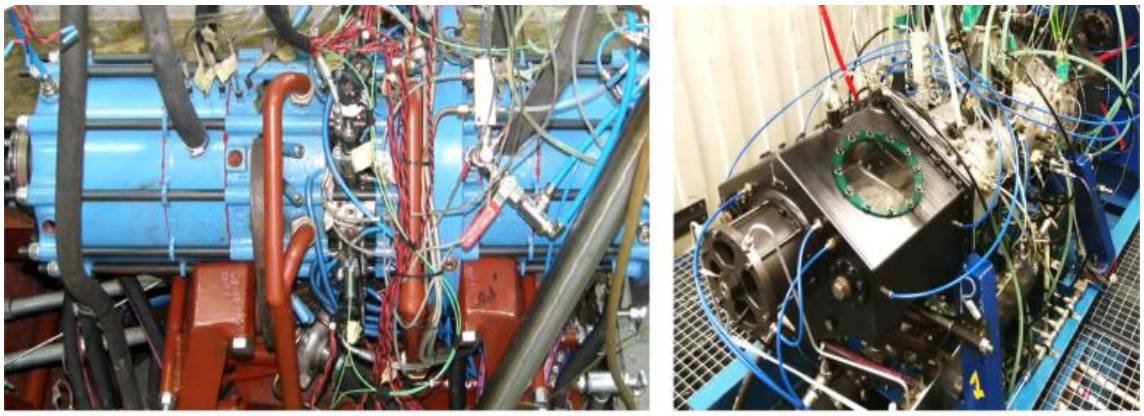

Figure 2.18 - PAMAR 3 and PAMAR 4 on the left and right, respectively [13]

Chapter 3

3 Methodology

3.1. Software Tools

- Microsoft Excel: is a spreadsheet program that enables to calculate, format, and organize data. This program is used throughout the work for the calculations of the different parameters of the engine movement.
- CATIA V5: is a CAD software developed by "Dassault Systèmes". This software is utilized to design the engine´s parts and the posterior assemble and motion simulation. It is also used to undergo a structural analysis of the engine crankshaft.

3.2. First Parameters

As already mentioned, the present work has the objective of designing and size an axial opposed-piston concept engine with a four-stroke distribution system fuelled by gasoline for possible aircraft use.

To begin the sizing of the engine and the posterior design, the first step is to identify and select some initial parameters crucial to any engine. The parameters selected are:

- Engine speed which is the maximum rotation speed of the engine crankshaft.
- Piston bore diameter which is the diameter of the surface in which the pressure resulting from the engine combustion will act upon.
- Stroke to bore ratio which is the ratio between the piston stroke and the piston bore diameter. So having the piston diameter and the stroke to bore ratio automatically selects the engine stroke, which in the case of this engine design, is the horizontal distance that the piston travels from TDC to BDC or vice versa, instead of vertical distance as seen traditionally in conventional engines.
- Compression ratio which is the ratio between the maximum cylinder volume and the minimum cylinder volume which means the ratio between the cylinder volume at BDC and the cylinder volume at TDC.

$$r_c = \frac{V_d + V_c}{V_c} \tag{3.1}$$

Where:

V_d is the swept/displacement volume.

V_c is the clearance volume.

The straight forward way to find these parameters is to compare it to other engines, with some parameters being better compared to engines with similar designs while others to engines with similar purposes.

The stroke to bore ratio (S/B), per example, in modern aircraft engines presents a value inferior to one, meaning that the piston bore diameter is larger than the stroke. That is because, most internal combustion engine aircraft designs are horizontal opposed piston engines and so the pistons reciprocate horizontally and perpendicular to the crankshaft. A large piston stroke creates a wider engine. Since those engines are placed in the front of the aircraft, it causes a large front sectional area which worsens the aircraft aerodynamics.

Despite horizontal opposed piston, this engine design is axial meaning the pistons reciprocate parallel to the crankshaft and thus the opposite happens. It´s a large piston bore diameter that creates a wider engine while a larger stroke only creates a longer engine which does not worsen the aircraft´s aerodynamics.

For the reason explained above, instead of comparing stroke to bore ratios and piston bore diameters with modern conventional aircraft engines, the comparison is made with engines with similar designs to that of the present engine.

Most of 20th century axial opposed piston engine designs have S/B ratios in the range of 1 to 1.3 except the Salmson engine with a S/B of almost 3.5 *[14]*, however the more modern engines like the Achates and the PAMAR engines, more specifically, the most recent PAMAR 4 engine have higher S/B ratios, closer to the Salmson engine.

According to Achates, which has a S/B ratio between 2.2 and 2.6 *[27]*, there are some significant advantages in higher stroke to bore ratios like reduced in-cylinder heat transfer which creates a higher thermal efficiency engine. Although the Achates engine is an opposed-piston engine, it´s not axial like the engine of this paper and the PAMAR 4 engine. When comparing to the PAMAR 4 engine, the S/B ratio is even higher being valued at 6.85 *[13]*. According to Pawel Mazuro and Barbara Makarewicz, there are even more benefits to a higher S/B ratio for axial engines including the one explained above. Also, in a conventional engine with a crank mechanism, higher S/B ratios are limited due to the increase piston side force caused by the deviation of the connecting rod from the cylinder axis or prohibitively long connecting rod to overcome the later problem, making a conventional engine extremely wide. In an axial engine, that deviation is

extremely small as will be shown forward when calculating the forces acting on the wobble plate and crankshaft.

It is worth mention that the values of the S/B ratios of the Achates and PAMAR 4 engines represent the displacement of both piston strokes because an opposed piston engine has two pistons reciprocating opposed per cylinder.

Because there are no modern four-stroke axial opposed-piston engines to compare, as the Achates and the PAMAR engines run on a two-stroke cycle, a more conservative choice of selecting a S/B ratio of 1.25 for each piston and thus making a total S/B ratio of 2.5 seems more appropriate.

Initially the criteria to select a piston diameter was the availability of the diameter and price of manufactured pistons to other existing engines. An initial thought was to use a "Volkswagen Type 3" piston with $83mm$ diameter *[28]*, however, the piston bore diameter size may be limited due to the possible lack of space between the cylinders and the crankshaft. As this engine is axial and will use a L-head cylinder with the valves turned to the crankshaft, a large bore diameter can be a problem further in the dimension of the engine. Despite many 20^{ths} century axial engines having large bores, comparing to the more recent PAMAR 4 engine which uses a $55mm$ piston bore diameter *[13]*, a reduction in the piston bore diameter is more reasonable and so the $83mm$ "Volkswagen Type 3" piston must be discarded for a smaller $60mm$ piston bore diameter *[29]*.

The maximum engine speed and the compression ratio are parameters that seem not to be affected by the type of engine design and thus is more reasonable to compare those parameters to other aircraft engines than to other opposed piston axial engines.

Giacosa says that the compression ratio of four-stroke Otto cycle aircraft engines is valued in the range of 5.5 to 7.5 *[30]*. Those values are likely outdated because when compared to more modern aircraft engines such as the Lycoming or the Continental engines, the compression ratio varies between 7 and 9 *[31] [32]*.

The selected value amongst the range values above must has in count a dimension factor. As already mentioned, initially a "Volkswagen Type 3" piston was chosen but dismissed for the possibility of being too large. In the research of the "Volkswagen Type 3" piston specifications, it was discovered that the compression ratio of its engine is 7.5 and thus being in the compression ratio range of modern aircraft engines *[28]*. Knowing the specifications of the "Volkswagen Type 3" engine and if this engine has the same compression ratio as the "Volkswagen Type 3" engine, the estimate of its maximum pressure will be easier as it will be further explained in the Section *3.3.* with more detail. For that reason, a 7.5 compression ratio is selected for the present engine design.

The maximum engine speed of those same modern aircraft engines varies between $2400rpm$ up to $3400rpm$ but most of them are in the range of $2400rpm$ to $2800rpm$ *[31] [32]*. This is mainly limited by the propeller radius. A higher engine speed limits the propeller diameter, causing a smaller propulsive efficiency for the same aircraft. Therefore, it is between that range that the maximum engine speed of this engine design of $2500rpm$ is selected.

3.3. Maximum Pressure

One of the first steps to size the engine is to find the maximum pressure reached inside the combustion chamber. The maximum pressure together with the diameter of the piston define the maximum force on the piston and, in consequence, the structural requirements of the whole engine. It is to that piston force that the engine parts will be dimensioned to withstand.

The maximum pressure reached inside a real combustion chamber is influenced by many parameters such as engine speed, air/fuel ratio, ignition timing, flame speed factor, residuals fraction and compression ratio *[33]*. In a theorical cycle thought, explained in the Section *2.1.1.*, where many simplifications of the combustion are assumed and many variables are considered constant, the maximum pressure varies mainly, among the parameters described in the last sentence, by the compression ratio *[34]*.

Because the result of the maximum pressure using a theoretical cycle is very unreasonable, a different strategy to estimate it is using reversed engineering.

In the beginning of the project, it was supposed to design the present engine to use “Volkswagen Beetle” piston with a bore of $83mm$. As already explained in the Section *3.2.*, later it was chosen not to use that piston due to an excessive bore compared to modern axial engines. Despite that and because the “Type 3” has a compression ratio that fits inside the range of aircraft internal combustion engines, it is decided to use the same compression ratio for the engine. By knowing the dimensions of the piston, the gudgeon pin and the small end of the connecting rod of the “Type 3” engine of the “Volkswagen Beetle”, it is possible to inversely dimension the parts mentioned in order to estimate the maximum pressure of the “Type 3” engine and thus, the engine of this paper as well.

Knowing the outer diameter and the supported length of the gudgeon pin by the small end of the connecting rod *[35]* and seeking the highest value for the allowable bearing pressure of the bronze bush between the gudgeon pin and the small end of the connecting rod *[36]*, it´s possible to find the maximum force on the “Type 3” piston engine through the following equation:

$$F_{max} = d_{pin} l_{pin} p_{bp} \quad (3.2)$$

Where:

$d_{pin} = 22mm$ is the outer diameter of the gudgeon pin.

$l_{pin} = 24.7mm$ is the supported length of the gudgeon pin by the small end of the connecting rod.

$p_{bp} = 50MPa$ is the maximum allowable journal lubrification bearing pressure of the bronze bearing found *[36] [37]*.

Once estimated the maximum force, the maximum pressure inside the combustion chamber is given by:

$$p_{max} = \frac{4F_{max}}{\pi D_{piston}^2} \quad (3.3)$$

Despite not the ideal way to find the maximum pressure of the engine, the value obtained is considered reliable because comparing to other engines such as the more powerful "Jaguar XK" engine with a compression ratio of 8 and a maximum pressure of $5.2MPa$ *[38]*, the maximum pressure of $5.02MPa$ for the present engine design seems reasonable due to, among other facts, the less favourable combustion chamber geometry, however, because the present work has the goal of preliminary sizing the concept engine and not perfecting it, an approximate value rather than an exact value is not a concern.

Rewriting the *Equation 3.3* but this time using the piston bore diameter for the present engine, the maximum piston force acting on it is found:

$$F_{max} = \frac{\pi}{4} D_{piston}^2 \, p_{max} \quad (3.4)$$

3.4. Point of Maximum Piston Force

According to Ajeet Singh *[39]*, in structurally sizing an internal combustion engine, two piston positions are considered to know which one produces the biggest forces on the engine mechanical components. The first one is when the piston is at TDC, the torque is zero and the pressure inside the combustion chamber is maximum. The

second is when the torque is maximum and the pressure peak inside the combustion chamber has passed. The piston is on its way to BDC.

The maximum torque happens when the tangential force is the largest which depends on the pressure inside the combustion chamber in that position and the mechanical equations of the design. The maximum torque for spark ignition engines in a conventional engine design happens at $25º$ to $35º$ degrees of the crankshaft rotation angle *[39]*.

The present engine is being designed as a spark ignition engine but because it has a different design from a conventional engine, the crankshaft angle range at which the tangential force is maximum may be different.

When considering that the maximum pressure is at TDC, it is assumed that the combustion happens with the considerations of a theoretical Otto cycle. In reality, looking to any engine graphic which relates pressure to crankshaft angle like the engine tested in *[33]*, the maximum pressure happens always after TDC and not at TDC.

Heywood says that in a spark ignition engine, the spark plug ignition happens between $10º$ and $40º$ degrees before TDC and the combustion lasts between $40º$ and $60º$ degrees of the crankshaft angle rotation *[8]*.

Rather than using the two moments described by Ajeet Singh and using *[33]* and *[8]* as references, instead the present engine will be sized assuming a maximum pressure, and thus, a maximum force at $20º$ degrees after TDC. This solution happens to be a midterm between the maximum pressure and the maximum torque positions and mathematically provokes slightly larger reactions in the engine components. An overestimation value rather than an underestimation value is not a problem and so this solution guarantees that the engine components are capable of withstand the pressure resulting from the engine combustion.

3.5. Connecting Rod

As already explained in the Section *2.3.*, in an axial engine design, spherical bearings are normally used to the joints of the wobble plate/connecting rod big end and connecting rod small end/piston due to the wobbling movement of the wobble plate.

The crosshead blocks any translation and rotation outside the plane where it is placed and connected to the wobble plate with the main objective of preventing the wobble plate to rotate together with the crankshaft. However, the crosshead also influences the motion behaviour of the connecting rod big end connected to the wobble plate where the point E is located as shown in *Figure 3.2*. The connecting rod big end

motion is rotating around the crankshaft center point O perpendicular to the plane where the crosshead is placed.

If the crosshead is placed in the plane xy, the same plane where the piston and the connecting rod small end translate, restricted by the cylinder, the connecting rod motion becomes purely rotational in turn of z-axis of the crankshaft center point O. If placed in any other plane, the connecting rod big end motion misaligns with the connecting rod small end attached to the piston. This causes the connecting rod to wobble with the wobble plate.

The conclusion of this fact is that if the crosshead is placed in the plane xy, then the small end of the connecting rod can be a piston pin joint like in a conventional engine instead of a socket and ball joint (spherical bearing). With this solution, a conventional piston can also be used instead of designing a completely new piston if a spherical bearing.

A regular connecting rod of a conventional engine is still not suitable for this engine design due to the rotation of the wobble plate in the point E in turn of the y-axis where the connecting rod big end is connected. Usually, axial engines use a socket and ball joint (spherical bearing) in the big end joint except Duke Engine that uses a cardan joint. For this engine connecting rod design, a socket and ball joint is used in the big end joint and a piston gudgeon pin in the small end joint.

In connecting rods with a spherical bearing, the usual is being designed with a circular section instead of an H section like a conventional connecting rod. The connecting rod design process is well explained in *[40]*. To design the column rod, the Rankine´s formula must be used:

$$F_{cr} = \frac{\pi^2 EI}{{L_e}^2} \tag{3.5}$$

Where:

F_{cr} is the maximum load acting on the connecting rod with a safety factor of 2.5:

$$F_{cr} = 2.5F_q \tag{3.6}$$

F_{q} is the resultant force acting on the connecting rod from F_{max} and is defined in *Equation 3.13* in *Section 3.7*.

I is the moment of inertia of the section with respect to the buckling-bending axis which in case of a circular section is:

$$I = \frac{\pi}{64} {d_{cr}}^4 \tag{3.7}$$

Where:

d_{cr} the diameter of the circular section of the connecting rod column in mm.

$E = 200 \times 10^3 MPa$ and is the modulus of elasticity of the connecting rod material which will be the same as that of the crankshaft shown forward.

L_e is the equivalent length of the connecting rod column. A connecting rod is considered to have both ends fixed meaning that for calculation purposes, it´s equivalent length is considered half of its length.

$$L_e = \frac{L}{2} \tag{3.8}$$

In the present engine design, the connecting rod length is influenced by the distribution mechanism system, more specifically, the length of the poppet valves.

The width of the small end is dependent on the piston pin diameter and the force acting on it:

$$w_{secr} = \frac{F_{max}}{p_{bp} d_{pp}} \tag{3.9}$$

Where:

d_{pp} is the outside diameter of the gudgeon piston pin *[29]*.

$p_{bp} = 50 MPa$ is the safe bearing pressure of the bronze bearing.

To reduce friction, a bronze plain bearing of $2mm$ is used between the gudgeon piston pin and the small end *[39]*. The inside diameter of the connecting rod small end is given by:

$$d_{i_{secr}} = d_{pp} + 4mm \tag{3.10}$$

The outside diameter of the small end is given by:

$$d_{o_{secr}} = \frac{F_{max}}{w_{secr} \tau_{cr}} + d_{i_{secr}} \tag{3.11}$$

Where:

τ_{cr} is the safe tensile stress of the connecting rod material with a safety factor of 2.5.

The socket and ball joint used in the big end of the connecting rod is designed by finding the radius necessary to withstand the maximum force acting on it:

$$r_{lecr} = \sqrt{\frac{F_q}{\pi p_{bp}}} \tag{3.12}$$

3.6. Wobble Plate Blocked by Crosshead

In a conventional engine, the connecting rod is connected directly to the crankshaft through the big end of the connecting rod and the journal bearing of the crankshaft.

In most axial engines, due to the parallel movement of the piston in relation to the crankshaft, that connection is made by an intermediate mechanical piece depending on the type of axial engine. In the present engine design, the wobble plate blocked by crosshead mechanism is used.

The structural dimensioning of the wobble plate is not part of the present work objective and it´s design is simplified considering similar designs of other wobble plate axial engines. The connection to the crankshaft is made with two rolling bearings which follows the abutment dimensions requirements of the bearing manufacturer. The joint linking to the connecting rod follows the measures of the socket and ball joint of the big end of the connecting rod. The cap of the socket and ball joint is screwed to the wobble plate and incorporates a pin to mate with the blocking crosshead. Finally, two halves of the wobble plates are screwed to each other inversely parallel and in between, are placed the roller bearings and crankshaft.

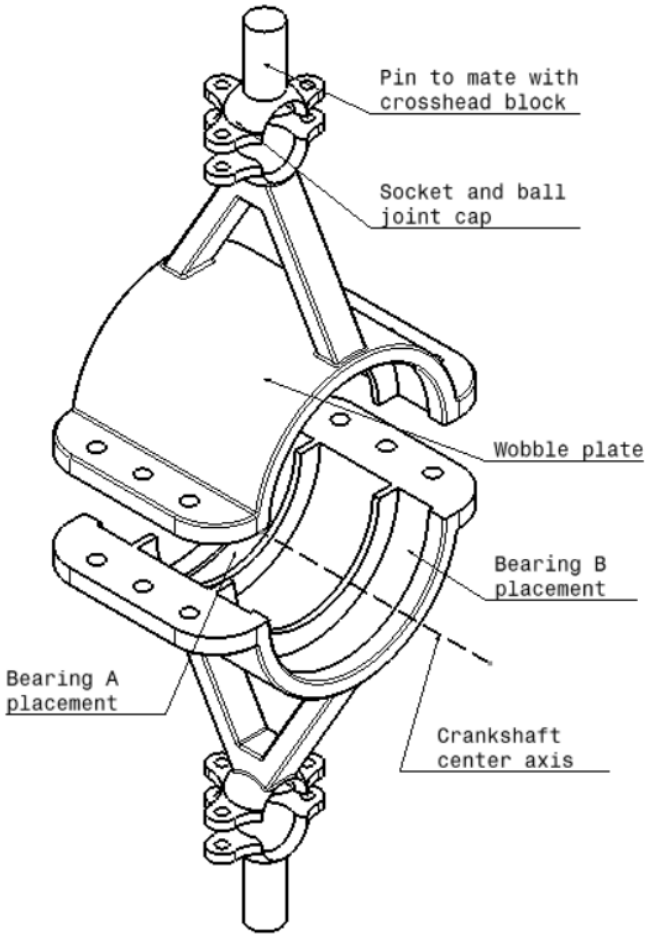

Figure 3.1 - Wobble plate configuration

The crosshead is built-in to the engine block/coverage which is connected to the crankshaft support bearings that allow the crankshaft to rotate. Per piston, the wobble plate mechanism has three different pieces, the wobble plate, the socket cap, and the crosshead built-in in the engine block.

3.7. Kinematics Analysis and Crankshaft Design

With the maximum pressure from the combustion chamber estimated and at which point it happens, it is now possible to find how the maximum force applied on the piston is transmitted to the other reciprocating components of the engine, that forces the crankshaft to rotate and produce torque and power. Those intermediate components are the connecting rod and the wobble plate. *Figure 3.2* illustrates the kinematics of the engine´s piston/connecting rod/wobble plate/crankshaft motion explaining how the movement works and the parameters in play to find the forces associated with the shaft torque.

The mechanical components such as the wobble plate are simplified and not at scale.

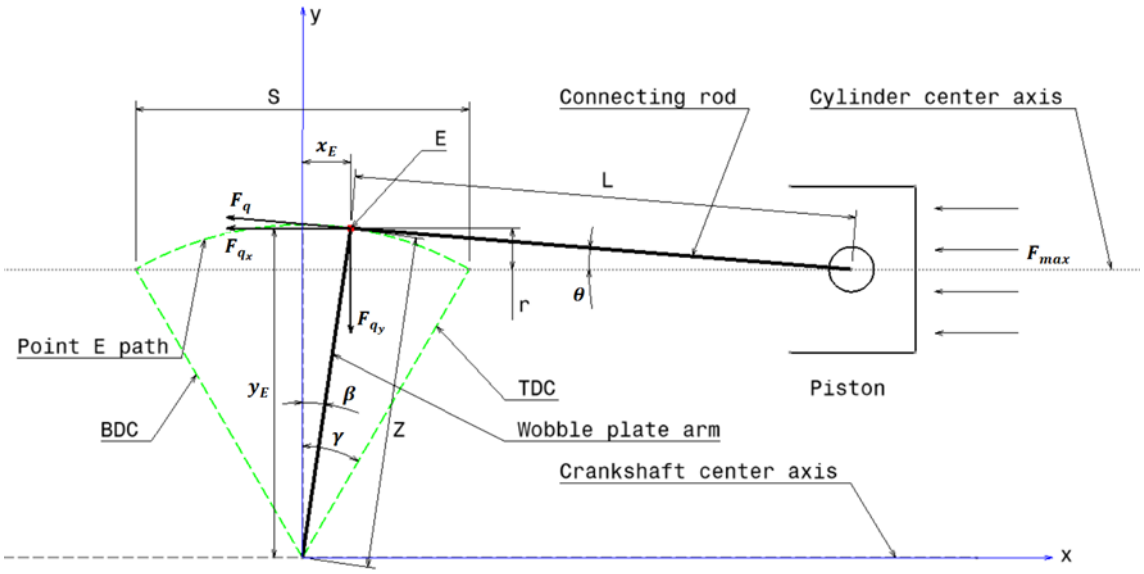

Figure 3.2 – Kinematic representation of wobble plate/connecting rod/piston

The stroke of the engine S is already indirectly defined through the S/B ratio. Because the S/B ratio is 1.25 and the piston bore diameter is $60mm$, the stroke is $75mm$.

To analyse the engine kinematics, thought, it is still necessary to define one last constant which is the maximum angular range γ of the wobble plate arm movement. Historical values are almost impossible to find except for the PAMAR engine. In *[13]* is mentioned that the maximum angle of the wobble plate for the PAMAR 4 engine is designed to have $18.1º$ degrees. Coincidentally or not, the "DIN 71802" socket and ball joint which is a spherical plain bearing similar to the joint which is used to connect the connecting rod big end and wobble plate also has a maximum angle of $18º$ degrees *[41]*. For those reasons, γ will be arbitrarily defined as $18º$ degrees.

It is worth mentioning that the movement of the reciprocating parts is in two dimensions because, as previously explained, the engine uses a mechanism to block the rotation of the wobble plate around the crankshaft center axis and thus cancelling any movement in the third dimension.

The force resultant F_q acting on the joint connecting rod/wobble plate, which in the future will be called point E, is the force along the connecting rod with the angle θ which is the angle that the connecting rod has during the reciprocating motion in relation to the centre line of the cylinder which is positioned at TDC:

$$F_q = \frac{F_{max}}{cos\,\theta} \tag{3.13}$$

That force is divided into two components, one for each direction:

$$F_{q_x} = F_q \cos\theta \tag{3.14}$$

$$F_{q_y} = F_q \sin\theta \tag{3.15}$$

Theta θ is the angle of the connecting rod relative to the cylinder centre line. The theta angle θ is given by the trigonometry relation between the length of the connecting rod L and the vertical distance variation r between the cylinder centre line and the joint where the connecting rod connects with the wobble plate arm:

$$L \sin\theta = r \tag{3.16}$$

And so, θ is given by:

$$\theta = sin^{-1}\left(\frac{r}{L}\right) \tag{3.17}$$

The connecting rod length L varies depending on the later full design of the crankshaft and other engine components because it is placed parallel to the crankshaft. The vertical distance variation r, thought is already given for any cylinder position:

$$r = Z \cos\beta - Z \cos\beta_{cylinder\ position} \tag{3.18}$$

Where:

β is the angle between the wobble plate arm and the y-axis in the plane Oxy and will vary according to the rotation of the crankshaft with a range of $[-\gamma; \gamma]$ degrees being $\beta = \gamma$ at TDC and $\beta = -\gamma$ at BDC.

Z is the length of the wobble plate arm in mm.

Because the cylinder centre line will be aligned in the TDC condition and in that position $\beta = \gamma$, the vertical distance variation is:

$$r = Z \cos\beta - Z \cos\gamma \tag{3.19}$$

The length of the wobble plate arm Z which r depends on is directly influenced by the engine stroke S and the maximum angular range γ of the wobble plate arm movement, both previously defined:

$$Z = \frac{S}{2\,sin\,\gamma} \tag{3.20}$$

To discover the resultant force F_q applied on the point E (joint wobble plate/connecting rod), it is necessary to find the angle β.

The angle β can be given by the trigonometric components of the wobble plate arm or the coordinates of the point E:

$$x_E = Z\,sin\,\beta \tag{3.21}$$

$$y_E = Z\,cos\,\beta \tag{3.22}$$

Where β is:

$$tan\,\beta = \frac{x_E}{y_E} \tag{3.23}$$

The two variables x_E and y_E define the position where the connecting rod connects with the wobble plate, and they are not known yet. Because the angle β varies with the crankshaft rotation, it´s necessary to define and analyse the variables of the crankshaft and its movement rotation to determine its value.

As obvious, the engine crankshaft is one of the main parts of any engine. Due to this axial design, the crankshaft is also one of the parts that is completely different form a conventional engine and thus requires a different mechanical and geometrical analysis to be sized and designed.

For the design of the crankshaft, two main constants are sufficient to completely define all the others and thus all the crankshaft: the angle of the arm γ which is equal to the maximum angular range of the wobble plate arm and the length of the arm X shown in *Figure 3.3*.

With those constants defined, trigonometric equations can be found to size the geometry of the crankshaft. *Figure 3.3* illustrates the crankshaft geometry in the TDC position with the other mechanical parts of the engine simplified for reference. The crankshaft is represented by a simplified center line for better perception and representation of the constants. The real crankshaft has two corners in each arm X as shown in *Figure 3.4*. Observing *Figure 3.3*, *Equations 3.24* to *3.27* are derived.

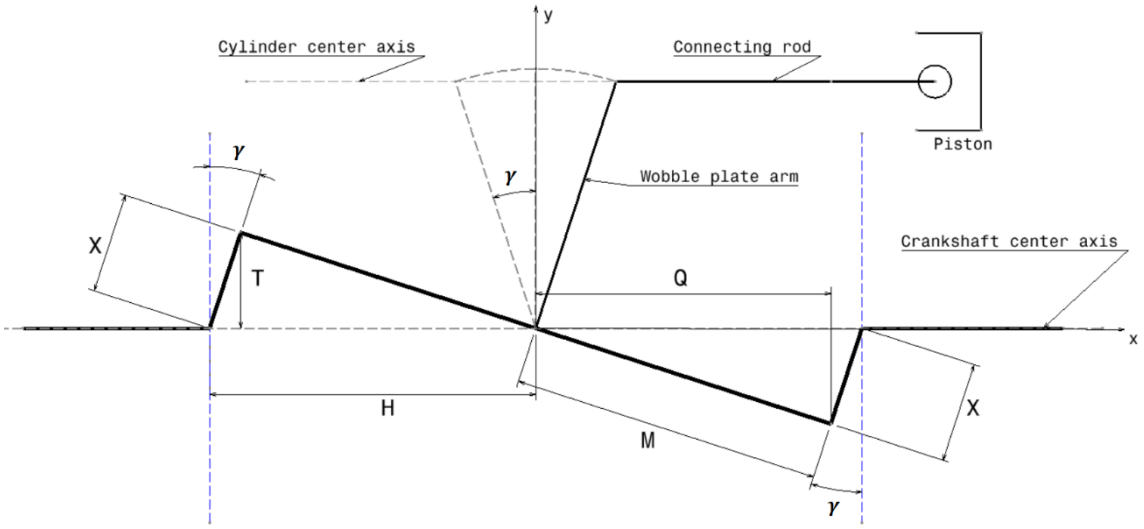

Figure 3.3 - Simplified crankshaft design

$$M = \frac{X}{tan\,\gamma} \tag{3.24}$$

$$H = \frac{X}{sin\,\gamma} \tag{3.25}$$

$$Q = M\,cos\,\gamma \tag{3.26}$$

$$T = X\,cos\,\gamma \tag{3.27}$$

Despite not shown in the previous figures, two bearings are used to connect the wobble plate to the crankshaft and, to fully complete the motion analysis of the reciprocating components, it´s necessary to define the position of those bearings as they heavily influence the reactions on the crankshaft. Their placement on the crankshaft is shown in *Figure 3.4* marked as the point A and B.

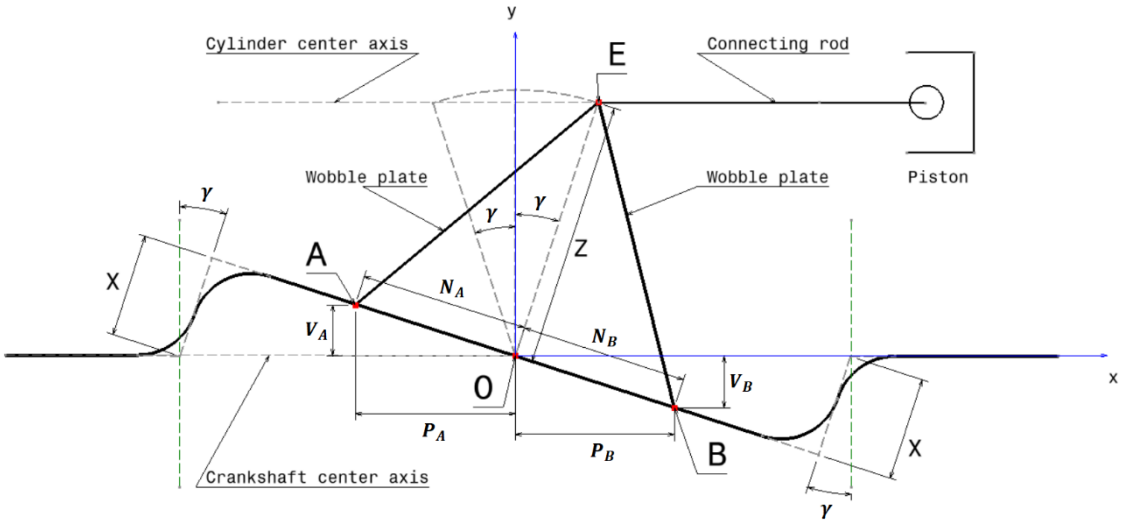

Figure 3.4 – Crankshaft/wobble plate joint bearings A and B coordinates

As it can be observed, there are two differences between the *Figure 3.4* and the previous *Figures 3.2* and *3.3*. The crankshaft has the correct center line with its curves on the arm X instead of the angles, and the wobble plate design is composed with two arms, each one connecting to each bearing instead of a single center arm. These changes do not interfere in any of the previous equations which still apply.

The bearings positions marked as points A and B can be defined by the variables N_A and N_B which are the distance of the bearings A and B, respectively, from the center of the crankshaft marked as point O. Furthermore, trigonometric relations are defined for the distances to the y-axis and x-axis of the bearings nominated P and V respectively for each bearing:

$$V_A = \frac{N_A T}{M} \tag{3.28}$$

$$P_A = \frac{N_A Q}{M} \tag{3.29}$$

$$V_B = \frac{N_B T}{M} \tag{3.30}$$

$$P_B = \frac{N_B Q}{M} \tag{3.31}$$

Further ahead, in Section *3.10.2.* is discussed how to choose the best value for N_A and N_B according to the crankshaft dimensions and bearing placement limitations and requirements.

Using a Cartesian coordinate system $Oxyz$ centred in the point $O(0;0;0)$ located in the center of the crankshaft between the bearings A and B as shown in *Figure 3.4*, at TDC, the point A where the bearing A is placed is:

$$A(-P_A; V_A; 0)$$

And the point B where the bearing B is placed is:

$$B(P_B; -V_B; 0)$$

The point E is located where the wobble plate and the connecting rod connects being:

$$E(Z\sin\gamma\,; Z\cos\gamma\,; 0) = E(x_E; y_E; 0)$$

Considering that referential but now with the angle of the crankshaft rotation around the x-axis denominated Φ, with $\Phi = 0$ being when the piston is at TDC, the exact location of the mentioned points A, B and E for each angle of the crankshaft rotation Φ can be found with the points coordinates:

$$O(0;0;0)$$

$$A(-P_A; V_A\cos\Phi\,; V_A\sin\Phi)$$

$$B(P_B; -V_B\cos\Phi\,; -V_B\sin\Phi)$$

$$E(Z\sin\beta\,; Z\cos\beta\,; 0) = E(x_E; y_E; 0)$$

The resultant vectors are:

$$\overrightarrow{AE} = E - A = (x_E - (-P_A); y_E - V_A\,cos\,\Phi\,; -V_A\,sin\,\Phi) \qquad (3.32)$$

$$\overrightarrow{OE} = E - O = (x_E; y_E; 0) \qquad (3.33)$$

The distance between the point O and the point A and the distance between the point O and the point E is constant:

$$\overline{OA} = N_A$$

$$\overline{OE} = Z$$

So, the distance between the point A and the point E which is the hypotenuse of the triangle AOE and according to the Pythagorean theorem is:

$$\overline{AE} = \sqrt{{N_A}^2 + Z^2} \tag{3.34}$$

And those same distances using the Cartesian coordinate system are:

$$\overline{AE} = \sqrt{\left(x_E - (-P_A)\right)^2 + (y_E - V_A \cos \Phi)^2 + (-V_A \sin \Phi)^2} \tag{3.35}$$

$$\overline{OE} = \sqrt{x_E^2 + y_E^2} \tag{3.36}$$

Equalizing both equations:

$$\overline{AE} = \sqrt{\left(x_E - (-P_A)\right)^2 + (y_E - V_A \cos \Phi)^2 + (-V_A \sin \Phi)^2} = \sqrt{{N_A}^2 + Z^2} \tag{3.37}$$

$$\overline{OE} = \sqrt{x_E^2 + y_E^2} = Z \tag{3.38}$$

Solving the equations system formed by the *Equations 3.37* and *3.38*, it can be found the exact coordinates of the point E, the variables x_E and y_E, in function of the crankshaft angle of rotation. Knowing the coordinates of the point E defines the value of angle β (*Equation 3.23*) which in turn gives the value of the resultant force F_q and its components acting on the point E. Despite finding the point E through this method, point E is independent of the bearings positioning.

The intention is to find the reactions acting on the crankshaft due to the piston force at maximum torque of the crankshaft rotation which was previously considered as happening at $20º$ degrees of the crankshaft rotation after TDC ($\Phi = 20º$). Those reactions acting on the crankshaft are located where the wobble plate connects to the crankshaft through the bearings in points A and B.

To achieve that goal, one vector to the resultant force and two vectors, one to each reaction are defined. Furthermore, two vectors uniting the three points where the force and reactions act are also necessary.

$$\overrightarrow{r_{AE}} = E - A = ((x_E + P_A)\,\vec{\imath}; (y_E - V_A \cos \Phi)\vec{\jmath}; (-V_A \sin \Phi)\vec{k}) \tag{3.39}$$

$$\overrightarrow{r_{AB}} = B - A = \left((P_B + P_A)\vec{\imath}; (-V_B - V_A) \cos \Phi\, \vec{\jmath}; (-V_B - V_A) \sin \Phi\, \vec{k}\right) \tag{3.40}$$

$$\vec{F} = (-F_{q_x}\vec{\imath}; -F_{q_y}\vec{\jmath}; 0\vec{k})$$

$$\overrightarrow{R_A} = (R_{A_x}\,\vec{\imath}; R_{A_y}\vec{\jmath}; R_{A_z}\vec{k})$$

$$\overrightarrow{R_B} = (R_{B_x}\,\vec{\imath}; R_{B_y}\vec{\jmath}; R_{B_z}\vec{k})$$

Determining the vector product of these vectors for the torques due to the defined vector forces:

$$\overrightarrow{r_{AE}} \times \vec{F} = \begin{vmatrix} \vec{\imath} & \vec{\jmath} & \vec{k} \\ x_E + P_A & y_E - V_A\cos\Phi & -V_A\sin\Phi \\ -F_{q_x} & -F_{q_y} & 0 \end{vmatrix}$$

$$= \left((x_E + P_A)\left(-F_{q_y}\right)\right)\vec{k} - \left((y_E - V_A\cos\Phi)\left(-F_{q_x}\right)\right)\vec{k}$$

$$+\left(V_A\sin\Phi\,F_{q_x}\right)\vec{\jmath} - \left(V_A\sin\Phi\,F_{q_y}\right)\vec{\imath} \qquad (3.41)$$

$$\overrightarrow{r_{AB}} \times \overrightarrow{R_B} = \begin{vmatrix} \vec{\imath} & \vec{\jmath} & \vec{k} \\ P_B + P_A & (-V_B - V_A)\cos\Phi & (-V_B - V_A)\sin\Phi \\ R_{B_x} & R_{B_y} & R_{B_z} \end{vmatrix}$$

$$= \left((P_B + P_A)R_{B_y}\right)\vec{k} - \left((P_B + P_A)R_{B_z}\right)\vec{\jmath}$$

$$+\left((-V_B - V_A)\cos\Phi\,R_{B_z}\right)\vec{\imath} - \left((-V_B - V_A)\sin\Phi\,R_{B_y}\right)\vec{\imath}$$

$$-\left((-V_B - V_A)\cos\Phi\,R_{B_x}\right)\vec{k} + \left((-V_B - V_A)\sin\Phi\,R_{B_x}\right)\vec{\jmath} \qquad (3.42)$$

The forces and torque components provide the six static equations of equilibrium:

$$\sum M_x = -V_A\sin\Phi\,F_{q_y} + (-V_B - V_A)\cos\Phi\,R_{B_z}$$

$$-(-V_B - V_A)\sin\Phi\,R_{B_y} \qquad (3.43)$$

$$\sum M_y = V_A\sin\Phi\,F_{q_x} - (P_B + P_A)R_{B_z} + (-V_B - V_A)\sin\Phi\,R_{B_x} = 0 \qquad (3.44)$$

$$\sum M_z = (x_E + P_A)\left(-F_{q_y}\right) - (y_E - V_A\cos\Phi)\left(-F_{q_x}\right)$$

$$+(P_B + P_A)R_{B_y} - (-V_B - V_A)\cos\Phi\,R_{B_x} = 0 \qquad (3.45)$$

$$\sum F_x = R_{A_x} + R_{B_x} - F_{q_x} = 0 \qquad (3.46)$$

$$\sum F_y = R_{A_y} + R_{B_y} - F_{q_y} = 0 \qquad (3.47)$$

$$\sum F_z = R_{A_z} + R_{B_z} = 0 \qquad (3.48)$$

The only movement the crankshaft can have, is the rotation around the x-axis which provides the crankshaft torque. All the equations should be equal to zero except the moment in turn of the x-axis.

$$T_{crankshaft} = M_x = -V_A \, sin\, \Phi \, F_{q_y} + (-V_B - V_A) \, cos\, \Phi \, R_{B_z} \\ -(-V_B - V_A) \, sin\, \Phi \, R_{B_y} \quad (3.49)$$

It is also worth noticing that the bearings A and B must be the same bearing but opposite to each other despite the bearing A carry more load than the bearing B. This is because the crankshaft must be balanced about the x-axis and so the bearing masses must be equal. For that reason, also, those bearings must be placed at the same distance of the point O and so their coordinates are equal but opposite:

$$N_A = N_B;\; V_A = V_B;\; P_A = P_B$$

Solving the equation system of the six static equations of equilibrium provides the six components of the reactions on the points A and B however, this system is impossible to solve if at least one assumption is not made, or one variable value assumed.

The main force acting on the crankshaft is the axial component of the piston force F_{q_x} and the axial reactions of the bearings A and B must counter it which is represented in the sum of forces of the x-component.

$$\sum F_x = R_{A_x} + R_{B_x} = F_{q_x} \quad (3.24)$$

Due to the present crankshaft design and opposed-piston axial configuration, the main bearing to counter the axial component force of the piston is the bearing A and thus, it´s axial reaction must be the largest. For that reason, the axial component of the bearing B is considered zero for the sake of selecting a bearing model with sufficient axial force specification and useful life determination.

To lock the crankshaft from moving in the x-direction relative to the engine block, another two bearings are used. Those bearings are the bearings C and D positioned in the point C and point D. Unlike the bearings A and B, those bearings are stationary in the same position for the support of the crankshaft.

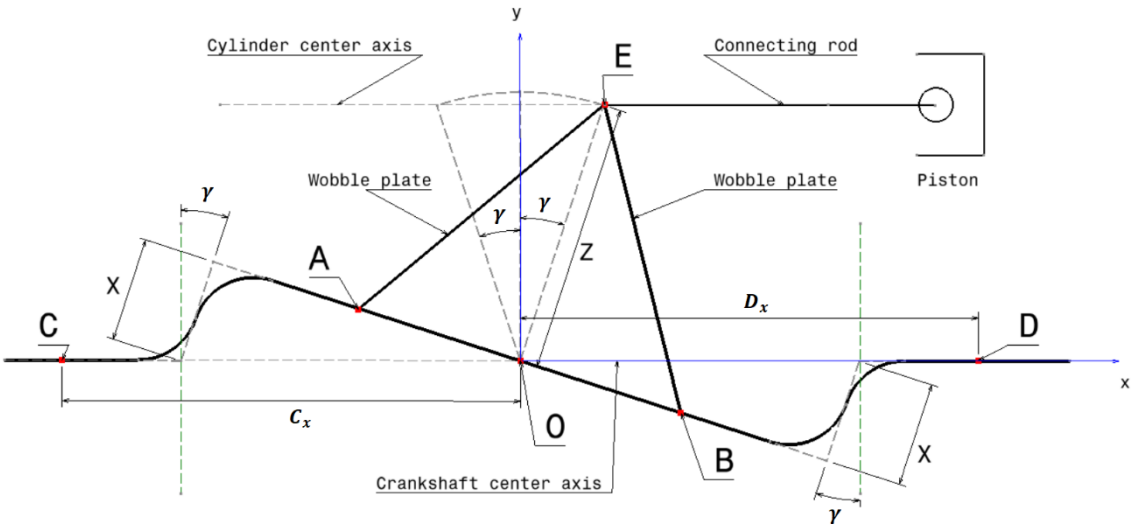

Figure 3.5 – Support bearings C and D coordinates

Using the same Cartesian referential system centred in $O(0;0;0)$, the coordinates of the points C and D are:

$$C(-C_x;0;0) = C(-\overline{OC};0;0)$$

$$D(D_x;0;0) = D(\overline{OD};0;0)$$

To calculate the reactions in bearings C and D the procedure is simpler, and it is only needed the three fundamental equations of statics in two dimensions as the z-component is zero: sum of forces in the x-direction, sum of forces in the y-direction and some of moments of a point which in this case is the point C:

$$\sum F_x = -F_{q_x} + R_{D_x} + R_{C_x} = 0 \tag{3.25}$$

$$\sum F_y = F_{q_y} + R_{D_y} + R_{C_y} = 0 \tag{3.26}$$

$$\sum M_C = -F_{q_x} \times y_E + F_{q_y} \times (x_E + \overline{OC}) + R_{D_y} \times (\overline{OC} + \overline{OD}) = 0 \tag{3.27}$$

Again, this equation system is also impossible to solve if at least one variable is not assumed like the equation system of bearings A and B. In this case, the x-component of the reaction at point D, R_{D_x} is zero and explained further ahead why, when arranging the bearings C and D.

3.8. Crankshaft Partition

There are two options to place the rolling bearings in their locations: through the middle of the crankshaft or through the ends.

Due to the present engine configuration, axial and opposed piston, the biggest forces act on the outside bearings A and C and so these bearings are supposed to be the larger ones. Nevertheless, if the bearings are placed through the ends, the first bearing to be placed which is bearing D, must be the largest to give space to the next ones: B, A and C to enter, when in terms of strength required, is the smallest. This option makes the bearings size complete opposite of what is required in terms of strength.

The other option which is that the bearings to be placed through the middle of the crankshaft, allows the bearing A and B to be placed first and in final the bearing D. The bearing C can still be placed thought the end of the crankshaft.

This configuration also allows the design of a backrest in the crankshaft to accommodate bearing A against it to withstand correctly against the axial force component of the resultant force F_{q_x}, which is the largest. To allow the bearings passage through the middle of the crankshaft, the crankshaft must be divided into two symmetrical pieces in relation to the y-axis. Once the bearings are placed in their proper locations, the crankshafts are reunited with a shaft coupling, designed further ahead.

With that being said, the crankshaft partition is executed in the middle of the crankshaft where the combustion chambers are placed in parallel.

3.9. Bearing Arrangements

As previous mentioned, two bearings denominated A and B are used to connect the wobble plate to the crankshaft while two other denominated C and D are used to hold the crankshaft to the engine block.

According to NSK catalogue *[42]*, a bearing and machining components company, there are many arrangements of bearings possible and a good procedure on how to choose the most appropriate is explained in the catalogue. Usually, a fixed-end bearing capable of carrying combined loads (axial and radial), and a free-end bearing carrying only radial loads are used to secure a shaft. In this arrangement, the fixed-end bearing needs to use a double bearing or two bearings because when radial loads are applied to these types of bearings, a component of load is produced in the axial direction. To balance this component load, bearings of the same type are used in pairs, placed in a face-to-face or back-to-back mounting *[42]*.

With this arrangement, in total, three bearings are necessary, two capable of carrying combined loads and one capable of carrying only radial loads. However, if the distance between the bearings is small and the elongation and contraction of the shaft due to temperature variations is negligible, an arrangement is possible where the bearing capable of carrying only radial loads is unnecessary and the two bearings capable of carrying combined loads are placed separately.

The bearings A and B match the requirements of the two bearings arrangement as their distance is sufficiently small, but the bearings C and D have to be arranged with the three bearings arrangement as their distance from one another is considerably superior. Also, the bearing D is the closest to the combustion chamber hence the most suitable to temperature variation which causes the shaft to elongate and contract more in that area. For that reason, the bearing D must be free to allow bearing axial displacement.

The type of bearings more common available for the positions A and B are angular contact ball bearings and tapered roller bearings, remembering that both bearings must be the same bearing type and model, for equal mass and engine balance.

To test which type of bearings are better suited for the position A and B, an estimation of the reaction values acting on the bearings and an early structural analysis of the crankshaft in CATIA V5 was made. Using the "SKF Bearing Select" tool *[43]* to test the bearing types for a minimum of 500 hours of bearing life, which is the minimum required for aircraft engines according to Shigley´s *[44]*, showed that the angular contact ball bearings need a disproportional large inner diameter to withstand the reactions compared to the diameter needed for the crankshaft to withstand the same reactions which would cause the crankshaft to be far heavier unnecessarily. The tapered roller bearings thought need a considerable smaller inner diameter giving the possibility to use smaller bearings saving weight. Also, according to NSK *[42]*, tapered roller bearings are more rigid and suited for shock loads (transient loads of very high amplitude and short duration) which is exactly what occurs in piston engines.

Unless the crankshaft has a very large diameter, the best arrangement for bearings A and B seems to be two tapered roller bearings in a back-to-back mounting like the *Figure 3.6* as it gives a far better bearing life for shock loads, a smaller weight and possible to use if the crankshaft diameter is small. To secure the bearings, a backrest is designed in the crankshaft for the bearing A like the bearing in the right and a locking nut is used for the bearing B like the bearing in the left.

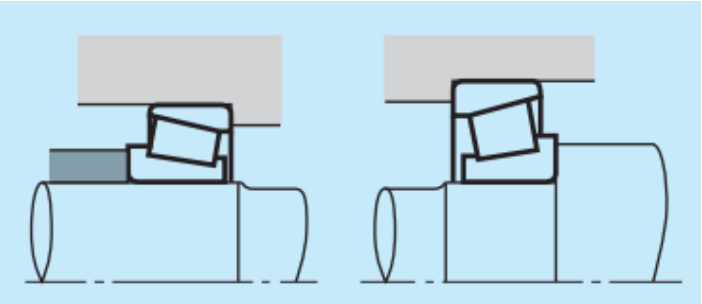

Figure 3.6 - Tapered bearings in a back-to-back mounting [42]

For bearing C, double-row angular contact ball bearings, double-row tapered roller bearings and spherical roller bearings are available.

To test which bearing types are better for the bearing C, the same procedure used to test the bearings A and B is applied. The results showed that the inner diameter of the angular contact ball bearings is too large for what the crankshaft possible requires. Again, the tapered roller bearings proved to have the better life for their size and weight but both spherical and tapered bearings have identical benefits including a rigid mounting and a good resistance to tilting moments, although tapered roller bearings are better suited for shock loads while spherical roller bearings have more permissible misalignment, both desired.

The position C diameter does not affect the analysis of the crankshaft or influences any other parameter or mechanical piece in the engine except the block that supports and fixes the bearing. It is only after designing the flying wheel in one side of the engine and in the other end, the output shaft to connect the propeller that the finished diameter of the position C can be optimized which means that both bearings type can be used since the position C can eventually be thicker and hollow or thinner and solid to meet the required inner diameter of the bearing. It terms of price, the double row tapered bearing price is not shown and for that reason cannot be compared to the spherical roller bearing price, but usually larger bearings have higher prices. So, for the execution of the present work, the double row tapered roller bearing was selected to be used in the position C.

For the position D, deep groove ball bearings and cylindrical roller bearings are available, both having an identical minimum inner diameter. The cylindrical roller bearing though presents far more benefits compared to the deep groove ball bearing making it more suitable for the engine:

- As the engine is axial and the combustion chamber is parallel and very close to the crankshaft´s centre and the position D, it is expected that the crankshaft expands and contracts slightly with the temperature variation and the cylindrical

roller bearings allows axial displacement in both directions if desired, acting as a free-end bearing.

- A cylindrical roller bearing provides a better rigidity to the crankshaft than a deep groove ball bearing as its rolling components have a larger contact area with its rings which is very useful as the biggest translational displacement of the crankshaft occurs in the region of the bearings B and D.
- Cylindrical roller bearings are better suited to deal with shock loads *[42]*.
- The cylindrical roller bearings are also easier to assemble and disassemble *[42]*.

Therefore, for the present engine, cylindrical roller bearings are more advantageous than deep groove ball bearings and it is that type which will be used in position D.

The bearing arrangement for the position C and D should be like shown in *Figure 3.7*, being in the left the double row tapered roller bearing as bearing C and, in the right, the cylindrical roller bearing as bearing D.

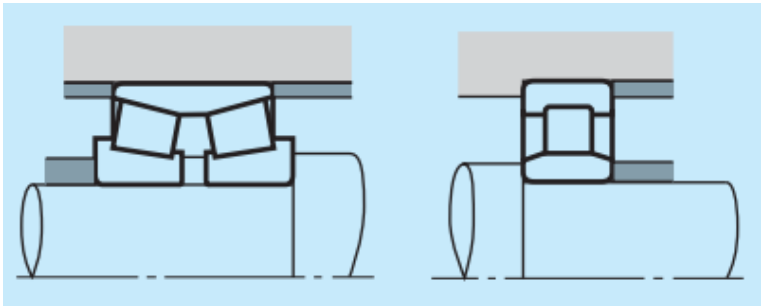

Figure 3.7 - Double row tapered roller bearing as fixed-end and cylindrical roller bearing as free-end [42]

The bearing C is secured to the crankshaft with a backrest on one side and a locking nut in the other like the *Figure 3.7*. The outer ring of the bearing D is free to move axially while to secure the inner ring to the crankshaft a backrest is used in one side and in the other, a retaining ring (circlip) or a spacer sleeve can be used *[45]*. By research, a spacer sleeve is wider than the retaining ring and thus means making a crankshaft longer and heavier and for that reason it is better to use instead a retaining ring “DIN 471” for shafts.

Because the outer ring of the bearing D can move freely in the x-direction, it does not carry any axial loads. It is for this reason that the x-component of the reaction at point D (R_{D_x}) is zero.

3.10. Crankshaft and Bearings Iteration

The following flowchart describes the procedure to select the bearings inner diameter together with the crankshaft sizing and how both affect each other to optimize the bearings placement and to save weight.

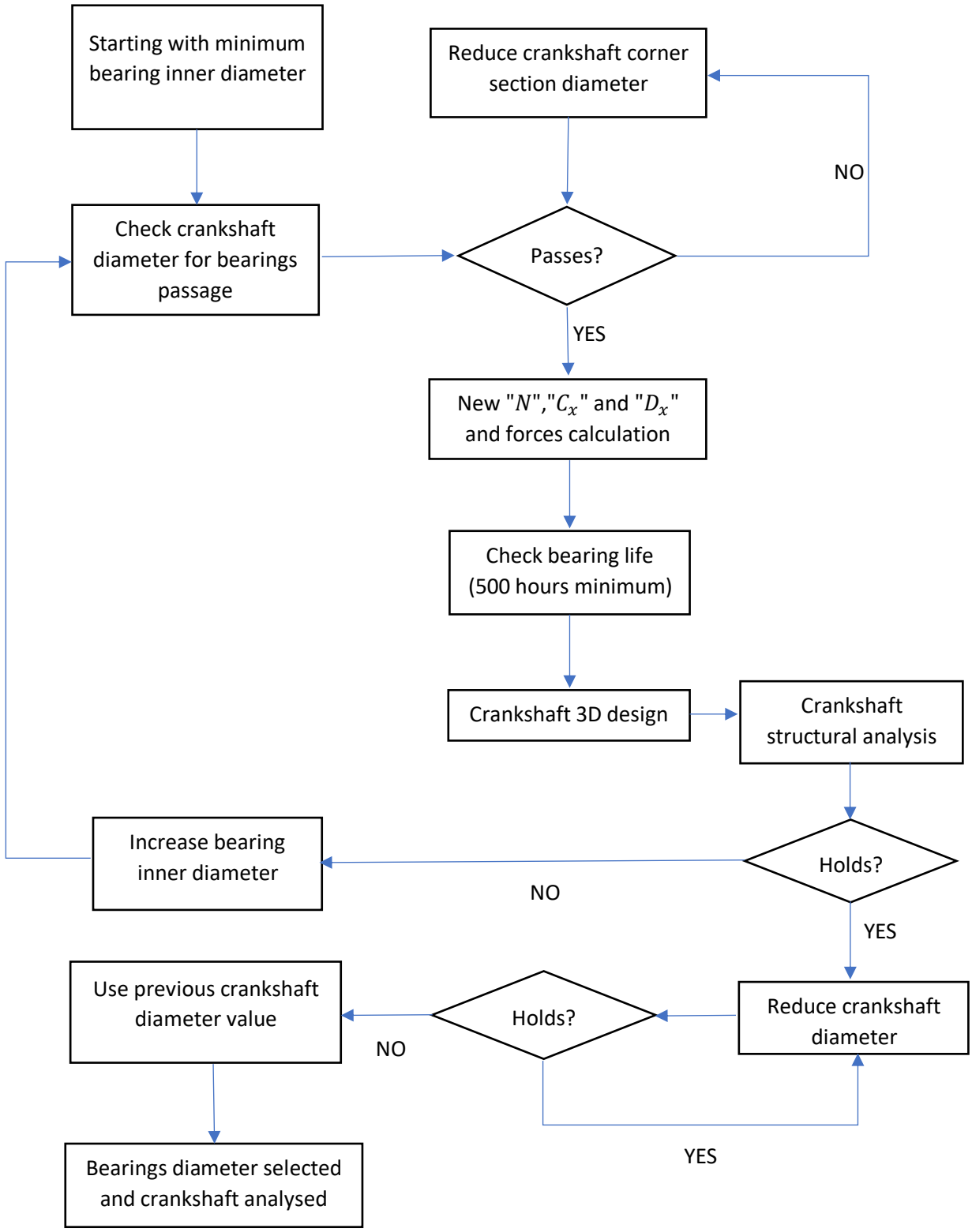

3.10.1. Bearings Passage

Due to the unique design of the crankshaft, the bearings placement is more complicated than usual. The bearings must be placed entering the middle end of the crankshaft halve and pass through the crankshaft corner through the positions of bearings B and D for bearing A, and bearing D for bearing B.

Conclusively, the bearings passage depends on the bearings and crankshaft specifications, more specifically on the inner diameter of the bearing and its width and on the diameter of the different zones of the crankshaft such as the crankshaft diameter where bearings B and D are placed and the crankshaft corner section diameter. Also, the crankshaft backrest of the bearing D can interfere with the bearings assembly depending on the minimum diameter required for the bearing model.

After defining the crankshaft specifications except its diameter along the different zones, a simulation in CATIA V5 is performed to successfully analyse the bearings passage path through the crankshaft. The simulation consists in the design in two dimensions of the crankshaft and the bearings A and B which are equal. Through tangency lines between the outer diameter of the crankshaft in its different zones and the inner diameter of the bearings, the path of each bearing is simulated, and it can be verified if the bearing passes thought or not without touching the outer walls of the crankshaft.

It is worth mentioning that because the CATIA V5 simulation is not perfectly accurate, the bearing width presented in the catalogue is used as a safety margin to not damage the bearings surface against the crankshaft in their passage through the corners section. The actual effective bearing width is slightly smaller, for assembly, than the catalogue bearing width because the bearings have filleted corners.

3.10.2. Bearing Positioning

Both bearings, A and B are placed at the exact same distance of point O to balance the engine. That distance is defined as N (*Figure 3.4*) and is the horizontal distance of the bearings in M (*Figure 3.3*).

The value N heavily influences the crankshaft structural analysis and the bearings life by changing the forces acting on those components, although the crankshaft output torque is not affected. Different values will be tested to provide the best results.

Because the main parameters of the crankshaft are already defined, the N value is primarily influenced by the bearings A and B model:

$$N = N_B = N_A = M - R_{arc_{A;C}} - D_{arc;nut} - L_{wall_A} - \frac{L_{brg_A}}{2} \qquad (3.28)$$

Where:

$R_{arc_{A;C}}$ is the radius of the corner of the crankshaft between the bearings A and C.

L_{wall_A} is the width of the crankshaft wall to support bearing A which is equal to that of the nut of the bearing B to maintain balance of the crankshaft.

L_{brg_A} is the width of the bearing A.

$D_{arc;nut}$ is the minimum distance necessary between the nut of bearing B and the corner of the crankshaft between the bearings B and D to allow the passage of the bearings A and B and its nut and can be found using the bearing passage simulation in CATIA V5.

Bearings C and D are placed the closest possible to point O, which represents the half crankshaft center. Because those bearings are meant to support the crankshaft to the engine block, the smaller the distance to one another, the smaller the crankshaft deflection but different values will be tested to verify this statement.

The minimum distance for the coordinates C_x and D_x is given by the following equations:

$$C_x = \overline{OC} = H + L_{wall_C} + \frac{L_{brg_C}}{2} + D_{arc_{A;C}} \qquad (3.29)$$

$$D_x = \overline{OD} = H + L_{wall_D} + \frac{L_{brg_D}}{2} + D_{arc_{B;D}} + D_{arc;wall\ D} \qquad (3.30)$$

Where:

L_{wall_C} is the width of the crankshaft wall to support bearing C.

L_{wall_D} is the width of the crankshaft wall to support bearing D.

L_{brg_C} is the width of the bearing C.

L_{brg_D} is the width of the bearing D.

$D_{arc;wall\ D}$ is the distance between the end of the corner of the crankshaft between the bearings B and D and the beginning of the backrest that secures the bearing D to the crankshaft axially which is only influenced by the minimum backrest height required by the supplier of bearing D. A taller backrest will result in a higher $D_{arc;wall\ D}$. If the

backrest is not high enough to influence the passage of bearings A and B, the optimum value should be zero.

$D_{arc_{A;C}}$ is the distance between the end of the corner of the crankshaft between the bearings A and C and the beginning of the crankshaft arm X.

$D_{arc_{B;D}}$ is the distance between the end of the corner of the crankshaft between the bearings B and D and the beginning of the crankshaft arm X.

The $D_{arc_{A;C}}$ is given for any angle of the crankshaft by the following equation:

$$D_{arc_{A;C}} = D_{arc_{B;D}} = \frac{sin\left(\frac{90-\gamma}{2}\right) \times R_{arc_{A;C}}}{sin\left(\frac{90+\gamma}{2}\right)} \quad (3.31)$$

Where:

$R_{arc_{A;C}}$ is the radius of the corner of the crankshaft between the bearings A and C.

$R_{arc_{B;D}}$ is the radius of the corner of the crankshaft between the bearings B and D.

The $R_{arc_{A;C}}$ is given for any angle and arm length of the crankshaft by the following equation:

$$R_{arc_{A;C}} = R_{arc_{B;D}} = \frac{X}{1 + \frac{sin\left(\frac{90-\gamma}{2}\right)}{sin\left(\frac{90+\gamma}{2}\right)}} \quad (3.32)$$

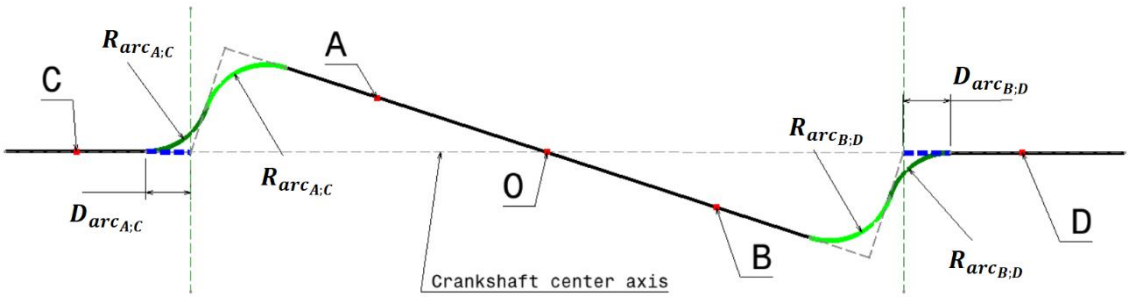

Figure 3.8 - Illustration of $D_{arc_{A;C}}$, $D_{arc_{B;D}}$, $R_{arc_{A;C}}$ and $R_{arc_{B;D}}$

3.10.3. Bearing life

One of the main requirements for the selection of a specific bearing for a certain application is the expected bearing life.

According to Shigley´s *[44]*, the expected bearing life for aircraft engines is between 500 and 2000 hours of operation.

To calculate the bearing life, the axial and radial loads applied on the bearings must be found. For bearings C and D, the loads are equal to the reactions acting on the point C and D, respectively. For bearings A and B however, the loads must be found using a rotation transformation matrix of the reactions acting on points A and B because the radial and axial loads of the bearings A and B are not in the same coordinate system of their reactions.

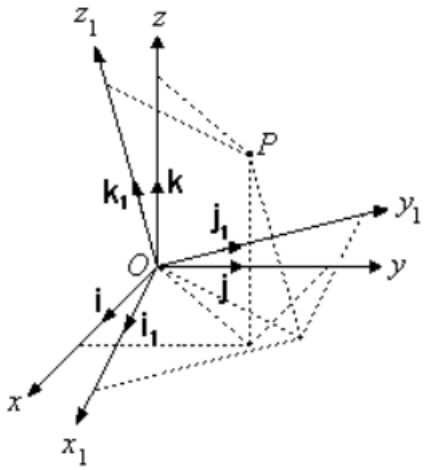

Figure 3.9 - Rotation transformation [46]

Points A and B reactions are represented in the coordinate system $Oxyz$ while the loads of the bearings A and B are represented in the coordinate system $Ox_1y_1z_1$. The rotation transformation matrix is given by the angles between the vectors of the different coordinate system:

$$\begin{bmatrix} \mathbf{i_1}.\mathbf{i} & \mathbf{j_1}.\mathbf{i} & \mathbf{k_1}.\mathbf{i} \\ \mathbf{i_1}.\mathbf{j} & \mathbf{j_1}.\mathbf{j} & \mathbf{k_1}.\mathbf{j} \\ \mathbf{i_1}.\mathbf{k} & \mathbf{j_1}.\mathbf{k} & \mathbf{k_1}.\mathbf{k} \end{bmatrix} = \begin{bmatrix} \gamma & 90+\beta & 90-\alpha \\ 90-\beta & \beta & 90 \\ 90+\alpha & 90 & \alpha \end{bmatrix}$$

Where, despite not represented in any figure, the alfa angle α is the angle of the third dimension and represents the rotation of the crankshaft in relation to the plane

Oxz and has a range of $[0;\gamma]$ degrees being zero at TDC. It can be obtained with the position of the point A defined further in this paper:

$$\alpha = tan^{-1}\left(\frac{V_A}{P_A}\, sin\,\Phi\right) \tag{3.59}$$

Consequently, the loads acting on the bearings A and B, R'_A and R'_B respectively are:

$$R'_A = \begin{cases} R'_{A_x} = cos\,\boldsymbol{i_1}.\boldsymbol{i} \times R_{A_x} + cos\,\boldsymbol{j_1}.\boldsymbol{i} \times R_{A_y} + cos\,\boldsymbol{k_1}.\boldsymbol{i} \times R_{A_z} \\ R'_{A_y} = cos\,\boldsymbol{i_1}.\boldsymbol{j} \times R_{A_x} + cos\,\boldsymbol{j_1}.\boldsymbol{j} \times R_{A_y} + cos\,\boldsymbol{k_1}.\boldsymbol{j} \times R_{A_z} \\ R'_{A_z} = cos\,\boldsymbol{i_1}.\boldsymbol{k} \times R_{A_x} + cos\,\boldsymbol{j_1}.\boldsymbol{k} \times R_{A_y} + cos\,\boldsymbol{k_1}.\boldsymbol{k} \times R_{A_z} \end{cases} \tag{3.60}$$

$$R'_B = \begin{cases} R'_{B_x} = cos\,\boldsymbol{i_1}.\boldsymbol{i} \times R_{B_x} + cos\,\boldsymbol{j_1}.\boldsymbol{i} \times R_{B_y} + cos\,\boldsymbol{k_1}.\boldsymbol{i} \times R_{B_z} \\ R'_{B_y} = cos\,\boldsymbol{i_1}.\boldsymbol{j} \times R_{B_x} + cos\,\boldsymbol{j_1}.\boldsymbol{j} \times R_{B_y} + cos\,\boldsymbol{k_1}.\boldsymbol{j} \times R_{B_z} \\ R'_{B_z} = cos\,\boldsymbol{i_1}.\boldsymbol{k} \times R_{B_x} + cos\,\boldsymbol{j_1}.\boldsymbol{k} \times R_{B_y} + cos\,\boldsymbol{k_1}.\boldsymbol{k} \times R_{B_z} \end{cases} \tag{3.61}$$

The resulted loads from the matrix are for the maximum forces carried by the bearings $F_{max_{brg}}$, however due to shock and vibration during the operation of the engine, it is advised to add a safety factor *[42]*. Due to this specific engine design, it is expected that vibrations are significantly less than in a conventional engine. A safety factor of 1.5 representing an operation with moderate vibration and shock loads seems reasonable.

$$F_{lf} = 1.5F_{max_{brg}} \tag{3.62}$$

As the loads on the bearings fluctuates during engine operation, an average load should be estimated to not overinflate the practical bearing life.

To find the exact value, the function of torque variation with the crankshaft angle like that of *Figure 3.10* must be obtained.

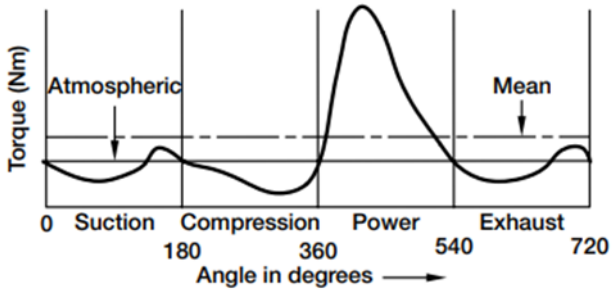

Figure 3.10 - Torque variation with crank angle due to gas pressure and inertia effects in a conventional engine [39]

In the present work, the function was not estimated, but an estimation for the average engine torque value can be found for the power stroke by assuming it like a sine wave, and so the average load in that phase is given by the following relation being "F_{max}" of *Figure 3.11* equal to $F_{max_{brg}}$ representing the reactions calculated above:

$$F_m = 0.65 F_{max_{brg}} \tag{3.63}$$

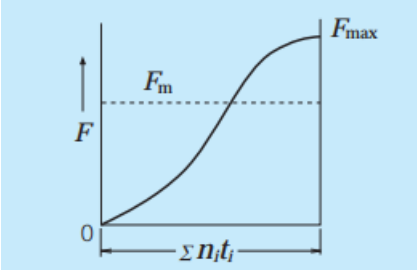

Figure 3.11 - Half sine wave for an eighth of revolution of engine operation [42]

Figure 3.10 only represents the torque variation for a single piston. Acknowledging the fact that this engine design has two pistons acting on the same bearings, results that in half of the engine operation two sine waves exist.

The other half of the engine operation is hard to estimate without the graph actual function of the torque variation despite being clear that the average load on this half is far inferior compared to that of the power phase. So, it is pessimistically assumed that the other half of the engine operation is equal to that of the power phases and that a minimum of 500 hours bearing life must be reached, the minimal value for aircraft engines *[44]*. The actual bearing life will, thus, significantly exceed the 500 hour minimum bearing life requirement.

Joining *Equations 3.62* and *3.63*, the actual force to calculate the bearings life is:

$$R^{''} = F_m F_{lf} = 0.975 F_{max_{brg}} \quad (3.64)$$

The bearing life calculation is a process dependent on different variables which also are dependent on the bearings model and type. That process is explained in detail in *[42]*, however a simpler way is provided by SKF, a bearing manufacturer, using a tool called "SKF Bearing Select" *[43]* that allows the calculation of the bearing life and other factors using only the forces acting on the bearing and the speed of operation to facilitate the selection process.

3.10.4. Crankshaft structural analysis

Once the bearings are chosen, the crankshaft 3D design is performed in CATIA V5 in the section "Mechanical Design", subsection "Part Design".

Next, to ensure the crankshaft integrity to the forces acting on it, a structural analysis simulation is made. Due to the crankshaft irregular geometry, the structural sizing equations were not derived like it is simply done for a conventional crankshaft. Instead, the engine crankshaft structural analysis is made in CATIA V5 in the section "Analysis & Simulation", subsection "Generative Structural Analysis".

The structural analysis provides the values necessary to ensure mechanical integrity and stiffness of the crankshaft.

The crankshaft is chosen to be made of annealed "AISI 4340" steel, a common material for crankshafts, with an ultimate tensile strength of $745MPa$ and a yield strength of $470MPa$ *[47] [48]*. Other structural properties of the material, and common for steels, necessary to the structural analysis in CATIA V5 are:

- Yield strength $\sigma_{4340} = 470MPa$
- Poisson´s ratio $\nu_{4340} = 0.29$
- Elastic modulus $E_{4340} = 2.0 \times 10^5 MPa$
- Density $\rho_{4340} = 7800kg/m^3$

Two main types of failures generally occur in a crankshaft: failure due to fatigue and failure due to plastic deformation. Failure due to fatigue is fracture due to the repeated application of many cycles of varying stress. According to Taylor *[49]*, no failures due to fatigue seem to occur in steels when stress is less than 48% of the ultimate tensile strength of the material.

Failure due to plastic deformation is when the stresses applied are larger than the yield strength of the material.

Adding a safety factor s_f of 2.5 to the yield strength of the crankshaft material is a reasonable value to not add to much unnecessary weight and is enough to protect the crankshaft from both types of failure.

Concluding the maximum stress in the crankshaft should be equal or less than:

$$\sigma_{max_{cranksahft}} \leq \frac{\sigma_{4340}}{s_f} \tag{3.65}$$

The allowable translational displacement or deflection of a shaft to measure its stiffness usually must be equal or lower than two ten thousandths the distance between the support bearings *[50]*:

$$\delta \leq 0.0002(C_x + D_x) \tag{3.66}$$

Being $D_x + C_x$ the distance between the bearings C and D which are the support bearings of the crankshaft.

The analysis consists of the reactions A and B where the bearings are placed acting on the crankshaft and restraints in the position C and D and in the middle face of the crankshaft. The position C and the middle face are restrained of all translations and rotations except rotation about the x-axis while position D allows translation and rotation about the x-axis.

3.11. Shaft Coupling

As mentioned above, the crankshaft is divided in half at the centre due to the need of a path to install the bearings in their proper placements to allow the connection of the crankshaft to the wobble plate. To reunite the crankshaft, a mechanism called shaft coupling is used.

Shaft coupling is a mechanical assembly, consisting of machine elements, used in the transmission of rotation movement between two shafts *[51]*. There are various types of shaft couplings, that allow two different collinear shafts to be connected to allow the transmission of torque to one another. The most common types of shaft couplings are attached through friction or through keys and some with both. Those categories subdivide themselves into more types with different characteristics to

adequately couple various types of shafts. In this case, a rigid shaft is required to not allow misalignment between both shafts.

The main parameters to select the coupling type is the length and the outer diameter of the coupling. The short distance available between the crankshaft and the cylinders to install the coupling meant that the coupling has a limited outer diameter to freely rotate with the crankshaft without crashing against the cylinders placed in both sides. A shorter coupling is desired to reduce the length of the crankshaft between the bearings D of both crankshaft halves, which in turn would also reduce the connecting rod and the cylinder length saving considerable weight in the engine and making it shorter.

Considering the parameters described above, a two-piece rigid shaft coupling is selected. This type of coupling is a two-piece metal cylinder revolving around both shafts and is screwed to one another preventing the rotation of the shafts independently through friction.

To dimension the shaft coupling, its assumed that one of the shafts is stationary while the other is rotating at maximum speed and at maximum torque.

The force that the screws must exert to create the friction necessary to transfer the torque of one crankshaft to the other is:

$$P_s = \frac{2T_{crankshaft}}{\pi\ \mu\ d_{coupling}} = p_{coupling} d_{coupling} L_{coupling} \qquad (3.67)$$

Where:

$T_{cranksahft}$ is the crankshaft torque in $N.mm$.

$d_{coupling}$ is the diameter of both shafts where the shaft coupling is installed in mm and the inner diameter of the coupling.

μ is the friction coefficient between the material of the shaft coupling and that of the shaft. Because both materials are steel, $\mu = 0.57$ *[52]*.

$p_{coupling}$ is the pressure acting on the projected area of the coupling in MPa.

$L_{coupling}$ is the length of the coupling in mm.

The number of screws necessary to withstand that force is:

$$n_{screw} = \frac{P_s}{P_p} \qquad (3.68)$$

Where P_p is the force of each screw given by:

$$P_p = S_p \, \sigma_{adm} \tag{3.69}$$

And σ_{adm} is the permissible tension of the screw which is usually approximately $98MPa$ *[53]* while S_p is the thread section area of the screw which varies depending on the screw size selected with d_{screw} being the thread internal diameter:

$$S_p = \frac{\pi {d_{screw}}^2}{4} \tag{3.70}$$

The shaft coupling needs to have a minimum length to function properly depending on the permissible maximum pressure p_{adm} of the material chosen:

$$L_{min} = \frac{P_s}{p_{adm} \, d_{coupling}} \tag{3.71}$$

The permissible maximum pressure of the steels normally used can vary between $65MPa$ up to $120MPa$ *[53]*. If the minimum length required is too large compared to the length necessary to accommodate the screws, a better steel can be selected to save weight.

The screws generally used are Allen screws to allow screwing from the top and an orienting distribution for the screws placement is shown in *[52]*, where the variable "d" of the *Figure 3.12* represents the diameter of the screw hole machined with drill.

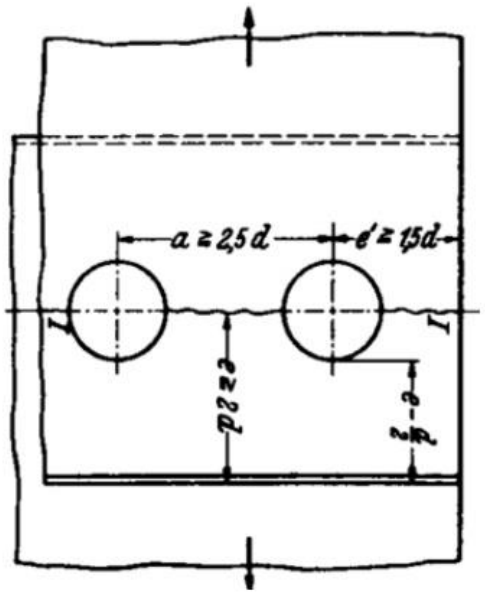

Figure 3.12 - Orienting distribution of a two-piece rigid shaft coupling [52]

3.12. Distribution System Mechanism

The distribution system is the mechanism of the engine responsible for gas exchange in and out of the cylinder.

In four stroke modern conventional engines, that system is driven by the crankshaft that connects to a set of gears which in turn drive the camshaft. The set of gears is designed such the gear connected to the crankshaft has half the diameter of the gear connected to the camshaft and thus, the camshaft rotates with half the speed of the crankshaft to actuate each valve once per every two revolutions of the crankshaft. Then, the lobe of the camshaft opens the valves in each rotation against a helical spring attached to the valves with the help of a valve retainer and a valve lock. When the lobe stops actuating on the valve due to the rotation of the camshaft, the helical spring forces the valve to close.

In most modern engines, the system is an overhead valve distribution system due to the valves being placed above the combustion chamber directly or slightly angled. This distribution system has some variations where the lobe is not in direct contact with the valve and instead actuates a rocker arm which in turn transfers the motion to the valve.

In L-Head engine thought, where the valves are placed aside the combustion chamber and are inverted compared to an overhead valve, usually a push rod must be placed between the rocker arm and the valve to clear the distance between the valve and the rocker arm. This distribution system is in disuse mainly because it leads to poor design of the combustion chamber, which causes a poor gas flow and low compression ratio and an inefficient combustion causing a low efficiency engine *[54]*. In the following figure, both distribution systems are illustrated in more detail with the nomenclature of the different mechanical pieces.

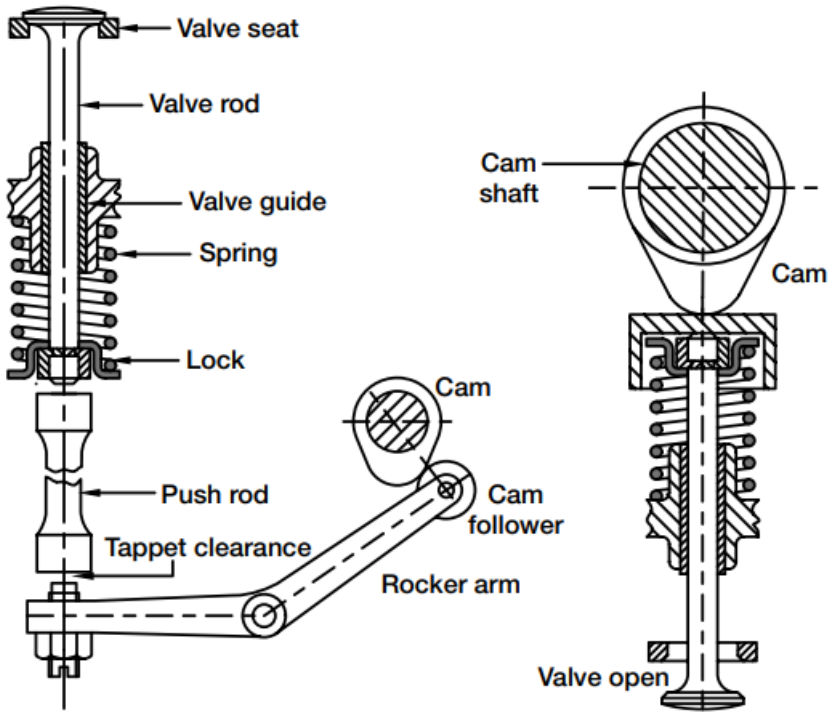

Figure 3.13 - In the left, a L-head distribution system and, in the right, an overhead valve distribution system [39]

Although not ideal, the lack of a cylinder head and the presence of two opposed pistons, mandates placing the valves of the present engine in a similar type to a L-head distribution system, despite being improved by opposing admission and exhaust valves, thus reducing the minimum volume of the combustion chamber. The chosen distribution system is thus a variation to the L-head distribution system type as it differs to the L-head distribution system presented in the *Figure 3.13* by not using a rocker arm or a lobe camshaft neither helical gears and any other mechanical pieces used to run that mechanism except the valves placed next to the combustion chamber together with the valves springs, retainers and valve locks.

Instead, a cylindrical groove cam is connected around the crankshaft through a parallel key where a cam follower translates inside the groove of the cam. The cam follower is connected to a follower, similar to a push rod, and with the rotation of the crankshaft which in turn rotates the cylindrical groove cam, the follower has a translation movement which presses the valve to open.

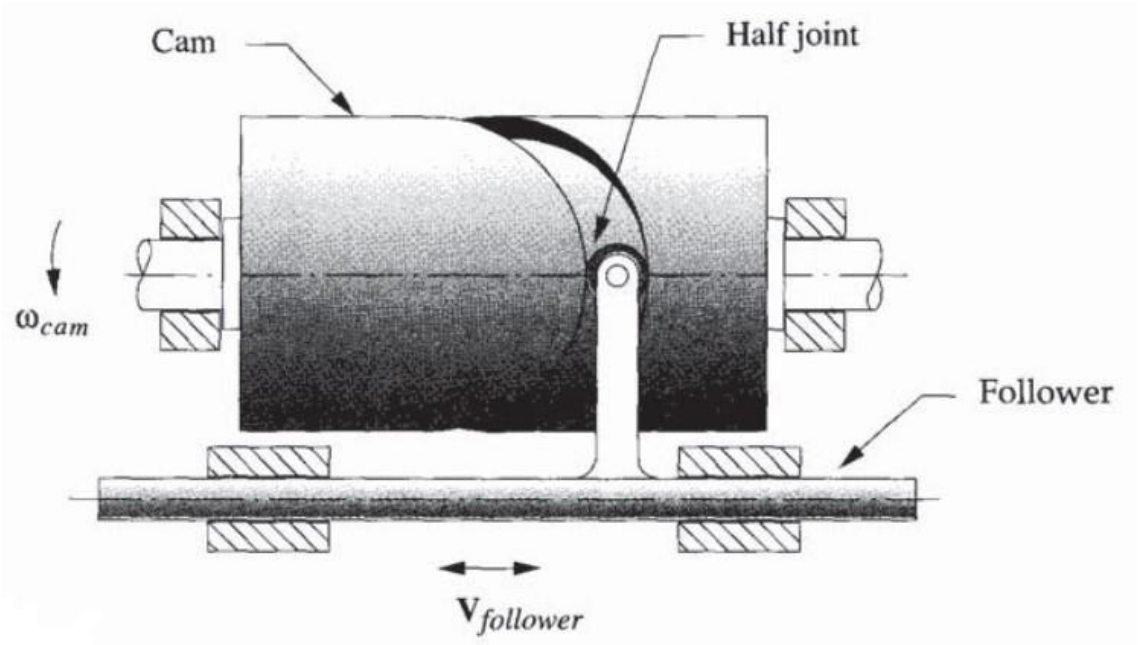

Figure 3.14 - Cylindrical/barrel groove cam with a translating follower [55]

The *Figure 3.14* of Robert L. Norton´s book *[55]* presents a very good visualization of the mechanism explained above however, there is a main difference in the mechanism for the present engine. The cylindrical/barrel cam groove of this engine is composed by two grooves that intersect each other similar to the groove of a self-reversing screw (*Figure 3.15*). Despite more complex, it is critical to be that way to create a mechanism where the follower only presses the valve once per two revolutions of the cylindrical groove cam and crankshaft to create the four-stroke engine distribution system.

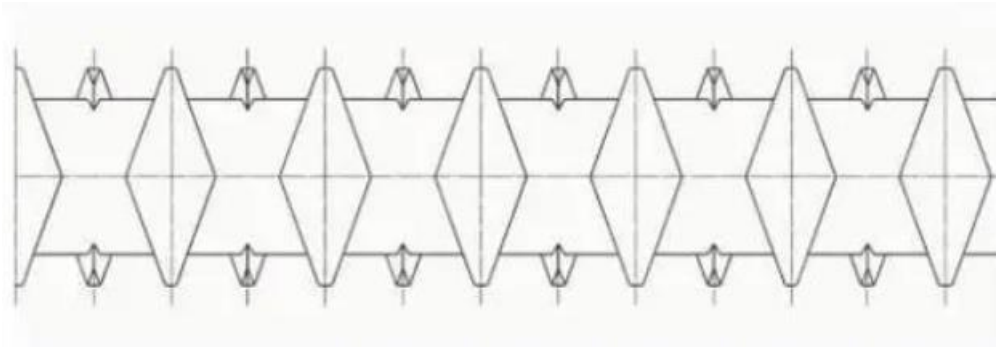

Figure 3.15 - Self reversing screw groove pattern [56]

3.12.1. Ports

The sizing of the distribution system begins by finding the flow rate of mixture needed to feed the engine and that of burnt gases of the exhaust. The mixture and burnt gases travel through the intake and exhaust ports where they enter and leave the combustion chamber when the intake and the exhaust valves open, respectively.

The flow rate necessary to feed any piston engine is directly proportional to its mean piston velocity and cylinder cross section area but because the present engine is an opposed piston engine, the volume of gas flow must be double:

$$Q_p = 2\left(v\frac{\pi}{4}{D_{piston}}^2\right) \tag{3.72}$$

Where:

D_{piston} is the piston bore in m.

v is the mean piston velocity in m/s given by:

$$v = \frac{2SN}{60} \tag{3.73}$$

Where:

N is the engine speed in rpm.

S is the engine stroke in m.

As said above, the gas necessary to feed the engine passes through the ports to enter or leave the combustion chamber when the valves are opened and thus it is the area of the ports and the gas velocity traveling through the ports that define the gas flow rate. The gas flow passing through the ports must be at least equal to the necessary gas flow to feed the engine. If the port area is too small, mixture/burnt gases choke the engine and the efficiency decreases.

$$Q_p = \frac{\pi}{4}v_g{d_p}^2 \tag{3.74}$$

Where:

v_g is the mean gas velocity in m/s.

d_p is the port diameter in m.

The mean gas velocity that travels through the ports vary accordingly with the speed of the engine with higher engine speeds have higher gas velocities and vice versa. For port sizing purposes, the value of maximum engine speed is the single necessary parameter.

Those values are found in Ajeet Singh´s book despite not properly scaled as they only get divided in low, medium, and high engine speeds without mentioning what range of speeds falls in each category *[39]*.

Using the examples provided in exercises in the rest of the book, it is concluded that the present engine maximum speed of $2500rpm$ should correspond between medium and high speed engine category, representing thus approximately an exhaust mean gas velocity of $70m/s$ and an intake mean gas velocity of $50m/s$.

In Giacosa *[30]*, high speed automobile engines have an intake mean gas velocity of approximately 65 to $75m/s$. So, it was decided to estimate the mean gas velocity of another engine for comparison.

As already mentioned, the sizing of the present engine has some of its parameters determined based on the "Volkswagen Type 3" engine. Knowing the specifications of that engine *[28] [57] [58]* and using the *Equations 3.72* and *3.74*, it is possible to estimate the mean gas velocity to which the "Type 3" is designed for, which is approximately $59.5m/s$ for the intake gas velocity and $74m/s$ for the exhaust gas velocity at $3800rpm$ which places the engine in the lower part of high speed engines in Ajeet Singh´s book. Taking that fact in consideration, it is decided to design the present engine in the medium scale gas velocity meaning that the value for the intake gas velocity is $42.5m/s$ while the exhaust gas velocity is $60m/s$.

Equating the *Equation 3.72* and *3.74*, the port diameter is given by:

$$d_p = \sqrt{\frac{2v}{v_g}} D_{piston} \tag{3.75}$$

It is worth noticing that the intake and the exhaust ports have different diameters due to the difference in mean gas velocities. Because the mean gas velocity is inversely proportional to the port diameter, the intake port diameter is larger than the exhaust port diameter as the mean gas velocity of the mixture is lower than the mean gas velocity of the burnt gases.

3.12.2. Valves and seats

Valve seats are one of the most important mechanical pieces in the valvetrain system as they work as sealing surfaces between the face of the valve and the inclined length of the seat when the valves are closed.

Valve seats are replaceable in aluminium cylinder heads, or cylinder blocks in case for the present engine, which means they are separable mechanical pieces *[59]*.

Using a correlation between the inclined length of the valve seat and the port diameter of about 0.085 *[39]*, the valve seat width is given by:

$$w = 0.085 d_p \cos \alpha \tag{3.76}$$

Where:

α is the inclined angle of the valve seat, the same as the valve face angle which is usually $45º$ degrees *[39]*.

The valve seat width calculated is the width to perfectly seal the passage with the valve. A significantly margin is always given to the seat to provide thickness so the seat can be placed in the cylinder head/cylinder block. The inner diameter of the valve seat is the port diameter of each valve.

The valves are a crucial part of the valvetrain mechanism as they are the components that directly control the entrance and the exit of gas in and out the cylinder. The most common and simplistic valvetrain designs use poppet valves (*Figure 3.16*) placed at the end of the port. When opened the mixture/burnt gases are free to flow in and out of the cylinder.

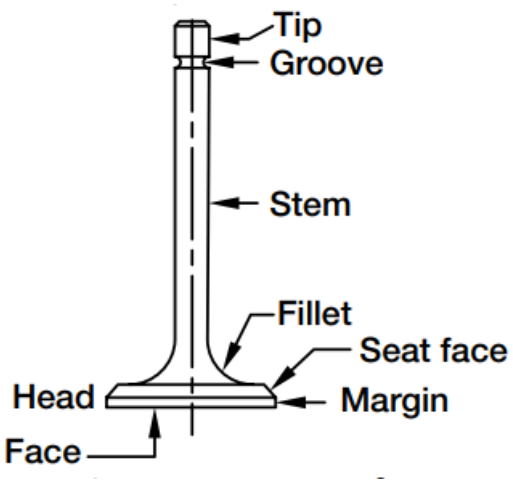

Figure 3.16 - Poppet valve [39]

Among the parameters of a valve, the most important ones are its valve head diameter and its seat face angle. The seat face angle must be equal to the inclined angle of the valve seat with only a slight interference angle of one degree to create a leak proof joint *[39] [59]*. The valve head diameter depends on the port diameter and the seat width and so it is different for the exhaust and the intake valves:

$$d_{iv} = d_{ip} + 2w_i \tag{3.77}$$

$$d_{ev} = d_{ep} + 2w_e \tag{3.78}$$

Where:

d_{iv} is the head diameter of the intake valve in mm.

d_{ev} is the head diameter of the exhaust valve in mm.

d_{ip} is the inlet port diameter in mm.

d_{ep} is the exhaust port diameter in mm.

w_i is the seat width of the intake valve in mm.

w_e is the seat width of the exhaust valve in mm.

Due to complex manufacturing design and cost, valves already manufactured for other engines are used for the present engine instead of designing new ones. Probably is not possible to find the exact size for the valve diameters of the exhaust and intake valves using the parameters calculated above but because some of those values used to find the diameters are arbitrated and not exact requirements, such as the inlet and exhaust gas velocities values, a valve diameter margin exists giving room to choose valves and corresponding seats of approximate size instead of precise diameter.

3.12.3. Valves Lift

The maximum valve lift is the valve total translation necessary to equalize the flow rate that travels thought the port (*Equation 3.74*) and the flow rate that passes through the valves.

$$Q_v = Q_p = \frac{\pi}{4} v_g {d_p}^2 \tag{3.79}$$

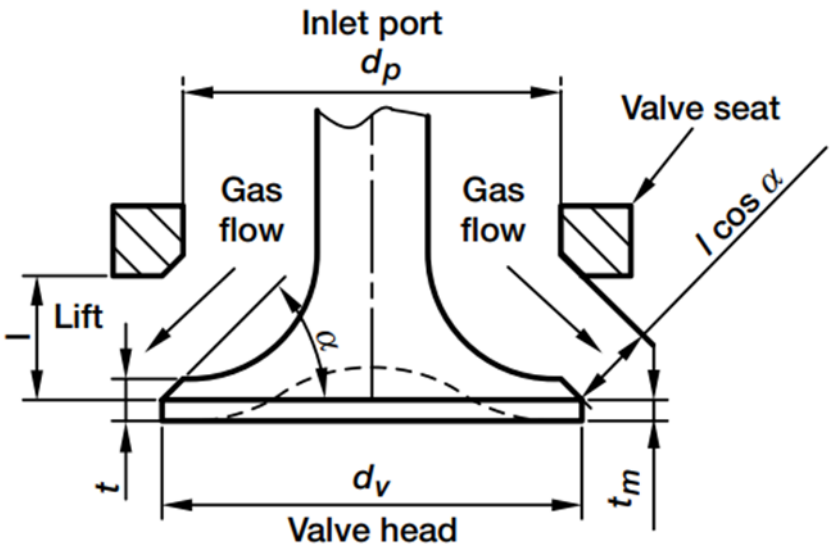

Figure 3.17 - Valve lift [39]

Also, the flow travels thought the valves with an area of the periphery of the port diameter and the inclined opening of the valve:

$$Q_v = \pi d_p v_{g_v} l \cos \alpha \tag{3.80}$$

Where:

l is the valve lift in mm.

v_{g_v} is the gas velocity through the valves in m/s.

By assuming a gas velocity through the valves equal to the gas velocity through the ports, the area that the flow passes through the valves must be equal to the area that the flow passes through the ports:

$$\frac{\pi}{4} {d_p}^2 = \pi d_p l \cos \alpha \tag{3.81}$$

And so, the maximum lift is given by:

$$l = \frac{d_p}{4 \cos \alpha} \tag{3.82}$$

As *Equation 3.82* shows, the maximum lift depends mainly on the port diameter and because the port diameter is significantly different for the intake and exhaust valves, so is the respective valve lift.

3.12.4. Valve Spring

Springs are elastic members that exert forces, or torques and absorb energy, which is usually stored and later released *[47]*. In an engine, the valve spring is used to keep the valve closed against its seat with the help of a valve lock and a valve retainer. Those pieces lock the valve and the spring together. When the spring is compressed, usually by a push rod and rocker actuated by a cam or directly by a cam, the valve is forced to open.

After an extensive search for multiple valve springs, none could fit perfectly to the specifications of the present engine. Most of the valve springs have the seat pressure to high and the maximum lift does not match that required for the present engine. The variables like the two mentioned above, the stiffness or the spring index create many combinations possible. For those reasons the best procedure is to design a valve spring specifically to the present engine.

To design the spring, the force that the spring must exert in the valve to properly close must be identified. That force must counter the inertia of the total mass of the valvetrain components that translate together with the valve and the spring when activated and must provide the valve with the acceleration of the push rod to maintain the valve in constant contact with the push rod during the valve closing motion *[30]*.

In the present engine design, the components that translate with the valve are the spring, the valve spring retainer and the two valve locks. It is worth noticing that only half the mass of the valve spring is considered to contribute to the inertial force of the valvetrain.

The cylindrical cam groove that forces the pushrod to translate and subsequently the valvetrain components is designed with a simple harmonic motion profile. The maximum acceleration of a simple harmonic motion is given by:

$$a = 0.5 l \omega^2 \qquad (3.83)$$

Where:

l is the maximum lift in mm.

ω is the angular velocity given by:

$$\omega = \frac{2\pi}{t} \tag{3.84}$$

Where:

t is the opening valve time in seconds.

In a four-stroke engine where the valve is actuated once in a two-revolution period and considering that the valve opens during half the duration of the translation and closes during the other half, the opening valve time is given by:

$$t = \left(\frac{120}{N}\right)\left(\frac{0.5\lambda}{360}\right) = \frac{\lambda}{6N} \tag{3.85}$$

Where:

λ is the duration of the valve opening which is $230º$ degrees for the intake valve and $235º$ degrees for the exhaust valve *[39]*.

N is the engine speed in revolutions per minute.

Thus, the inertia force due to acceleration of the mass of the valvetrain components is given by:

$$F_a = 0.5l\left(\frac{12\pi N}{\lambda}\right)^2 m \tag{3.86}$$

Where:

m is the mass of all components that translate with the valve including half of the mass of the valve spring.

$$m = m_{valve} + m_{retainer} + 2m_{lock} + \frac{1}{2}m_{spring} \tag{3.87}$$

Where, as already mentioned above:

m_{valve} is the mass of the valve, usually the intake valve because its larger and so slightly heavier.

$m_{retainer}$ is the mass of the valve retainer.

m_{lock} is the mass of the valve lock.

m_{spring} is the mass of the spring given by:

$$m_{spring} = \frac{\pi^2}{4} d^2 D N \rho \tag{3.88}$$

Where:

d is the wire diameter of the spring in mm.

D is the mean coil diameter of the spring in mm.

N is the total number of turns of the spring.

ρ is the density of the material spring in kg/mm^3.

Because the mass of the spring is only known after designing it, and it can only be designed knowing the inertia force, an initial reasonable value for the spring mass is guessed between $0.02kg$ and $0.05kg$.

Although very low and thus not very influential, the values for the masses of the valve retainer and the valve lock used for calculation purposes are an average estimation using historic values. The mass of the valve is far more important due to its greater value, and an average value can be found through *[60]*:

$$m_{valve} = 0.130kg$$

$$m_{lock} = 0.002kg$$

$$m_{retainer} = 0.015kg$$

Adding a recommended safety factor of 1.5 *[30]* to prevent valve float, the maximum force that the valve spring as to exert is:

$$F_{max_{spring}} = 1.5F_a \tag{3.89}$$

The maximum force will be exerted when the valve is compressed at his maximum lift which is the intake valve lift.

Having only these two parameters to design the valve spring, the next procedure is to attribute a reasonable value to the spring index and the stiffness that minimizes the spring mass to be able to calculate other parameters needed to successfully dimension the spring. Also, a proper spring wire material must be chosen.

The spring index measures the coil curvature and is given by the ratio between the mean coil diameter of the spring and its wire diameter usually having a value between 6 and 12 *[39]*.

$$C = \frac{D}{d} \tag{3.90}$$

The spring stiffness or spring rate is the force needed to compress the spring one millimetre. For engine valve springs, the preferred value for the spring stiffness ranges from 10.9 to $49 N/mm$ *[30]*.

Aircraft engine valve springs are mainly manufactured with chrome vanadium spring steel which are alloy spring steels used for high fatigue resistance, long endurance and suitable for shock and impact loads at high temperatures. All-important properties desired for an engine valve spring. Among the many chrome vanadium spring steels, the "ASTM 232" or "AISI 6150" seem the best reasonable choice mainly due to its constant mention as a suitable material for engine valve springs *[37] [44] [47]*.

An engine valve spring usually is designed for infinite life as it must sustain millions of cycles of operation without failure. Because of that reason, its fatigue strength is extremely important, however the mechanical properties that determine its fatigue strength vary with the diameter of the wire.

An infinite-life fatigue diagram for engine valve spring wires with a maximum of $5mm$ diameter presented in *[47]* gives the maximum shear stress for infinite life for carbon or alloy steels using the maximum and the minimum forces acting on the spring.

The minimum force or the seat pressure of the spring is given by:

$$F_{min_{spring}} = F_{max_{spring}} - k\delta \tag{3.91}$$

Where:

k is the spring stiffness in N/mm.

δ is the maximum deflection which is the valve lift in mm.

According to that diagram, the "ASTM A232" carbon steel maximum shear stress allowed with shot peening treatment is approximately:

$$\tau_{spring} = 770 MPa$$

While the modulus of rigidity is:

$$G_{spring} = 77200MPa$$

The density material is common to steels:

$$\rho_{spring} = 7.85 \times 10^{-6} kg/mm^3$$

Without shot peening treatment the maximum shear stress is significantly lower which makes the spring too heavy and too wide. Since half the mass of the spring contributes to the inertia force, a light spring is desired.

All the variables to dimension the main parameters of a spring are known. The wire diameter of the spring is given by:

$$d = \sqrt{\frac{8KF_{max_{spring}}C}{\pi\tau_{spring}}} \tag{3.92}$$

Where:

K is the Wahl´s correction factor given by *[39]*:

$$K = \frac{4C-1}{4C+4} + \frac{0.615}{C} \tag{3.93}$$

Knowing the wire diameter, the dimension of the mean coil diameter through the spring index (*Equation 3.90*) as well as the outer and inner diameter of the spring which are needed to size the valve spring retainer are:

$$D_O = D + d \tag{3.94}$$

$$D_I = D - d \tag{3.95}$$

Where:

D_O is the outer diameter of the spring in mm.

D_I is the inner diameter of the spring in mm.

The active number of turns represents the turns that twist under load and deflect:

$$N = \frac{G_{spring} d^4}{8D^3 k} \tag{3.96}$$

Engine valves are designed with squared and ground ends and thus the total number of turns are:

$$N_t = N + 2 \tag{3.97}$$

The main parameters of the spring are dimensioned, allowing now to calculate it´s different lengths. The solid length where the spring is full compressed, or coil bonded is given by:

$$L_s = N_t d \tag{3.98}$$

The maximum valve lift length is where the spring is compressed with the maximum force of operation. This length is the solid length plus a safety margin for clash allowance to avoid coil binding.

Spring solid or coil binding is the phenomenon where the spring reaches its solid length where it can´t be compressed any further. If compressed when already in its solid length, the valve spring develops an almost infinite load on the valvetrain components. This leads to the weakest component to fail and break or possibly worse, the entire valvetrain system collapse. To avoid this, a 10% deflection allowance of the maximum working deflection is advised meaning that when the valve spring reaches the maximum lift to which is designed, there is a gap where the valve spring can still be compressed beyond maximum lift *[39]*.

$$L_{max\ lift} = L_s + \frac{0.1 F_{max_{spring}}}{k} \tag{3.99}$$

The installation length is where the spring is compressed with a force called minimum force or seat pressure and then fixed to the valve:

$$L_I = L_{max\ lift} + \delta \tag{3.100}$$

The total length or the free length of a spring is where there are no forces applied on the spring and its fully decompressed:

$$L_F = L_I + \frac{F_{min_{spring}}}{k} \tag{3.101}$$

The natural frequency is a very important parameter of a spring. As the name suggest, it measures the frequency of the motion of the spring. If not high enough, generally at least thirteen times higher than the external cyclic forces which in an engine is the rotation speed of the cam, the deflections caused by the phenomenon called spring surge can lead to the failure of the spring.

Spring surge happens when the spring is rapidly compressed and then suddenly released too fast and too often. The coils are pushed against each other before having time to share the displacement causing them to touch. When the valve is suddenly released, the disturbance is reflected backwards until it is dissipated. This can cause effects like spring solid and can cause valve float due to the bouncing of the spring. This problem is more likely to happen at higher engine speeds. Thus, the natural frequency of the spring is a parameter to measure the maximum speed of an engine for the certain spring. The higher the natural frequency, the better it is to avoid spring surge.

The minimum natural frequency of the valve spring in Hertz for the maximum speed rotation of the present engine is:

$$f_{n_{minimum}} = 13\frac{N}{2}/60 \tag{3.102}$$

The actual natural frequency for steel springs in Hertz using millimetres is given by:

$$f_n = \frac{353000d}{ND^2} \tag{3.103}$$

After all the process explained above, the real mass spring is calculated to give the true inertia force. Then the stiffness and the spring index is re-estimated which changes the spring mass again. The process is repeated until the spring mass does not change.

3.12.5. Valve Locks and Valve Retainers

The valve lock and valve retainer are the intermediate pieces that lock the spring and the valve. They reciprocate together directly influencing the design and mass of the spring, a key piece of the distribution system. Their influence is small though due to their lower mass. The present design of these two parts does not have in context their structural analysis, instead they are only made for functional purposes to fit the valve

and spring for the assembly and simulation of the engine using existent parts as examples. The valve lock only depends on the valve itself and influences the retainer. Because the valves are purchased, the most obvious choice is to purchase the valve locks that fit with the same valves. If not purchased, the design of the valve locks will have into account their inner diameter which must be equal to the valve´s stem diameter and the groove design existing in the stem which must be the same.

The retainer is dependent on the spring design and the valve lock. As the spring is designed specifically for the present engine, the valve retainer also must be specifically designed to secure the spring to the selected valves. The retainer is accurately sized to have the outer and the inner diameter of the spring wire as its outer and middle diameter, respectively. The inner surface of the retainer coincides with the angled valve lock outer wall. All other details of the design like thickness of the various parts of the retainer are designed approximately to existent retainers because no structural analysis was performed for this part and so, must be verified for integrity after the procurement of the parts and the manufacturing of the spring. It is worth noticing that the cylinder block has clearance to increase and decrease the support of the spring if needed. As the inertia force of this engine is small, a carbon steel “1020” coated for corrosion resistance is suitable.

3.12.6. Cylindrical Groove Cam

An explanation of the cylindrical groove cam design and its objective has already been given in the beginning of the Section *3.12*. The most important part of the cylindrical groove cam is the cam groove profile. It is the part that differentiates this cam design from others and is crucial for the present engine design.

3.12.6.1. Cam Groove Profile

The cam groove profile can be divided into four sections: the lift section, the crossing section, the deceleration section, and the static section.

The lift section is the section where the valves will be forced to open and close. This section is designed following a simple harmonic motion (*Figure 3.18*) and the steps described to draw it are the following *[39]*:

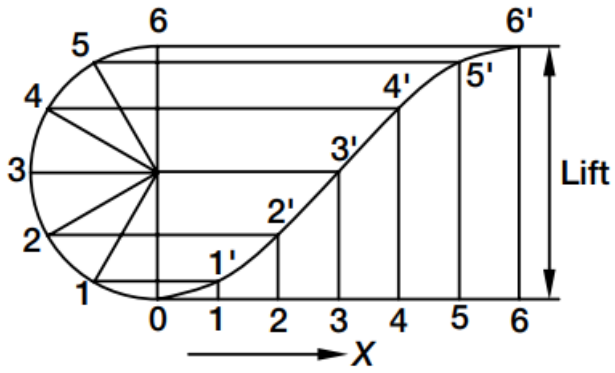

Figure 3.18 - Lift diagram following a simple harmonic motion [39]

1. Draw a horizontal line 0-6 as degrees of rise period to a suitable scale.
2. Divide the base line 0-6 in six equal part and number them as 1, 2, … 6.
3. Draw vertical line 6-6´ equal to lift.
4. Draw lines on right side of vertical line 0-6 at points 1, 2, … 5.
5. Draw line 0-6 at left point 0 of the base line.
6. Draw a semicircle with diameter 0-6.
7. Divide the semicircle at intervals of 30º.
8. Draw radial lines to cut the semicircle from its center at points 1, 2, … 5.
9. Draw horizontal lines from 1, 2, … 5 to cut the vertical lines on RHS of line 0-6.
10. Mark the intersections as 1´, 2´, … 5´.
11. Join these points 1´, 2´, … 5´ by a smooth curve.

The static section is the section where the cam follower does not translate and instead only rotates inside the groove.

The deceleration section, between the crossing section and the lift section, is a small static section required to decelerate the cam follower which in turn decelerate the follower before forcing the valve to open to not damage it with a shock load.

The crossing section is the section where the cam groove intersects itself. Due to the intersection, the groove must be distanced at the minimum of the cam follower diameter, so the groove of the deceleration section and the static section do not touch.

The cam curvature profile is especially important in this section because its value is the smallest here. According to *[61]*, a minimum radius of curvature of 3 to 5 times the radius of the cam follower should be implemented so that the cam follower does not jam.

The radius of curvature of the cam groove profile directly affects the dimensions of the cylindrical groove cam design. A greater radius of curvature means a greater outside

perimeter of the cylindrical cam and a greater length of the cam groove profile. This means that the distance the follower must travel increases but because the cam angular speed, being the same as the crankshaft, does not change, the rotation speed of the follower will increase, and a faster cam follower is more likely to jam.

However, a greater radius of curvature also means a smaller pitch angle of the cylindrical groove cam which means greater smoothness of the curvature of the cam groove profile because the cam follower has more distance to travel which makes it less likely to jam.

To choose the best curvature of the cam groove profile, different values must be simulated, and a more detailed theoretical analysis in hand. McGraw-Hill´s book *[61]*, presents detailed study and theoretical analysis of various cams and their designs including cylindrical groove cams but for the present work, a minimum curvature radius of 4 times the radius of the cam follower is selected.

3.12.6.2. Cam Follower

The largest forces that the cam follower must be capable of withstand are the combination of the spring compressed at maximum lift together with the gas flow pressure acting on the exhaust valve when fully opened:

$$F_{ls_{camfollower}} = F_g + F_{max_{spring}} \tag{3.104}$$

During the exhaust stroke, the gas pressure inside the combustion chamber is higher than the atmospheric pressure outside. This gas pressure creates a flow outward acting against the exhaust valve opening trying to close it. It is the cam follower that must be strong enough to counter act that pressure and allow the valve to be kept open.

$$F_g = \frac{\pi}{4} p_g {d_{ev}}^2 \tag{3.105}$$

Where:

d_{ev} is the exhaust valve diameter in mm.

p_g is the pressure variation between the maximum gas pressure inside the combustion chamber during the exhaust stroke and the ambient pressure outside the combustion chamber and according to Giacosa *[30]*, the average value is approximately $4kg/cm^2$ or approximately $0.4MPa$.

The cam follower also must withstand an acceleration force during the crossing section applied by the groove cam while during the static section no forces are applied on the cam follower.

$$F_{cs_{camfollower}} = m_{camfollower} \frac{{v_{camfollower}}^2}{r_{cs}} \tag{3.106}$$

Where:

$m_{camfollower}$ is the mass of the cam follower plus the follower assembly, arm follower and roller in kg.

r_{cs} is the radius of the maximum curvature of the crossing section in meters which also is the maximum curvature of the entire cam profile and, as mentioned, is 4 times the radius of the cam follower.

$v_{camfollower}$ is the cam follower velocity in m/s:

$$\begin{aligned} v_{camfollower} &= \frac{P_{camfollower}}{1000} \frac{{l_{groove}}/{2}}{\overline{P_{camfollower}}} \times rpm_{max_{crankshaft}} \\ &= \frac{{l_{groove}}/{2}\, rpm_{max_{crankshaft}}}{6 \times 10^4} \end{aligned} \tag{3.107}$$

Where:

l_{groove} is the full length of the cylindrical cam groove profile in mm which corresponds to two revolutions of the crankshaft and its exact value can be found through the CATIA V5 sketch. For one revolution the value must be divided in half.

$rpm_{max_{crankshaft}}$ is the maximum rotational speed of the crankshaft which has been set to be $2500rpm$.

$P_{camfollower}$ is the perimeter of the cam follower in mm:

$$P_{camfollower} = \pi d_{camfollower} \tag{3.108}$$

Where:

$d_{camfollower}$ is the diameter of the cam follower in mm.

Two main parameters are necessary to choose the correct cam follower: the maximum speed of the cam follower and its bearing life of 500 hours minimum.

The maximum speed of the cam follower is given by the manufacturer *[62]* while the bearing life calculation process is explained in *[63]*.

Equally to bearings A, B, C and D, the cam follower does not support the maximum force through the entire engine operation time and if so considered, the actual cam follower life will be greatly inflated. For that reason, the average load must be found using the following equation found in *[63]*:

$$F_{m_{camfollower}} = \sqrt[\frac{10}{3}]{\frac{t_{ls}{F_{ls}}_{camfollower}^{\frac{10}{3}} + t_{cs}{F_{cs}}_{camfollower}^{\frac{10}{3}} + t_{ss}{F_{ss}}_{camfollower}^{\frac{10}{3}}}{t_{ls} + t_{cs} + t_{ss}}} \quad (3.109)$$

Where:

${F_{ss}}_{camfollower}$ is the force acting on the cam follower during the static section and the deceleration section which is zero.

t_{ls} is the time fraction of the duration of the lift section.

t_{cs} is the time fraction of the duration of the crossing section.

t_{ss} is the time fraction of the duration of the static section and the deceleration section.

The nominal life of the cam follower in revolutions is given by *[63]*:

$$L_{10_{camfollower}} = \left(\frac{1}{f_w} \times \frac{C}{F_{m_{camfollower}}}\right)^{\frac{10}{3}} \times 10^6 \quad (3.110)$$

Where:

f_w is the load factor to account for vibrations and shocks and can be assumed to be 1.5.

C is the basic dynamic load which is given by the manufacturer.

The service bearing life in hours for a linear motion of the cam follower is given by:

$$L_{h_{camfollower}} = \frac{P_{camfollower} L_{10_{camfollower}}}{2\,{}^{l_{groove}}/_{2}\, rpm_{camfollower} 60}$$
$$= \frac{{P_{camfollower}}^{2} L_{10_{camfollower}}}{3.6 \times 10^{6} l_{groove} v_{camfollower}} \quad (3.111)$$

Where:

$rpm_{camfollower}$ is the cam follower velocity in rpm:

$$rpm_{camfollower} = 60 \frac{1000 v_{camfollower}}{P_{camfollower}} \quad (3.112)$$

3.12.6.3. Cylindrical Groove Cam Key

Keys are used on shafts to secure rotating elements and to enable the transmission of torque from the shaft to the shaft-supported element *[44]*. To connect the cylindrical groove cam to the crankshaft, a parallel key is a simple and easy key to install. This type of key (*Figure 3.19*) usually has the same depth in the shaft as in the hub and its width is equal to its height. A common material for this type of key is the "AISI 1060" with a yield strength of $370MPa$ *[44]*.

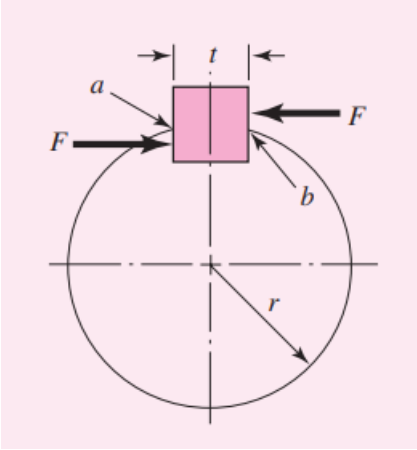

Figure 3.19 - Parallel key sizing [44]

The force acting on the surface of the crankshaft is:

$$F_{key} = \frac{T_{crankshaft}}{r_{crankshaft}} \quad (3.113)$$

Where:

$r_{crankshaft}$ is the radius of the crankshaft in mm where the cylindrical groove cam is placed.

The force F_{key} creates a shear stress in the key across the area "ab". Adding a safety factor f of 2.5, the maximum shear stress that the key can withstand for a certain force F_{key} is:

$$\frac{\tau_{key}}{f} = \frac{F_{key}}{t_{key} L_{key}} \tag{3.114}$$

Where:

t_{key} is the width of the key in mm.

L_{key} is the length of the key in mm which must be smaller than the length of the cylindrical groove cam for milling purposes.

By the distortion-energy theory *[44]*, the shear strength of the material can be given by the yield strength:

$$\tau_{key} = 0.577 \sigma_{key} \tag{3.115}$$

To resist crushing, one half the face of the key is used:

$$\frac{\sigma_{key}}{f} = \frac{F_{key}}{\frac{t_{key} L_{key}}{2}} \tag{3.116}$$

Whatever width of the key t_{key} is larger between the *Equations 3.114* and *3.116*, is the width necessary to resist the force applied on the key.

There are various sizes and predesigned keys that can be purchased. It is a matter of choosing a suitable width and find the necessary length.

3.12.7. Follower, Arm follower and Roller

As already mentioned, to press the valve due to the translational movement of the cam follower in the cylindrical groove cam, a follower is required similar to the one in *Figure 3.14*. The follower translates in a built-in part of the cylinder right above the valves. In this way, the follower can translate to press the valve to open. To connect the follower to the cam follower moved by the cam groove, an arm follower is designed to connect both parts. Because the cam follower is hanging and not fixed to any part except the follower, its weight pushes him down because the follower can rotate in its own axis. To prevent this, a roller is attached in the arm follower and secured to the built-in part of the cylinder. This solution stops completely the rotation of the follower and the fall of the cam follower.

In the present work, these parts are not structurally sized only being designed to simulate the engine mechanisms in CATIA V5.

3.13. Cylinder and Combustion Chamber

The present engine cylinder is different from a conventional engine for two main design features. The first is the combustion chamber design as a L-head/side valve due to the impossibility to add a cylinder head as the pistons are opposed to one another. The second change is that the combustion chamber is a single mechanical part, so it won´t be divided like in a conventional engine where the cylinder head is screwed to the engine block and a head gasket is put in between to seal the joint. According to Richard Stone *[6]*, this design has some advantageous like avoiding gasket failure and improving thermal conductivity.

Instead, to be able to open the combustion chamber for maintenance of its parts like valves and valve seats, the intake port and valve support is the separable part, and it connects to the flat zone of the combustion chamber like a nut. When required, the nut can be unscrewed with the entire intake valve assembly (intake valve, seat, spring, retainer, seal, guide, and both locks). Once disassembled of the cylinder, the exhaust valve spring on the opposite side can be loosed freeing the exhaust valve and its seat. With this procedure, all the components of the valves and cylinder can be reached for maintenance or replacement. This is an alternative to the head gasket that probably would not support the high temperatures of the combustion chamber and would need a solid connection of two cylinder halves thus heavier than the present solution.

The piece that holds the follower, arm follower and roller necessary to connect the cam follower to the valves is built-in to the outside of the cylinder wall. Their placement is the closest possible being the limiter factor the length of the intake valve plus the thickness of the intake valve support nut to give room to unscrew and disassemble the intake valve assembly and its components.

Two options are available for the material of the cylinder and the intake valve support nut. Cast-iron, which is the most used material for engine blocks, or aluminium alloys. Despite more expensive and with lower stiffness *[6]*, an aluminium block has major properties that are very advantageous for this type of engine design. Being an aircraft engine, the weight saving is especially important as the aluminium alloys have a density of approximately $2700 kg/m^3$ while cast-iron has about $7850 kg/m^3$ *[64]*. Also, the thermal conductivity of an aluminium alloy is three times larger than that of the cast-iron which is an immense help to cool the combustion chamber specially if the engine is air-cooled like most possibly in this case. Engines air-cooled tend to present more problems with cooling than water-cooled engines due to the low thermal conductivity of the air compared to the water.

Due to their weaker mechanical properties, usually, an aluminium engine block has a cast-iron sleeve. Those sleeves are the ones in contact with the combustion chamber combining the weight saving using aluminium as the main material of the block with the durability and trueness of the cast iron *[59]*.

The exact material selected is the aluminium alloy "A319 T5", a common material used for aluminium engine blocks with an ultimate tensile strength of $180 MPa$. A safety factor of 2.5 is adopted.

According to Ajeet Singh *[39]*, there are three types of stresses in the cylinder generally the third being neglected which is the bending stress caused by the side thrust of the piston. The other two types are the longitudinal stress acting on the piston and the flat zone of the combustion chamber and the circumferential stress acting on the wall of the cylinder, both caused by the gas pressure.

The cylinder wall thickness can be given by the following equation:

$$t_{cylinder} = \frac{D_{piston} p_{max}}{2\sigma_h} + C \qquad (3.117)$$

Where:

σ_h is the permissible circumferential stress which is the same magnitude of the safe tensile stress.

C is the re-boring allowance of the cylinder being equal to $1.5 mm$ for bore diameters up to $75 mm$ *[39]*.

The area of the combustion chamber must have enough room to fit the M8 spark plug, the intake, exhaust valve and its seats, the pistons, the cylinder sleeve and the

intake valve nut while having at least the maximum lift of the valves as height but the design of the combustion chamber is relatively open.

The height of the combustion chamber can be found through the volume represented in *Equation 3.1* and the area of the combustion chamber design can be found using the measuring tool in CATIA V5.

Finally, it is worth to remind that the cylinder center axis must be located at TDC with a distance of $Z \cos \gamma$ from the center axis of the crankshaft.

Chapter 4

4 Results and Discussion

4.1. Connecting Rod and Piston

The connecting rod dimensions achieved through the equations presented in the Section *3.5.* result in the circular column of the rod with a diameter of $9mm$ for a length of approximately $260.5mm$ using the annealed "AISI 4130" steel.

The selected off-the-shelf piston of $60mm$ bore comes with a gudgeon pin with an outside diameter of $13mm$ can be found in reference *[29]*.

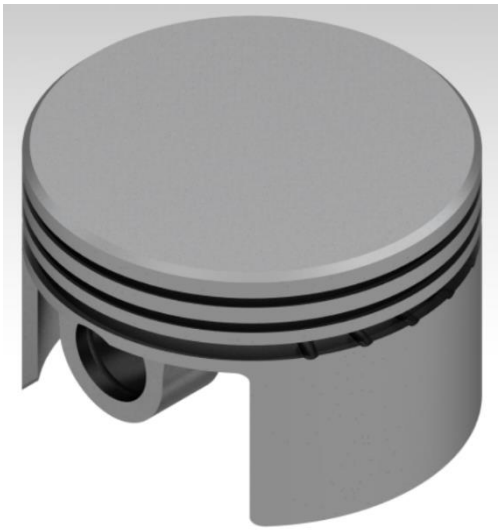

Figure 4.1 - Piston with $60mm$ bore in CATIA V5

Figure 4.2 – Gudgeon pin with $13mm$ outside diameter in CATIA V5

Figures 4.1 and *4.2* are the piston and gudgeon pin drawn in CATIA V5 but differences exist when compared to the real piston and gudgeon pin like that of reference *[29]*. One important parameter, that is not known, is the distance between the face of the piston and the center axis of the gudgeon pin, which influences the length of the connecting rod. The length of the connecting rod of $260.5mm$ is achieved using a distance between the face of the piston and the center axis of the gudgeon pin of $21mm$.

To withstand the force due to the pressure achieved inside the combustion chamber of $14198.3N$, the connecting rod small end must be $22mm$ in width while its outside diameter must be $21mm$ if a $2mm$ bearing sleeve is used between the gudgeon pin and the small end.

The socket and ball joint used in the big end connecting rod must have a radius of nearly $10mm$ meaning a diameter of $20mm$.

Using these dimensions, the 3D design of the connecting rod in CATIA V5 is presented in the following figure.

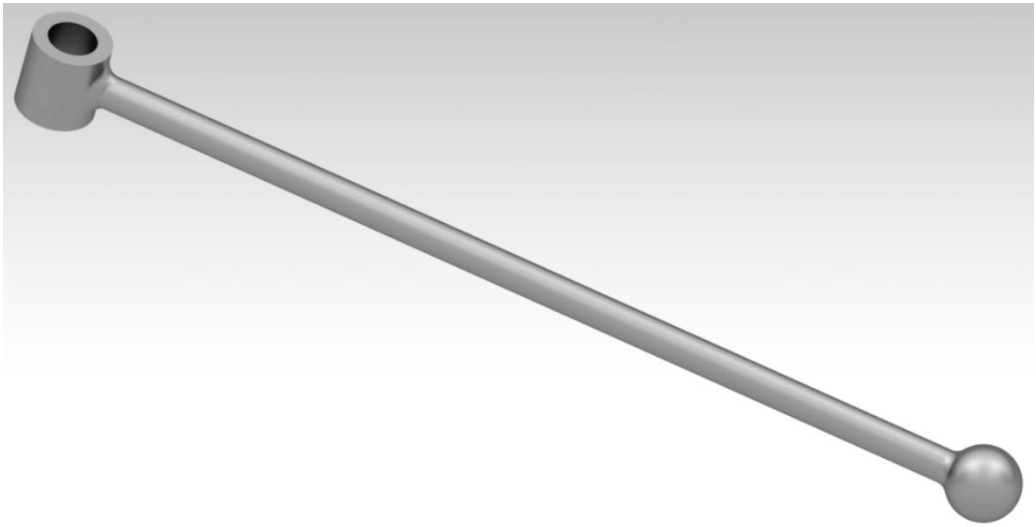

Figure 4.3 - Connecting rod in CATIA V5

4.2. Wobble Plate and Crosshead

As mentioned in Section *3.6.*, the socket and ball joint cap and the wobble plate design only have in account the abutment dimensions of bearings A and B and the small end of the connecting rod. All other details are for aesthetic purposes.

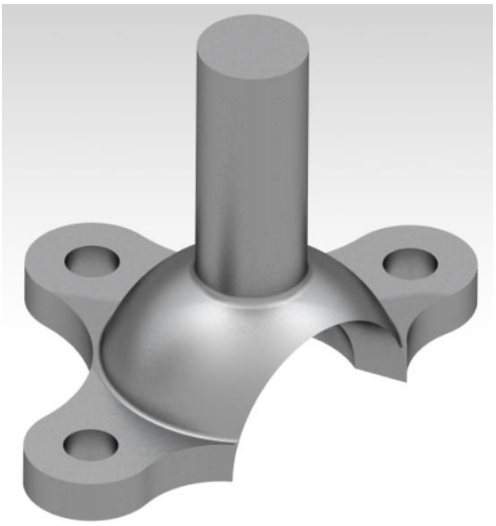

Figure 4.4 - Socket and connecting rod ball joint cap with crosshead engagement pin in CATIA V5

Figure 4.5 - Wobble plate in CATIA V5

Figure 4.6 only shows the design of the crosshead, despite the crosshead being built-in the engine block. The cavity is where the pin of the socket and ball joint of *Figure*

4.4 fits to block the wobble plate from rotating about the x-axis with the crankshaft. The block is then designed around the crosshead.

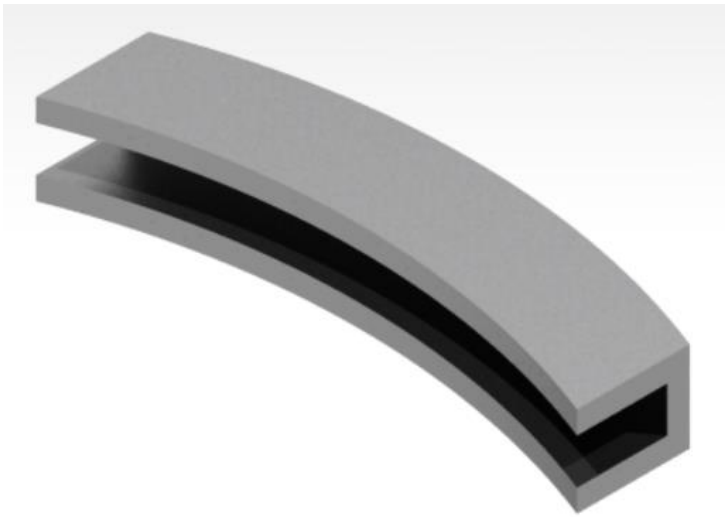

Figure 4.6 - Aluminium crosshead in CATIA V5

4.3. Kinematics analysis and crankshaft design

The initial parameters and considerations for the kinematic analysis and crankshaft dimensions that affect every parameter of the present engine are:

- A maximum pressure of $5.02MPa$ at peak combustion pressure.
- Peak combustion happening at $20º$ degrees of crankshaft rotation angle Φ after TDC.
- Stroke to bore (S/B) ratio of 1.25.
- Piston diameter of $60mm$.
- Maximum angular range γ of $18º$ degrees.

The kinematics analysis is functional for any point E position and thus any crankshaft rotation angle Φ but for the realization of the present work, the only important value is for peak combustion at $20º$ degrees after TDC. For that position, the coordinates of point E are approximately:

$$x_E = 35.44mm$$

$$y_E = 116.06mm$$

The beta angle β for those coordinates is approximately $16.98º$ degrees.

For a S/B ratio of 1.25, the engine stroke S is $75mm$ which corresponds to a wobble plate arm Z of approximately $121.35mm$. The vertical distance variation r between the point E and the cylinder centre line aligned with TDC is approximately $0.65mm$. The angle theta θ correspondent to that distance variation and a connecting rod length L of $260.5mm$ is approximately $0.14º$ degrees.

The maximum pressure of $5.02MPa$ during combustion applied on a piston with a diameter of $60mm$, creates a maximum force $F_{máx}$ of approximately $14198.3N$. The force resultant F_q of the maximum force applied on the joint of the point E is practically the same and its components F_{q_x} and F_{q_y} for the x-axis and y-axis are approximately $14198.3N$ and $35.4N$, respectively.

The values obtained from the kinematic analysis show very little to insignificant variation on the resultant forces acting on the point E and, on the distance and angle with the cylinder centre axis. In a conventional engine design, these variations are much greater, which confirms the results of *Figure 2.6* which states that an axial engine blocked by crosshead like the present one presents a much lower piston side thrust force than a conventional engine design.

Even at the most distant point from the cylinder centre axis at a crankshaft rotation angle Φ of $90º$ after TDC, the vertical distance variation r is approximately $5.94mm$ and the theta angle θ is approximately $1.31º$ degrees.

The crankshaft design has only two initial parameters:

- A crankshaft angle arm which must be equal to the maximum angular range γ of $18º$ degrees.
- A length of crankshaft arm X which is valued at $31mm$.

With those initial parameters, the values of *Figure 3.3* parameters are:

$$M \cong 95.41mm$$

$$H \cong 100.32mm$$

$$Q \cong 90.74mm$$

$$T \cong 29.48mm$$

To complete the simple design of the crankshaft, the variables of *Figure 3.8*, especially the corners radius $R_{arc_{A;C}}$ and $R_{arc_{B;D}}$ must be calculated determined:

$$R_{arc_{A;C}} = R_{arc_{B;D}} \cong 17.96mm$$

$$D_{arc_{A;C}} = D_{arc_{B;D}} \cong 13.05mm$$

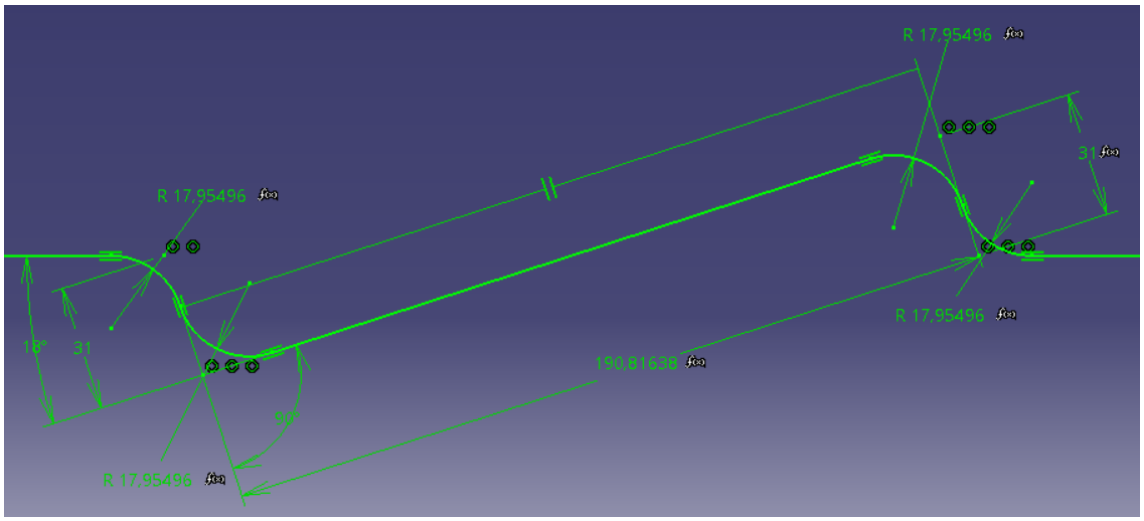

Figure 4.7 - 2D crankshaft design in CATIA V5

4.4. Crankshaft and Bearings Iteration

Following the flowchart presented in Section *3.10.*, the bearings selected, all from SKF company are, for position A and B (see *Figure 3.4*), a single row tapered roller bearings model "31308" *[65]* with $40mm$ inner diameter represented in *Figure 4.8*, for position C (see *Figure 3.5)*, a tapered roller bearing with two matched single row bearings arranged face-to-face model "31306/DF" *[66]* with $30mm$ inner diameter represented in *Figure 4.9* and for position D (see *Figure 3.*), a single row cylindrical roller bearing model "N 206 ECP" *[67]* with $30mm$ inner diameter represented in *Figure 4.10*. The lock nuts required to secure bearings B and C are, respectively, the "KMK 8" *[68]* and "KMK 6" [69] and are represented in *Figure 4.11* while the shaft circlip "DIN 471" with $30mm$ diameter *[70]* required to secure bearing D is represented in *Figure 4.12*.

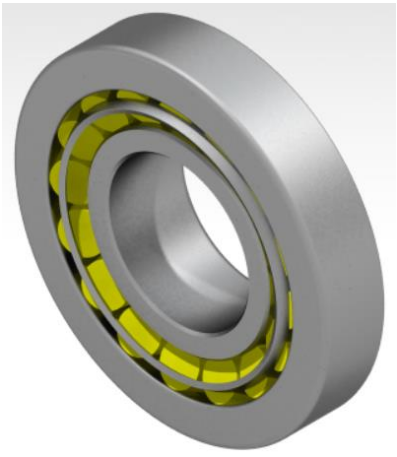

Figure 4.8 - Bearings A and B, "31308" in CATIA V5 by SKF [65]

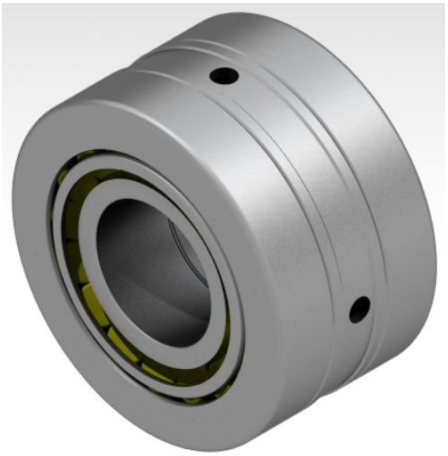

Figure 4.9 - Bearing C, "31306/DF" in CATIA V5 by SKF [66]

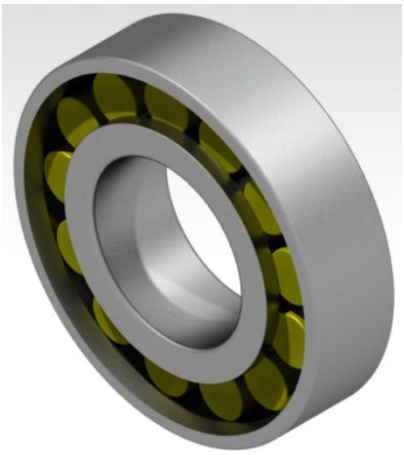

Figure 4.10 - Bearing D, "N 206 ECP" in CATIA V5 by SKF [67]

Figure 4.11 - Lock nut for bearing B, "KMK 8" in CATIA V5 by SKF [68]

The lock nut “KMK 6” 3D design in CATIA V5 is exactly equal to the lock nut “KMK 8” but smaller, with $30mm$ of inner diameter instead of $40mm$.

Figure 4.12 - Circlip for bearing D, “DIN 471” for a $30mm$ shaft in CATIA V5 by Norelem [70]

4.4.1. Bearings Assembly Clearance

The bearings assembly simulation in CATIA V5 allows testing the maximum diameter possible of the crankshaft corners between bearings D and B to make sure it is possible to assemble bearings A and B and the locking nut of the bearing B. The lock nut for bearing B has an inner diameter of $38.376mm$ counting with the thread and a width of $11mm$ while bearings A and B have an inner diameter of $40mm$ and a width of $23mm$ *[65] [68]*. The bearing D requires a minimum diameter backrest of $35.3mm$ *[67]*. *Figure 4.13* represents the design of the crankshaft following the specifications of the bearings and nut and provides a crankshaft diameter as well as a distance between the crankshaft corner and the locking nut placement $D_{arc;nut}$ to simulate the bearings passage.

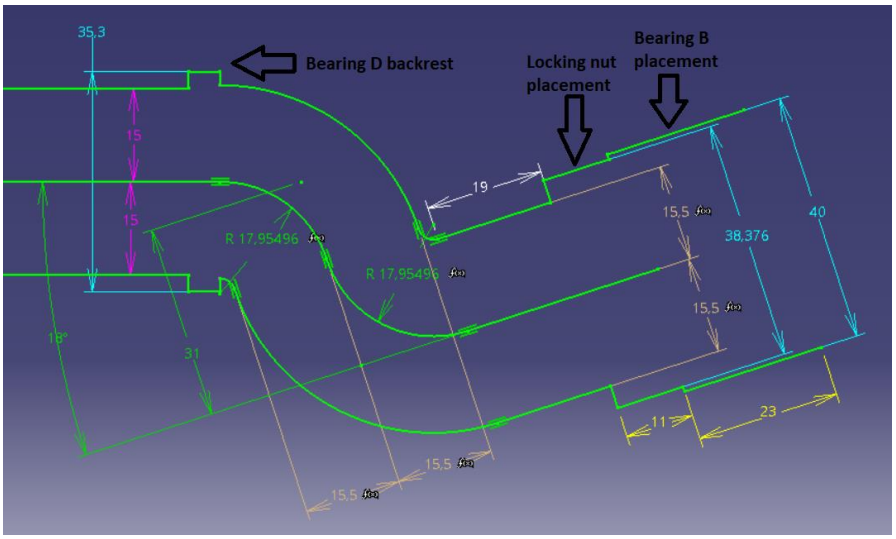

Figure 4.13 - Crankshaft and bearing specifications for bearing passage simulation

The simulation starts by placing the bearing/nut near the backrest of the bearing D. The bearing/nut passes through the backrest with ease due to the significant difference in diameter. Next, the upper part of the bearing/nut is made tangent to the upper crankshaft corner while the bottom right is made coincident to the bottom crankshaft corner. When the bearing/nut passes through half the path and the crankshaft corner reverses, as it can be seen in *Figures 4.14* and *4.15*, the coincident and tangent constrains are ceased. New constrains are made but now it is the left upper corner of the bearing/nut that is made coincident to the upper crankshaft corner while the bottom part of the bearing/nut is made tangent to the bottom crankshaft corner. This way, it is possible to simulate and verify if the bearing can pass depending on the established dimensions.

The locking nut and the bearing pass with relative ease thought the backrest of the bearing D and the first half of the path. It is worth noticing that in the simulation, the backrest of the bearing D is as close to the crankshaft corner as possible because it is at this distance that the bearing/nut has the most difficulty passing through.

It is during the final curvature, before the bearing and nut placement, that the bearing is close to the crankshaft boundary while the locking nut still passes with ease. *Figures 4.14* and *4.15* show the two points where the bearing is closer to the crankshaft boundary and it is these two points that define the maximum possible crankshaft corner diameter and the minimum possible distance between the crankshaft corner and the locking nut placement $D_{arc;nut}$, respectively.

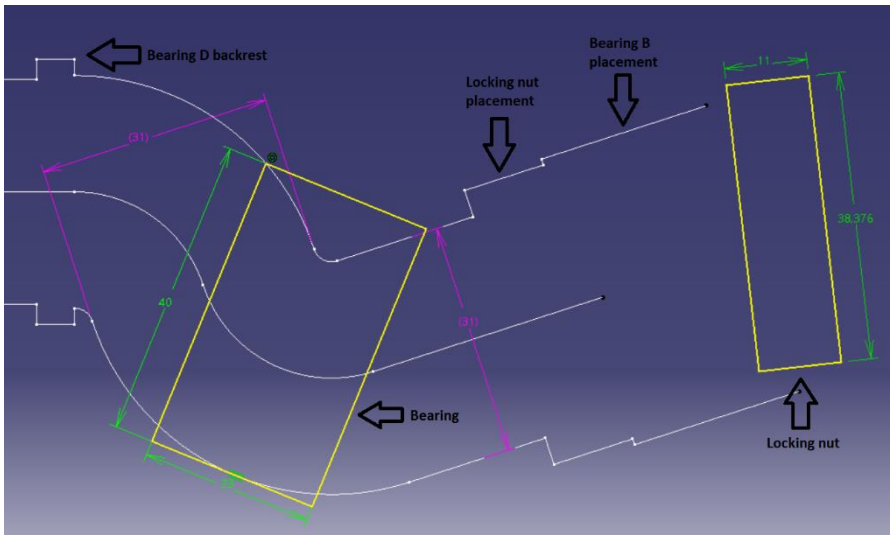

Figure 4.14 - Bearing passage point that defines the maximum crankshaft corner diameter

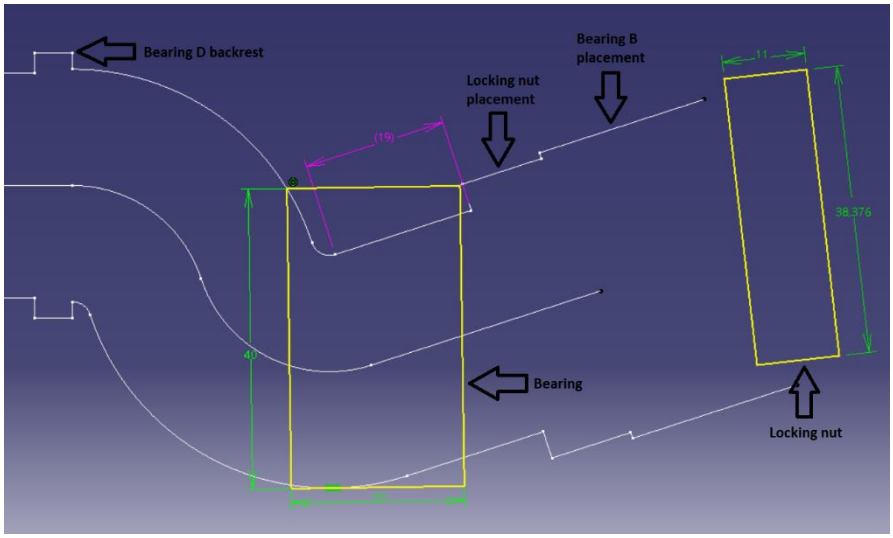

Figure 4.15 - Bearing passage point that defines the minimum $D_{arc;nut}$

It is worth remembering that bearings A and B design have fillets in their corners which makes its apparent width inferior by $3mm$ *[65]*. That difference works as a safety margin for the safe passage of the bearings. So, the simulation is made with the full width of $23mm$.

The simulation concludes that, for a crankshaft with the specifications shown in the *Figures 4.7* and *4.13* and the bearing specifications mentioned above, a maximum of $31mm$ diameter is possible for the crankshaft corners and a minimum distance between the nut of bearing B and the corner of the crankshaft $D_{arc;nut}$ of $19mm$ is required for bearings A and B and lock nut of bearing B to successfully pass.

4.4.2. Bearing Positioning and Crankshaft Structural Analysis

Bearings A and B positioning are only dependent on the N length which only depends on $D_{arc;nut}$ which has a minimum value of $19.00mm$. All other variables presented in *Equation 3.54* that defines N are bearings specifications or initial crankshaft specifications. Different N values are tested to verify the differences obtained and which one provides the best structural crankshaft analysis and bearings life.

For $N \cong 31.45mm$, the crankshaft loads are:

$$R_A = \begin{cases} R_{A_x} = 14198.3N \\ R_{A_y} = 25379.9N \\ R_{A_z} = -788.9N \end{cases} \qquad R_B = \begin{cases} R_{B_x} = 0.0N \\ R_{B_y} = -25415.3N \\ R_{B_z} = 788.9N \end{cases}$$

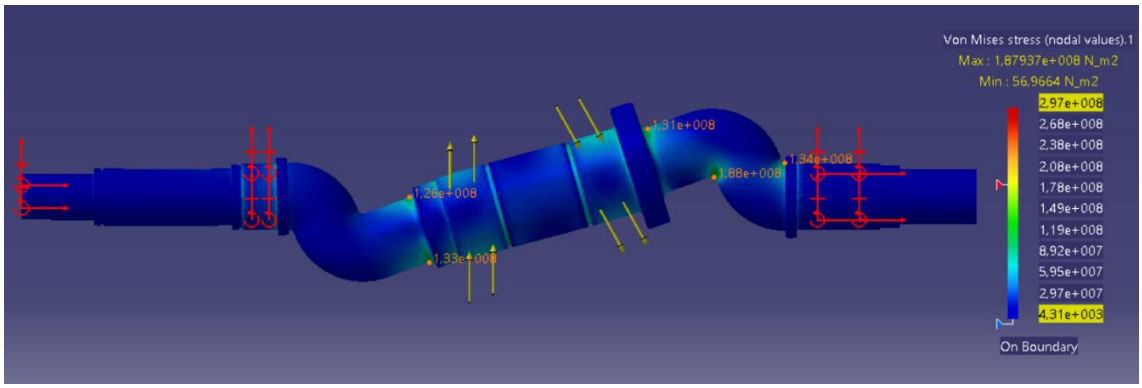

Figure 4.16 - Stress distribution for a crankshaft with $N \cong 31.45mm$

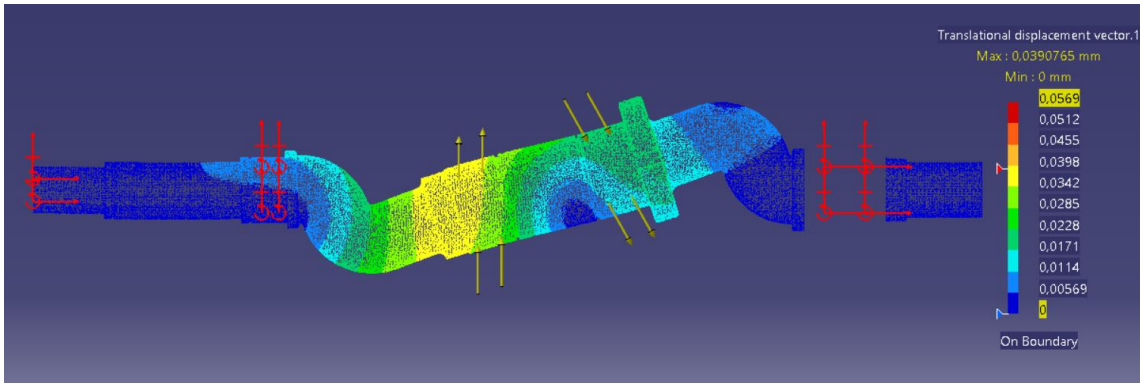

Figure 4.17 - Translational displacement for a crankshaft with $N \cong 31.45mm$

For $N \cong 31.45mm$, the bearing loads are:

$$R_A^{''} = \begin{cases} R_{A_x}^{''} = 20476.8N \\ R_{A_y}^{''} = 19624.3N \\ R_{A_z}^{''} = 764.5N \end{cases} \qquad R_B^{''} = \begin{cases} R_{B_x}^{''} = -7321.1N \\ R_{B_y}^{''} = -23699.8N \\ R_{B_z}^{''} = 764.5N \end{cases}$$

According to "SKF Bearing Select" tool *[43]*, for the represented bearing loads above and a maximum speed of operation of $2500rpm$, a bearing life of 682 hours for bearing A and 1960 hours for bearing B are expected.

For maximum $N \cong 35.95mm$, the crankshaft loads are:

$$R_A = \begin{cases} R_{A_x} = 14198.3N \\ R_{A_y} = 21929.7N \\ R_{A_z} = -788.9N \end{cases} \qquad R_B = \begin{cases} R_{B_x} = 0.0N \\ R_{B_y} = -21965.2N \\ R_{B_z} = 788.9N \end{cases}$$

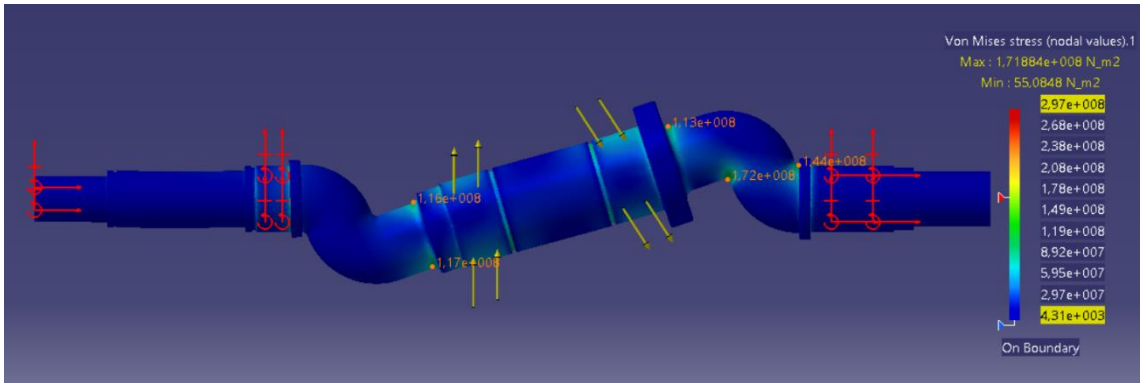

Figure 4.18 - Stress distribution for a crankshaft with $N \cong 35.95mm$

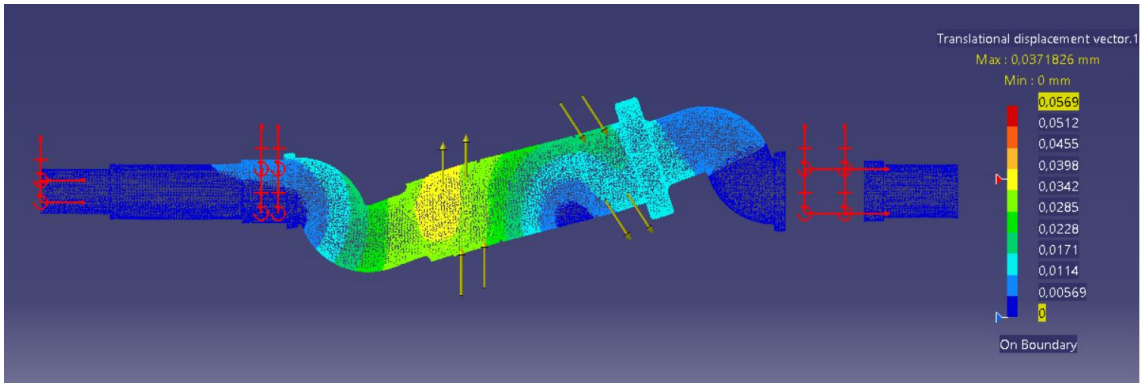

Figure 4.19 - Translational displacement for a crankshaft with $N \cong 35.95mm$

For maximum $N \cong 35.95mm$, the bearing loads are:

$$R_A^{''} = \begin{cases} R_{A_x}^{''} = 19494.5N \\ R_{A_y}^{''} = 16407.1N \\ R_{A_z}^{''} = 764.5N \end{cases} \qquad R_B^{''} = \begin{cases} R_{B_x}^{''} = -6338.8N \\ R_{B_y}^{''} = -20482.6N \\ R_{B_z}^{''} = 764.5N \end{cases}$$

According to "SKF Bearing Select" tool *[43]*, for the represented bearing loads above and a maximum speed of operation of $2500rpm$, a bearing life of 850 hours for bearing A and 2770 hours for bearing B are expected.

The crankshaft analysis results of *Figures 4.16*, to *4.19* are made with a distance $D_{arc;wall\ D}$ equal to zero which represents the smaller distance between the support bearings C and D because it should be the optimal value as it is verified further ahead. Analysing the results, it is possible to notice that an N of approximately $31.45mm$ resulting in a $D_{arc;nut}$ of $23.50mm$ is the minimum value possible to secure the integrity of the crankshaft because the maximum stress allowed $\sigma_{max_{crankshaft}}$ is $188MPa$ and coincidentally also the maximum of the crankshaft as shown in *Figure 4.16*.

As already mentioned, an N of approximately $35.95mm$ resulting in a $D_{arc;nut}$ of $19.00mm$ is the maximum value to allow the bearings passage. Comparing the two N values and their results, it is concluded that a larger N value creates smaller stresses through almost the entire crankshaft and a smaller deformation as well providing a larger expected bearing life for both bearings A and B. In depth analysis, it is noticed that the most fragile zone of the crankshafts is the interior corner between bearings A and C followed, secondly, by the corner near the backrest of bearing C as shown in *Figures 4.16* and *4.18*. The crankshaft with the maximum N has a maximum stress of $172MPa$ in the interior corner between bearings A and C. However, for the corner near the backrest of the bearing C, the crankshaft with the maximum N has a maximum stress of $144MPa$ while the crankshaft with the minimum N has a maximum stress of $134MPa$.

For a $D_{arc;wall\ D}$ equal to zero, the distance between C_x and D_x of the points C and D is approximately $263.72mm$ which represents a maximum allowable deformation displacement δ, obtained through *Equation 3.66*, of approximately $0.0527mm$.

For both crankshafts, the deformation displacement is very similar being stronger in the bearing B placement and its surroundings. The crankshaft with the maximum N has a maximum deformation displacement of approximately $0.0372mm$ as shown in *Figure 4.19*, slightly inferior relative to the crankshaft with the minimum N which has a maximum translational displacement of approximately $0.0391mm$ as shown in *Figure 4.17*.

It is clear by now that the crankshaft with the maximum N represented in *Figures 4.18* and *4.19* is more advantageous in every aspect. When increasing the N value, the

maximum stress and the maximum deflection on the crankshaft reduces and the expected bearing life increases. When decreasing the N value, the opposite happens.

The support bearings C and D have their placement in coordinates C_x and D_x given by *Equations 3.55* and *3.56*, respectively. The value $D_{arc;wall\ D}$ is the only variable that is not included in the bearings specifications or initial crankshaft specifications and so is the only that can vary.

For a $D_{arc;wall\ D} = 0mm$, representing a C_x of approximately $137.36mm$ and a D_x of approximately $126.36mm$, the bearing loads are:

$$R_C = \begin{cases} R_{C_x} = 13843.3N \\ R_{C_y} = 6080.4N \\ R_{C_z} = 0.0N \end{cases} \qquad R_D = \begin{cases} R_{D_x} = 0.0N \\ R_{D_y} = -6114.9N \\ R_{D_z} = 0.0N \end{cases}$$

According to "SKF Bearing Select" tool *[43]*, for the represented bearing loads above and a maximum speed of operation of $2500rpm$, a bearing life of 1270 hours for bearing C and 4770 hours for bearing D are expected.

For a $D_{arc;wall\ D} = 5mm$, representing a C_x of approximately $137.36mm$ and a D_x of approximately $131.36mm$, the bearing loads are:

$$R_C = \begin{cases} R_{C_x} = 13843.3N \\ R_{C_y} = 5966.6N \\ R_{C_z} = 0.0N \end{cases} \qquad R_D = \begin{cases} R_{D_x} = 0.0N \\ R_{D_y} = -6001.1N \\ R_{D_z} = 0.0N \end{cases}$$

According to "SKF Bearing Select" tool *[43]*, for the represented bearing loads above and a maximum speed of operation of $2500rpm$, a bearing life of 1280 hours for bearing C and 5080 hours for bearing D are expected.

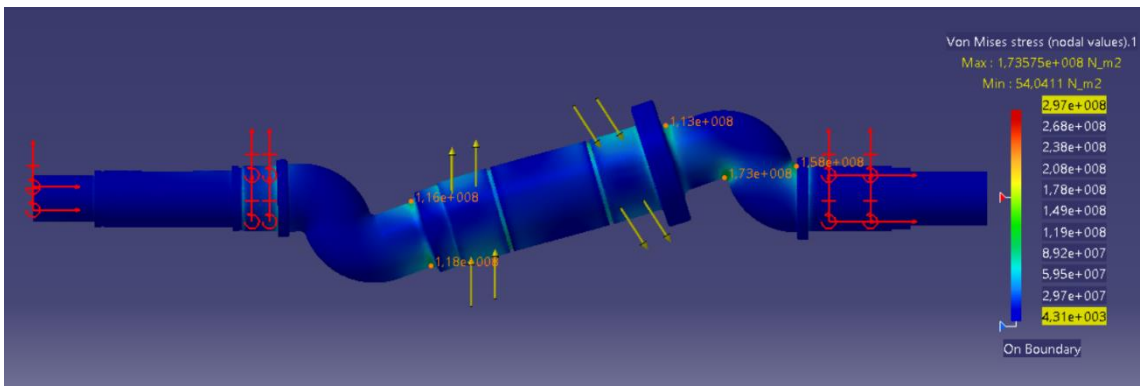

Figure 4.20 - Stress distribution for a crankshaft with $D_{arc;wall\ D} = 5mm$

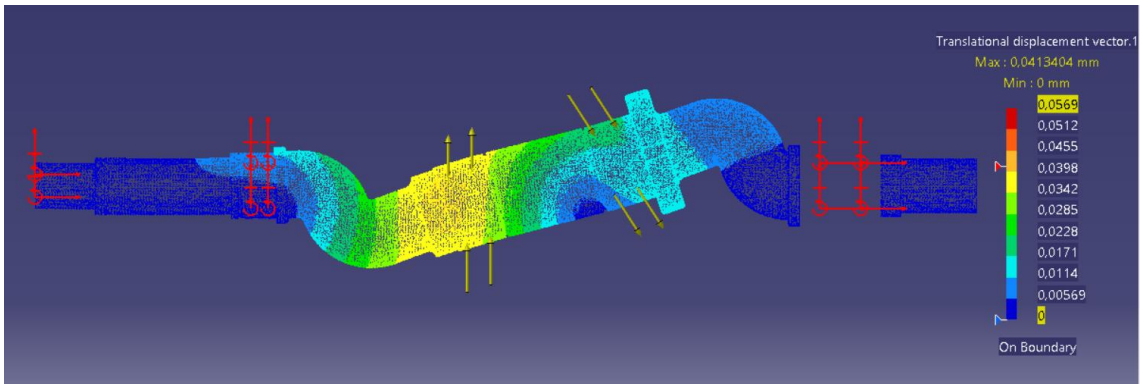

Figure 4.21 - Translational displacement for a crankshaft with $D_{arc;wall\ D} = 5mm$

The crankshaft of the *Figures 4.20* and *4.21* is designed with the maximum N of approximately $35.95mm$ as it has been concluded that it is the optimal value for this crankshaft design. For that reason, it makes sense to use that value for the comparison of crankshafts with different $D_{arc;wall\ D}$ values. Comparing *Figures 4.18* and *4.20*, it is observed that most of the maximum stresses acting on the different zones of the crankshafts remain almost identical apart from the maximum stress in the corner near the backrest of bearing C which increases from $144MPa$, in the crankshaft with a $D_{arc;wall\ D}$ equal to $0mm$, to $158MPa$ in the crankshaft with a $D_{arc;wall\ D}$ equal to $5mm$, although still in the allowable range. The significant difference between both crankshafts is noticed when comparing the deformation displacement, seen in *Figures 4.19* and *4.21*, where it is clear a significant increase from $0.0372mm$, in the crankshaft with a $D_{arc;wall\ D}$ equal to $0mm$, to $0.0413mm$, in the crankshaft with a $D_{arc;wall\ D}$ equal to $5mm$. In terms of expected bearing life, the crankshaft with a $D_{arc;wall\ D}$ equal to $5mm$ presents a very slight larger value for both bearings C and D compared to the crankshaft with a $D_{arc;wall\ D}$ equal to $0mm$.

Concluding, the smaller the $D_{arc;wall\ D}$ value, the smaller the distance between the support bearings C and D which results in a better structural integrity of the crankshaft. The downside is a smaller expected bearing life although the difference is so small that it can be considered irrelevant.

All the crankshafts analysed previously are designed with the maximum possible fillet against the backrest of bearing A and against the locking nut of bearing B which has a radius of approximately $3.69mm$. The crankshaft of the following *Figures 4.22* and *4.23* is exactly equal to the crankshaft of the *Figures 4.18* and *4.19* with a N value of approximately $35.95mm$ and a $D_{arc;wall\ D}$ of $0mm$ but without a fillet in the mentioned zones.

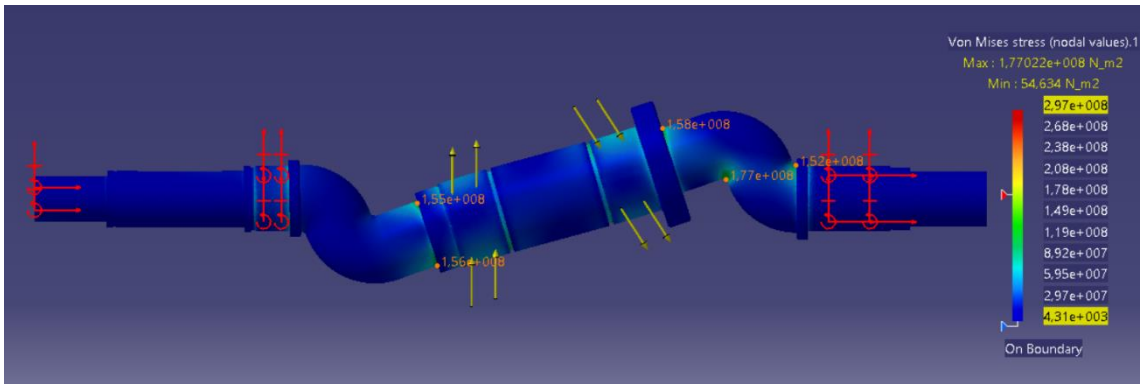

Figure 4.22 - Stress distribution for a crankshaft with no fillets

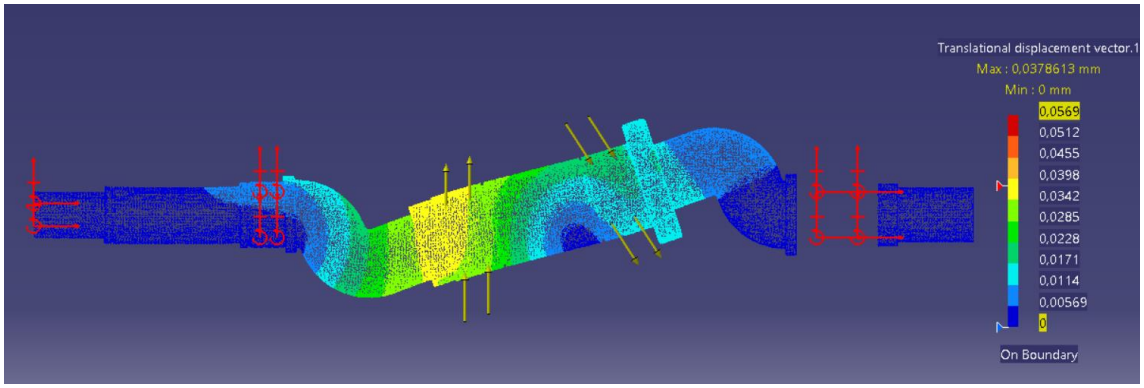

Figure 4.23 - Translational displacement for a crankshaft with no fillets

The CATIA V5 analysis shown in *Figure 4.22* shows a slight increase in the maximum stresses on the most critical zones but a very significant increase of near $40MPa$ in the zones where the fillets should be located compared to the analysis of the *Figure 4.18*. The deformation displacement also increased very slightly being the difference practically irrelevant. The analysis shown in *Figures 4.22* and *4.23* prove that it is advantageous to use fillets with the bigger radius possible in the crankshaft.

The following image provides the final 3D CAD design of each crankshaft halve with a $N \cong 35.95mm$ and $D_{arc;wall\ D}$ equal to zero:

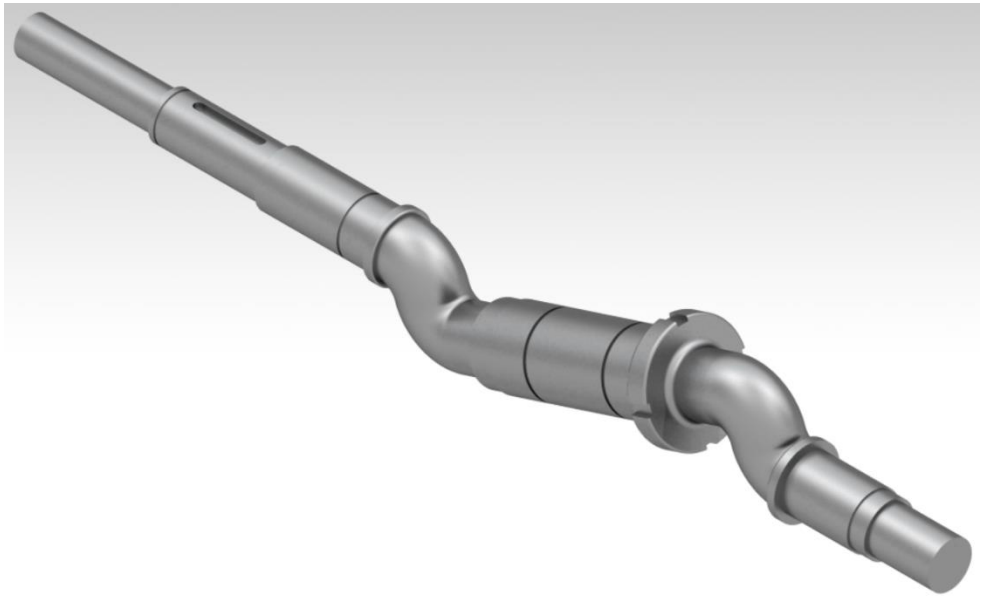

Figure 4.24 - Final crankshaft in CATIA V5

If observed, it is noted that the zone between the bearing D and the shaft coupling is quite long solely because of the length necessary for the valves and distribution system.

4.5. Shaft Coupling

For a crankshaft torque $T_{crankshaft}$ of approximately $1.83 \times 10^5 Nmm$, different combinations of numbers and internal thread diameters of screws, n_{screw} and d_{screw} respectively, and crankshaft diameters $d_{coupling}$ are available. Those values heavily affect the dimensions of the shaft coupling mainly the length, the outer diameter and the mass: $L_{coupling}$, $D_{coupling}$ and $\mathrm{m_{coupling}}$ respectively. *Table 1* shows the different possible combinations for different Allen screw sizes with $18mm$ length and the effect on the dimensions of the shaft coupling.

Table 4.1 - Shaft coupling combinations for different size screws

	d_{screw}	n_{screw}	*Minimum* $d_{coupling}$	$L_{coupling}$	$D_{coupling}$	$m_{coupling}$
M4	3.141	10	27	62.4	51	0.699
M4	3.141	12	23	74.4	47	0.749
M6	4.773	6	20	56	52	0.760
M8	6.466	4	16	52.25	55	0.842

The first three variables of the table are obtained using the calculation procedure used in the shaft coupling methodology, the length and outer diameter are obtained using a common distribution shown in *Figure 3.12* while the mass of the coupling is obtained using CATIA V5.

Analysing the values of the table is easy to conclude that the M8 shaft coupling is the thickest and heaviest but shortest. The M4 shaft couplings are the opposite of the M8 being lighter and thinner but longer. The M6 shaft coupling is in between with moderate dimensions. The M6 and M4 with 10 screws shaft couplings are the best choices. The M4 is a lighter shaft coupling but the minimum inner diameter is the largest being very close to that of bearing D with $30mm$. The bearing must pass through the crankshaft and, in between the shaft coupling and the bearing, is the cylindrical cam. Although possible, a reduced inner diameter may be better. For the present work, the M6 shaft coupling is selected but later on, slight modifications can be made to incorporate the M4 with 10 screws shaft coupling. To conclude the shaft coupling, between the screw and the surface of the shaft coupling, a flat washer is used.

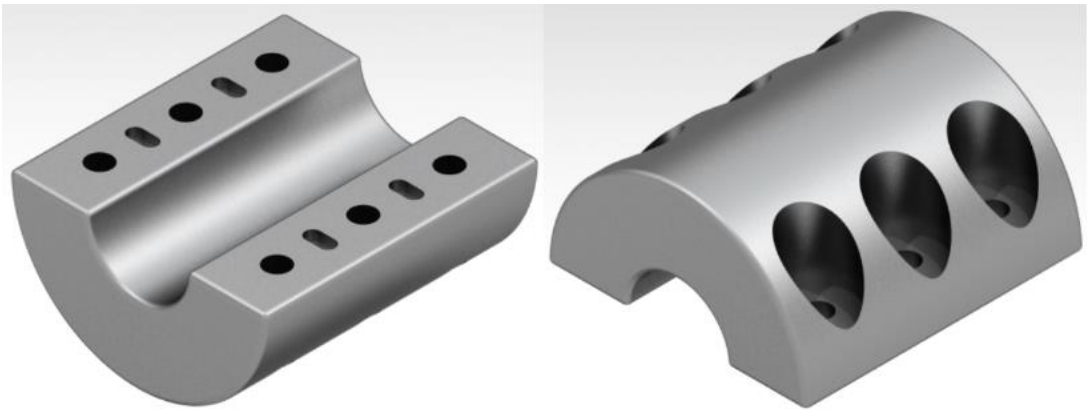

Figure 4.25 - Bottom and upper shaft coupling body in CATIA V5, respectively

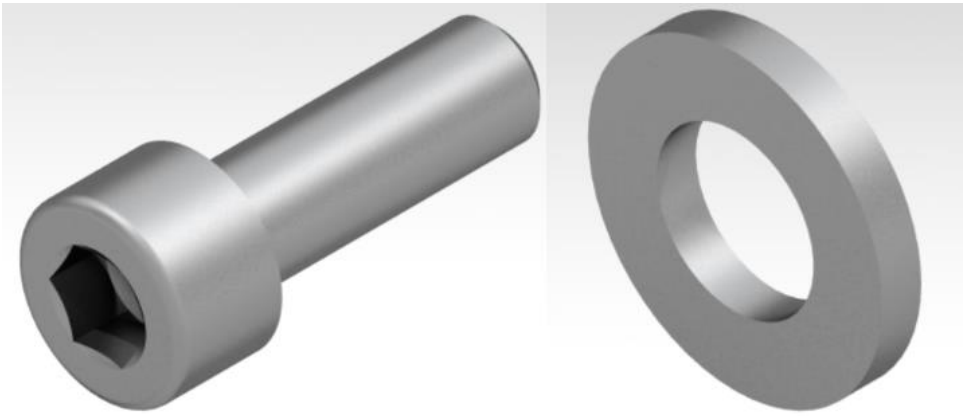

Figure 4.26 - Allen M6 screw with $18mm$ length and the respective flat washer in CATIA V5 by Bossard [71] [72]

Figure 4.27 - Shaft coupling assembled in CATIA V5

4.6. Distribution Mechanism System

4.6.1. Valves and Seats

The following table presents the values of the main parameters to size the engine valves and their seats considering an intake gas velocity of $42.5m/s$ and an exhaust gas velocity of $60m/s$, estimation values obtained and dependent on the engine´s maximum speed.

Table 4.2 - Theorical valves parameters

	Intake valve	*Exhaust valve*
Port diameter (mm)	32.54	27.39
Seat width (mm)	1.96	1.65
Valve head diameter (mm)	36.45	30.68

The values of *Table 2* are the theoretical values that are used to size the ports, the valves, and the valve seats for the engine. Because valves and seats with these exact dimensions do not exist, close dimensions were searched.

The search led to a marketplace website for racing engine components and catalogue where it is possible to filter the valves according to size and price. Among the cheapest valves in the market, an exhaust valve with a head diameter of $1.222in$ or $31.04mm$ was found which is very close to the value presented in *Table 2*. For the intake valve, though, two very similar valves with a $1.455in$ or $36.96mm$ and a $1.46in$ or a $37.08mm$ head diameter valve were found.

In doubt between these two intake valves, it is taken into consideration the fact that Giacosa says that engine designers tend to increase the port diameters to the maximum possible to reduce the gas velocity and thus diminishing the pressure drop losses *[30]*. The intake valve with $37.08mm$ head diameter is selected because it represents the larger port diameter and the lower mean gas velocity values.

Table 3 gives the actual values for the seat width and the port diameter according to the selected valves head diameters.

Table 4.3 - Selected valves parameters

	Intake valve	*Exhaust valve*
Valve head diameter (mm)	37.08	31.04
Seat width (mm)	1.99	1.67
Port diameter (mm)	33.11	27.71
Mean gas velocity (m/s)	41.06	58.61
Tip length (mm)	9.144	7.62
Overall length (mm)	119.89	108.59
Stem diameter (mm)	5.99	5.96

Both intake and exhaust valves have a seat face of $45º$ degrees *[60]*.

The valves that represent the values obtained in the *Table 3* are the intake valve "Ferrea F6310 6000 Series" and the exhaust valve "Ferrea F6312 6000 Series" *[73] [74] [75]*.

In the catalogue and website, additional information about the other valve parameters is provided which are useful to design in CATIA V5 the valves and other mechanical pieces connected to the valves to use in the engine simulation. Those parameters are the tip length, the overall length and the stem diameter and are also shown in *Table 3*.

There is one parameter that is important to design the valve in CATIA V5 that the supplier did not provide and that is the margin of the valve. It is possible to find that value through an article wrote by Ferrea that says the margin of an exhaust valve should be at least $0.08in$ or $2.03mm$ while the intake valve should be $0.05in$ or $1.27mm$ *[76]*. This value is influenced if the valve is exposed inside the combustion chamber or if it is placed perfectly aligned with the combustion chamber wall.

The result of the valves and their seats design in CATIA V5 are shown in *Figures 4.28* to *4.30*. The valves are designed with the parameters mentioned above that influence the engine simulation along with the other engine mechanical parts attached to the valves but probably there are differences to the real valves that must be checked to build the actual engine prototype but are irrelevant to the purpose of the present work. The valve seat is a piece made of steel as it is not possible to find one that matched the port diameters of the intake and exhaust valves.

Figure 4.28 - Intake valve "Ferrea F6310 6000 Series" in CATIA V5

Figure 4.29 - Exhaust valve "Ferrea F6312 6000 Series" in CATIA V5

The valve seats of both valves have the inner diameter equal to the port diameter and a ring width of $4.5mm$ giving an outer diameter of $42.11mm$ to the intake valve seat and an outer diameter of $36.71mm$ to the exhaust valve seat.

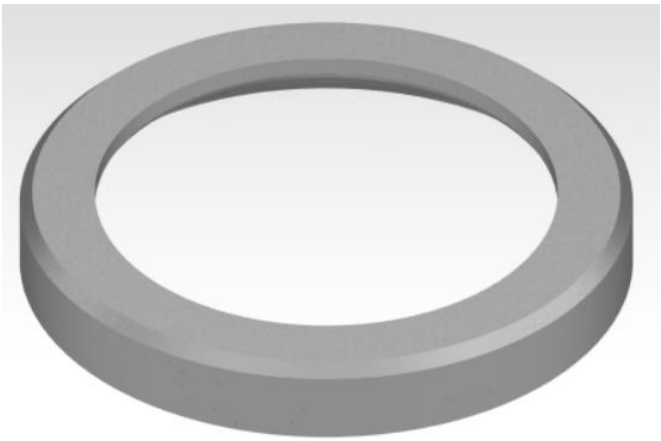

Figure 4.30 - Intake and exhaust valve seat in CATIA V5

4.6.2. Valve Lift

The results obtained for the maximum lift for both valves are:

Intake valve: $l_{iv} = 11.70mm$

Exhaust valve: $l_{ev} = 9.80mm$

Usually, an engine valve lift is equal for both valves and determined by the intake valve for being the larger value and so both cam groove profiles were designed with the intake valve lift of $11.70mm$ despite the cam groove profile design being different for the two valves due to the different duration of the opening phase, $230º$ degrees for the intake valve and $235º$ degrees for the exhaust valve.

4.6.3. Valve Spring

The valve spring must withstand the acceleration force with a 1.5 safety factor which give the maximum force of:

$$F_{max_{spring}} = 222.97N$$

Selecting a stiffness and a spring index among the usual values for engine valves of:

$$k = 11.5N/mm$$

$$C = 7.9$$

The minimum force of the spring is equal to:

$$F_{min_{spring}} = 88.36N$$

Using the procedure explained to design the valve spring in the Section *3.12.4.*, the parameter values to dimension the spring are:

Table 4.4 - Spring dimensions

Wire diameter "d"	$2.63mm$
Mean coil diameter "D"	$20.80mm$
Outer diameter "D_O"	$23.43mm$
Inner diameter "D_I"	$18.17mm$

The spring has 4.48 active turns N and 6.48 total turns N_t totalling a mass of $0.0181kg$. With those total number of turns, the spring lengths are:

Table 4.5 - Spring lengths

Solid length "L_s"	$17.04mm$
Maximum lift length "$L_{máx\ lift}$"	$18.98mm$
Installation length "L_I"	$30.69mm$
Free length "L_F"	$38.37mm$

Finally, the last requirement to complete the spring design is to verify if the spring is viable for this engine requiring a minimum natural frequency $f_{n_{minimum}}$ of $270.8Hz$. The spring obtains a natural frequency f_n of $479.0Hz$ making it viable for this engine.

It is worth noticing that the spring designed has small diameters and stiffness because the inertia force is also small and that is caused by the medium maximum speed rotation of the engine compared per example to an automobile engine which easily has more than the double. Because the speed engine is exponential to the inertia force, an engine with double the speed has four times the inertia force and that causes the spring to be significantly larger and far stiffer to not be too long.

To use the valve spring in the simulation of the movement of the engine in CATIA V5, it is not possible to use the spring with the design of the free length. Instead, it must use a different 3D design of the spring with the installation length ready to be placed next to the engine cylinder.

The only difference between the two designs, as the *Figure 4.33* show, is the difference in lengths simulating how the spring looks when compressed with its seat pressure.

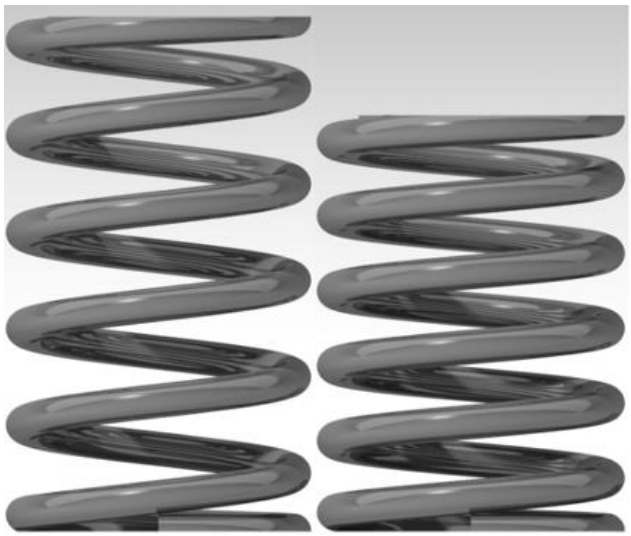

Figure 4.31 - In the left, the valve spring in its free length and in the right, in its installation length

Verifying the design with a spring manufacturer *[77]*, no flaws are presented. Also, the website has the capability to search in the market for similar spring valves that, with smaller changes in some spring parameters, can fit in the engine although none of the springs presented are manufactured with a suitable material for shock loads applications like an engine.

4.6.4. Valve Lock and Retainer

The valve lock is designed with a 7-degree angle, a single groove and their inner diameter equating to the stem diameter of the valves. Because the stem diameter is different between the exhaust and the intake valves, two pieces need to be designed. The intake valve lock with an inner diameter of $5.99mm$ and the exhaust valve lock with an inner diameter of $5.96mm$. The difference between them is not perceptible to the naked eye and so a single image in CATIA V5 of the piece is presented.

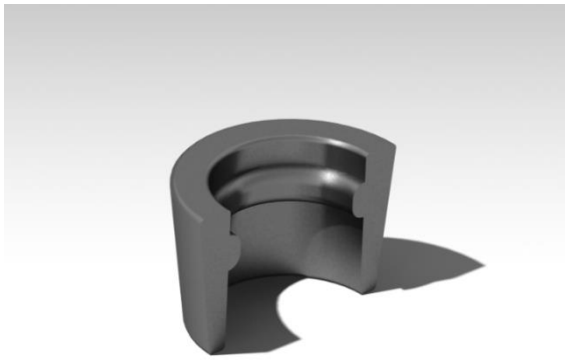

Figure 4.32 - Valve lock in CATIA V5

The valve retainer is designed using an outside diameter equal to the outer wire diameter of the spring of $23.43mm$ and a middle diameter equal to the inner wire diameter of the spring of $18.17mm$. The inner diameter of the valve retainer is equal to the angled valve lock outside wall, and it is rounded to $8mm$ with a 7-degree angle.

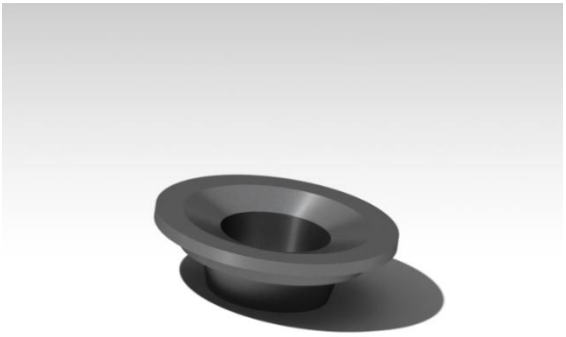

Figure 4.33 - Valve retainer in CATIA V5

4.6.5. Cylindrical Cam

4.6.5.1. Cam groove profile

The cam groove profile design begins by selecting a cam follower radius. Checking the catalogue of a bearings manufacturer *[62]* for possible cam follower radius values, it is possible to find various values. The cam follower with a radius of $8mm$ is the smaller that passes the bearing life requirement of 500 hours as is shown in Section *4.6.5.2.*

All four sections of the groove profile described in Section *3.12.6.1.* correspond to two revolutions of the crankshaft rotation. The lift section is the only with pre-defined crankshaft rotation degrees. This parameter was defined by comparing to other engines as a rule of thumb *[39]* while all other parameters groove profile are defined according to the following procedure.

One revolution of the crankshaft represents half of the crossing section, the deceleration section and the lift section while the other revolution represents the other half of the crossing section and all the static section. To make the crossing section even and symmetrical on both revolutions, the static section must have the same rotation degrees as the deceleration and lift sections combined. Furthermore, the crossing and the lift sections are the only sections that have curves being the crossing section curves far more sharper (smaller radius). The four curves of the crossing section are designed with the requirement of 4 times the cam follower radius meaning a curvature radius of $32mm$ for each curve. The connection between the four curves of the crossing section is made at $45º$ degrees. The deceleration section is designed with a relative very small rotation degrees compared to the other sections to allow the smallest possible length, diameter, and perimeter of the groove profile. Also, a $5mm$ boundary plus the diameter

of the cam follower between the deceleration section and the static section is implemented to separate the grooves and for structural integrity of the cylindrical cam.

The intake groove profile designed is divided as follows: the lift section has approximately $230º$ degrees ($100º$ degrees rise and fall each and $30º$ degrees in dwell following a simple harmonic motion) [39], the deceleration section has approximately $30º$ degrees, $15º$ degrees for each before and after the lift section, the static section has the same duration of the lift and the deceleration sections combined with approximately $260º$ degrees and the crossing section has the final $200º$ degrees, $100º$ degrees for each before and after the lift section. For the exhaust groove profile, the lift section is increased to $235º$ degrees ($102.5º$ degrees rise and fall and $30º$ degrees in dwell following a simple harmonic motion) *[39]* while the deceleration section is reduced to $12.5º$ degrees for each before and after the lift section to not affect any other measure and part of the profile. The remaining two sections are equal to the intake groove profile.

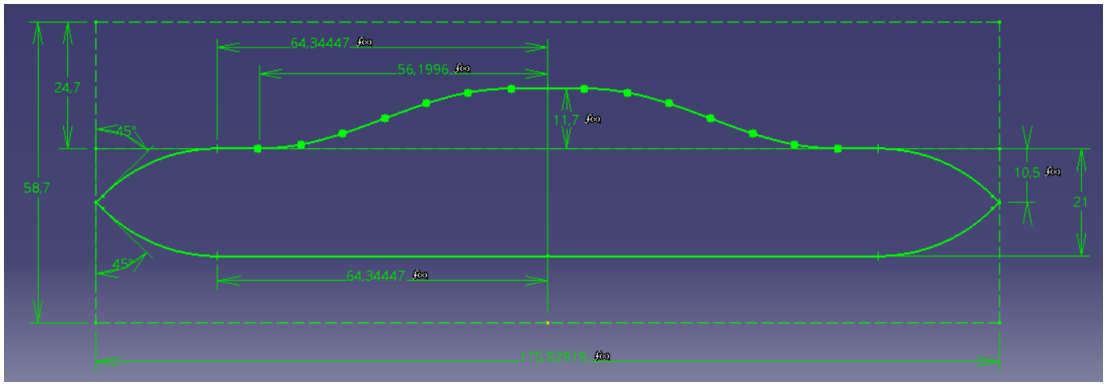

Figure 4.34 - Two dimensional intake groove profile in CATIA V5

The groove profile design with the conditions explained above results in a groove profile perimeter of approximately $175.93mm$ representing a radius of $28mm$. The *Figure 4.36* further shows the positions and sizes of the start of each section and the height of the cylindrical cam using the $5mm$ boundary plus the diameter of the cam follower rule.

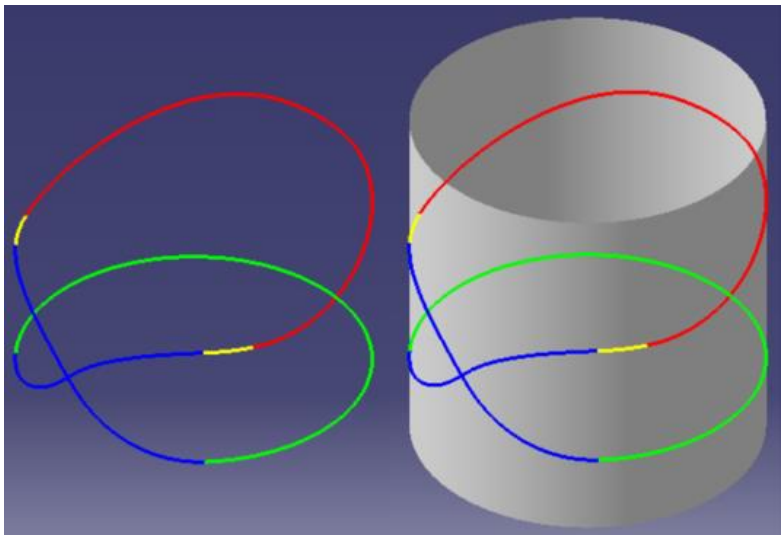

Figure 4.35 - Three dimensional intake groove profile in CATIA V5

Figure 4.37 presents the same groove profile presented in the *Figure 4.36* but now represented in three dimensions. The right side image adds a cylindrical shape that shows the groove profile radius of $28mm$ in the cylindrical cam. In colour red is the lift section, in colour yellow is the deceleration section, in colour blue is the crossing section and in green is the static section.

4.6.5.2. Cam Follower

The selected cam follower is the "FCR-16" of the company NSK capable of withstand a maximum load of $2360N$ at a maximum speed of $16000rpm$. The cam follower has a $16mm$ diameter, an $11mm$ width and weighs approximately $0.02kg$ *[62] [78]*. The assembly follower, arm follower and roller weights $0.078kg$ equating to a total mass pushed by the cam follower of $0.098kg$.

For this engine, the maximum load $F_{ls_{camfollower}}$ is at maximum lift during the lift section of the groove profile equating approximately $525.6N$. During the crossing section of the groove profile, the cam follower experiences an acceleration force $F_{cs_{camfollower}}$ equating approximately $246.7N$.

The exact length l_{groove} of the groove profile of *Figure 4.36* is found measuring the profile design in CATIA V5 which equals to $380.8mm$ per two revolutions. To travel that distance while the crankshaft is rotating at $2500rpm$, the cam follower must be capable to rotate at a maximum speed $v_{camfollower}$ of approximately $9470rpm$ or approximately $7.93m/s$ which it does.

The time percentage of the different sections of the groove profile are slightly different for the intake and exhaust cylindrical cam. For the intake cylindrical cam, the time fraction of the duration of the lift section t_{ls} is approximately 0.319, the crossing section t_{cs} is approximately 0.278 and the static section together with the deceleration section t_{ss} is approximately 0.403. For the exhaust cylindrical cam, the time fraction of the duration of the lift section t_{ls} is approximately 0.326, the crossing section t_{cs} is approximately 0.278 and the static section together with the deceleration section t_{ss} is approximately 0.396. Because the exhaust cylindrical cam has a larger lift section and in this section the forces are significantly larger, the average load acting on the cam follower $F_{m_{camfollower}}$ will be higher and subsequently the bearing life lower.

Supposing a constant maximum force through the entire of each section, for the lift section $F_{ls_{camfollower}}$ equating to $525.6N$, for the crossing section $F_{cs_{camfollower}}$ equating to $246.7N$ and for the static and deceleration section $F_{ss_{camfollower}}$ equating to $0N$, the average load $F_{m_{camfollower}}$ acting on the exhaust cam follower during the entire engine operation is about $383.1N$.

The basic dynamic load C of the cam follower "FCR-16" is $5800N$ *[62] [78]*. Considering a load factor f_w of 1.5 to account vibrations and shock loads, the nominal life L_{10} of the exhaust cam follower is about 2.223×10^9 revolutions. Supposing an engine operation at constant full speed, the service bearing life of the cam follower in hours L_h is slightly above 516 hours which complies with the requirement of 500 hours minimum service bearing life.

Figure 4.36 - Cam follower "FCR-16" in CATIA V5 by NSK [78]

4.6.5.3. Groove

The groove follows the path of the profile with the dimensions of the cam follower with slight safe margins. The depth of the groove is $12mm$, $11mm$ of the width

of the cam follower plus $1mm$ safe margin between the cam follower and the inner wall of the cylindrical cam. Its height is $16.2mm$, $16mm$ of the cam follower diameter plus $0.10mm$ of safe margin for each side of the cam follower.

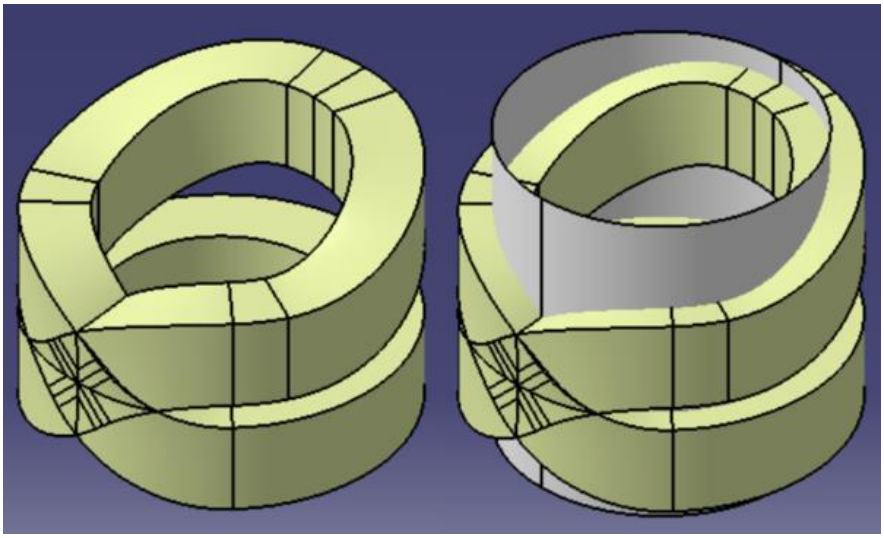

Figure 4.37 - Cylindrical cam groove in CATIA V5

4.6.5.4. Key and Keyway

The crankshaft radius where the cylindrical cam is placed is $13mm$. The force F_{key} resulted from the crankshaft torque $T_{crankshaft}$ for that radius is approximately $14100.3N$.

The length of the key L_{key} must be lower than the cylindrical cam length presented in *Figure 4.36* and equating to $58.7mm$.

For a key width t_{key} of $5mm$, the length of the key L_{key} must be at least $38.1mm$.

Predesigned keys with various sizes are found in a mechanical parts website and in their datasheet of parallel keys *[79]*. One of the keys complies with the requirements for this engine having a width of $5mm$ and a length of $40mm$.

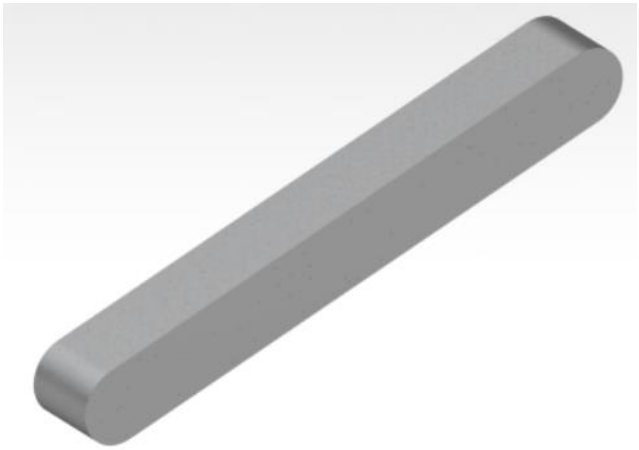

Figure 4.38 - Parallel key "DIN 6885 A" in CATIA V5 by Norelem [79]

The keyway in the cylindrical cam is $2.5mm$ deep and $5mm$ wide but its length is equal to length of the cylindrical cam entire having $58.7mm$. Its design is equal on both intake and exhaust cylindrical cams, but their placement is not. The placement of the keyway in the cylindrical cam depends on the placement of the keyseat in the crankshaft. In the crankshaft, the keyseat is designed in the position of TDC for two pistons and BDC for the other two. The intake valve opens at $10º$ degrees before TDC and it is at this position that the lift section of the groove profile of the intake cylindrical cam begins. So, the keyway of the intake cylindrical cam is placed $10º$ degrees after the start of the lift section or $105º$ degrees before the middle of the lift section at the center of the maximum lift. The exhaust valve closes at $10º$ degrees after TDC and it is at this position that the lift section of the groove profile of the exhaust cylindrical cam finishes. So, the keyway of the exhaust cylindrical cam is placed $10º$ degrees before the finish of the lift section or $107.5º$ degrees after the middle of the lift section at the center of the maximum lift. Concluding, the difference in the keyway placement between both cylindrical cams will be only $2.5º$ degrees and may not be perceptible by the cylindrical cam images.

4.6.5.5. Cylindrical Cam 3D Model

Both cylindrical cams are very similar and the differences between them are not perceptible. Instead of placing an image of both, one images with different sections of the intake groove cylindrical cam is shown.

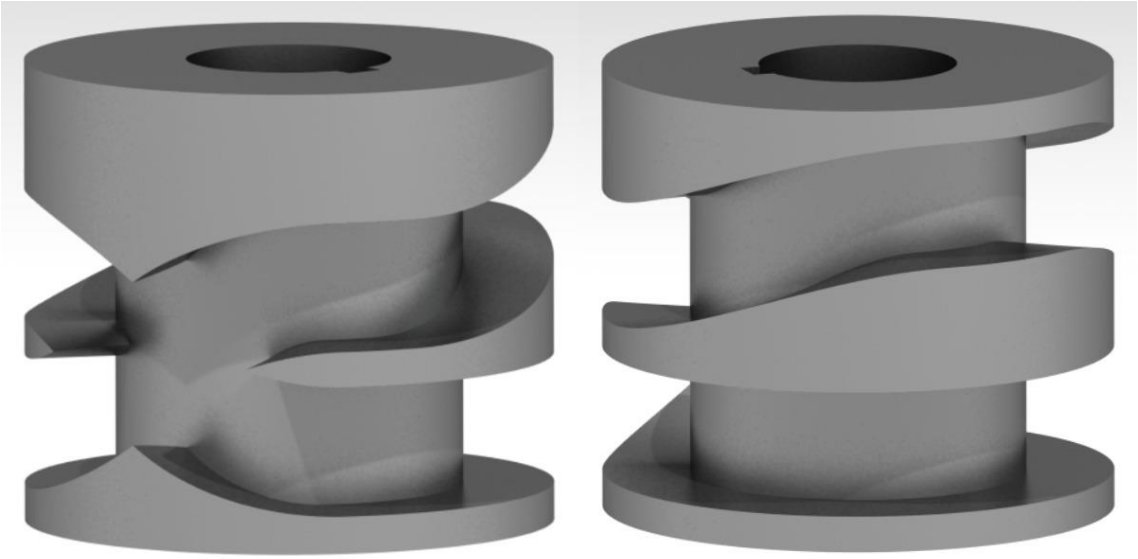

Figure 4.39 - Cylindrical cam in CATIA V5, crossing section sideview in the left and lift section sideview in the right

To prevent translation of the cylindrical cam along the x-axis of the crankshaft, on one side there is a wall of $30mm$ that serves as support for the placement of the bearing D while on the other side a circlip "DIN 471" like the one in *Figure 4.12* but for a $26mm$ shaft is used.

4.6.6. Follower, Arm Follower and Roller

The support roller selected is the "RSTO 5 TN" *[80]* of the company SKF which is the smallest that was possible to find. Its function is only to hold the weight of the assembled cam follower, follower and arm follower which are very light. Of course, the alternate translation movement creates inertial forces, but the mass of the assembled follower, arm follower, and cam follower is only about $0.0900kg$ with this roller weighting eight grams. Still, if the roller must be changed on a later stage due to not standing the inertial forces, the built-in support can easily be changed.

For curiosity, the velocity of the roller in rpm is far smaller than the cam follower which is given by:

$$rpm_{roller} = \frac{h_{groove}}{P_{roller}} rpm_{max_{crankshaft}} \quad (4.1)$$

Where:

h_{groove} is the height of the cylindrical cam groove profile in mm. The roller travels that distance per revolution of the crankshaft.

P_{roller} is the perimeter of the roller in mm:

$$P_{roller} = \pi d_{roller} \tag{4.2}$$

Where:

d_{roller} is the outer diameter of the roller in mm.

The height of the cylindrical cam groove h_{groove} is only $32.7mm$ and for this roller, the velocity is about $1626rpm$. For larger rollers, with a larger outer diameter, the rpm_{roller} decreases.

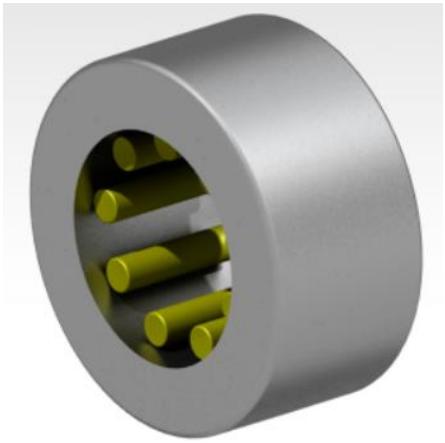

Figure 4.40 - Support roller "RSTO 5 TN" in CATIA V5 by SKF [80]

The intake valve and exhaust valves have different lengths, being the intake valve the longer. To press the valves, some piece in the distribution system mechanism must have a different length or placement. To maintain perfect symmetry in the engine specially with the placement of the cylindrical cams, it was chosen to only change the length of the follower. All the other pieces such the arm follower and the built-in support have the same length and placement. The difference in length of the followers is the difference in lengths of the valves which is approximately $11.30mm$.

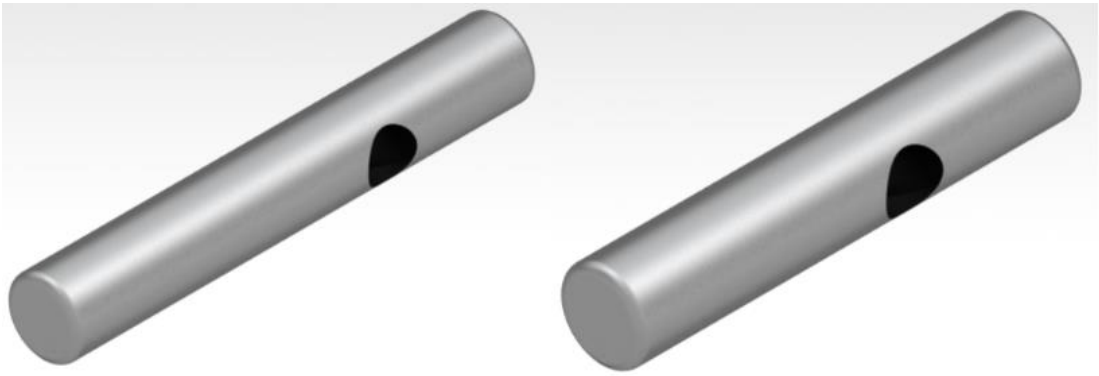

Figure 4.41 - Exhaust and intake follower in CATIA V5, in the left and right, respectively

Figure 4.42 - Arm follower in CATIA V5

4.7. Cylinder and Combustion Chamber

According to *Equations 3.117* and *3.118*, the cylinder wall thickness necessary for the cylinder is approximately $3.6mm$ but it will be rounded to $4mm$.

The combustion chamber is a single piece made of two sides, each corresponding to one piston. One side includes half the cylinder length, the intake valve nut, intake valve and intake valve seat. The other side has the exhaust valve, exhaust valve seat and the M8 spark plug and the other half of the cylinder. To the conclusion of this work, the combustion chamber is designed to have a single M8 spark plug in the center of the combustion chamber but using two instead can be advantageous by allowing a smaller combustion chamber area.

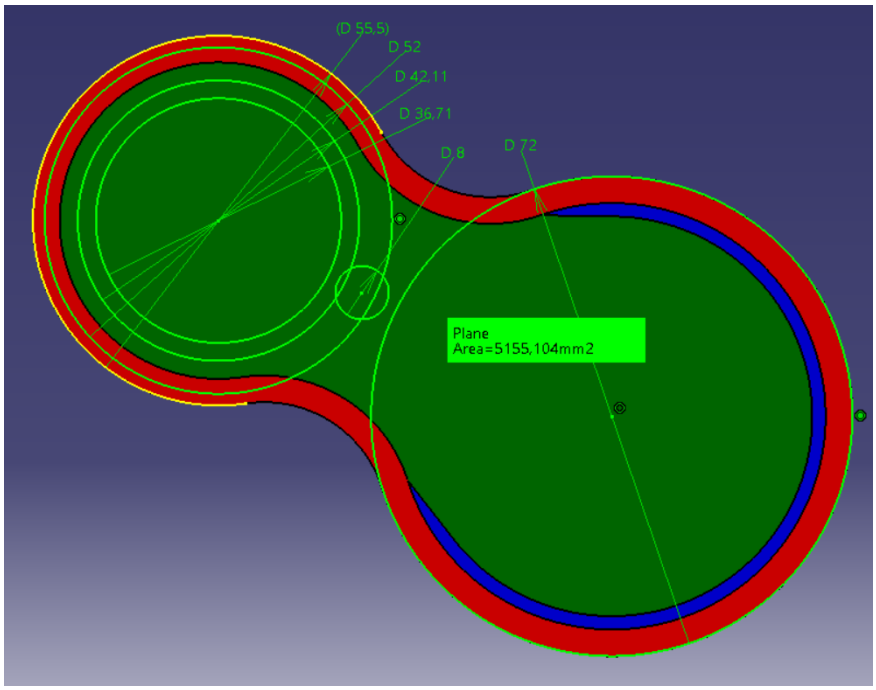

Figure 4.43 - Combustion chamber sketch in CATIA 5

Figure 4.43 shows how the dimensions of the combustion chamber sketch match the requirements of both sides despite simplistic. The exhaust valve seat seen on the upper left side has an outer diameter of $36.71mm$ and its axis is aligned with that of the intake valve seat. Between the exhaust valve seat and the outer wall of the cylinder which has a $72mm$ diameter, there is enough room to fit the M8 spark plug centred in the middle of the combustion chamber. It is this side that has the tighter room to fit all the components. The minor diameter of the intake valve support nut should be at least the outer diameter of the intake valve seat which is equal to $42.11mm$ and the outer diameter should be smaller than the outer wall of the secondary cylinder body where the valves are placed which is equal to $55.5mm$. A M52 nut, with a center hole for the intake valve seat, matches the requirements for the intake valve nut with a minor diameter of $46.587mm$ and giving a margin for a good thickness of the nut wall. Marked as red is the thickness of the cylinder wall and marked as blue is the design and thickness of the cast-iron sleeve. The area of the combustion chamber design marked as green is approximately $5155.1mm^2$ as shown in *Figure 4.46*. The cylinder has a length between pistons giving a total height for both sides of the combustion chamber equal to $12.657mm$, with the valves lift being $11.70mm$.

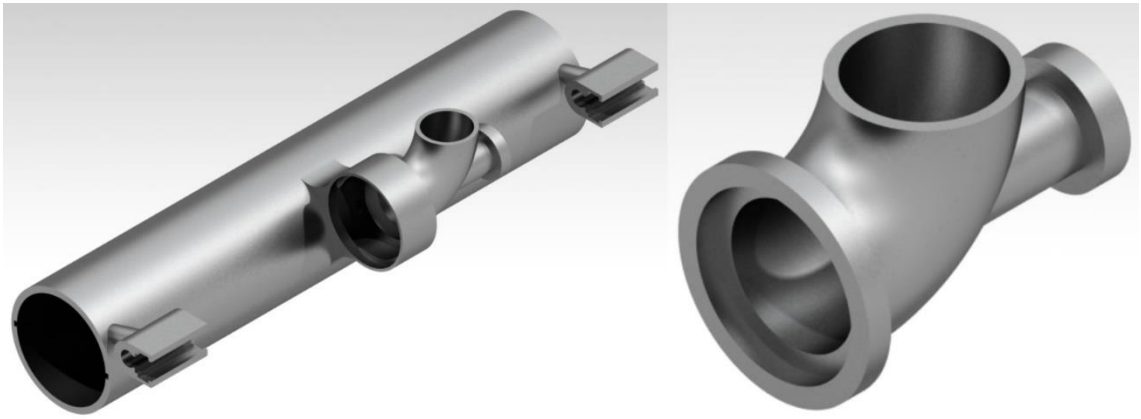

Figure 4.44 – Aluminium cylinder and intake valve nut in CATIA V5

In the point of each cylinder is possible to see the built-in support for the follower, arm follower and roller. They are located at $130mm$ from the base of the valves in the combustion chamber and the length of the intake valve plus the thickness of the nut to unscrew them is about $126mm$.

Because the lengths of the valves are different with the intake valve being longer, the supports for the spring also have different lengths.

The cast-iron sleeve between the cylinder and the piston has a $2mm$ thickness and is shown in *Figure 4.45.*

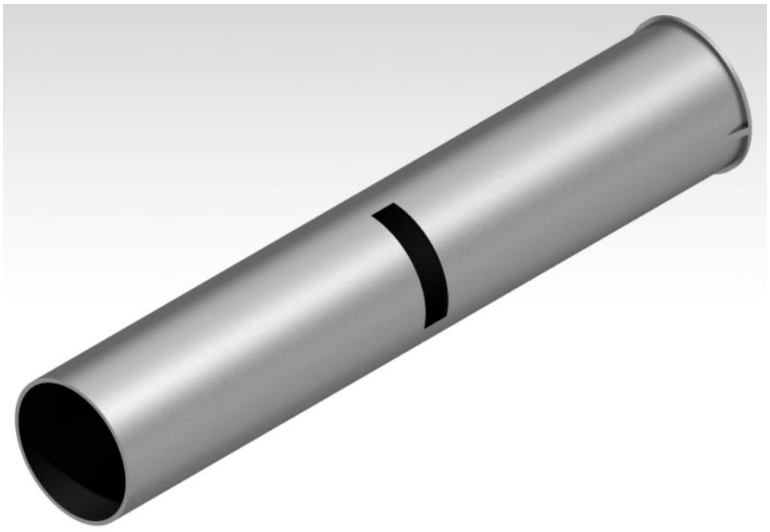

Figure 4.45 - Cast-iron sleeve in CATIA V5

4.8. Engine Assembly

In the present document, only the engine virtual model assembly can be shown. The actual simulation is not possible to show because it is a video.

The engine assembly in CATIA V5 is not visualized with material. Instead, for better visualization of the whole engine and movement in the simulation, the different components have different arbitrary colours as shown in *Figures 4.46* to *4.49*.

- Support bearings C and D are clear blue.
- Cylinder, intake valve nut and block with crosshead are grey
- Crankshaft is white
- Follower and arm follower are yellow
- Connecting rod is orange
- Piston and gudgeon pin are purple
- Wobble plate and socket and ball joint cap are dark green
- Cylinder sleeve, shaft coupling, and valve seats are brown
- Bearings A and B, roller and cam follower are yellow for the roller parts and dark grey for the cages
- Intake cylindrical cam and valve are red
- Exhaust cylindrical cam and valve are blue
- Spring, valve retainer and valve locks are different shades of green
- Lock nuts, circlip and key are dark grey

Figures 4.46 to *4.49* show the engine with different focuses for a better understanding and location of the different components according with colours mentioned above. All figures show one cylinder with its pistons in TDC and the other cylinder in BDC.

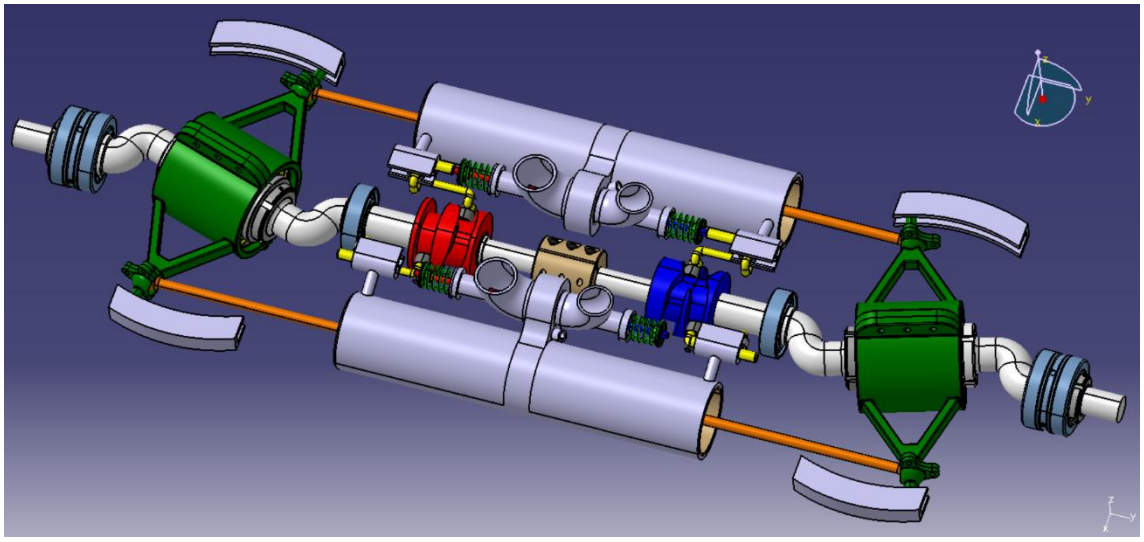

Figure 4.46 - Complete engine assembly in CATIA V5

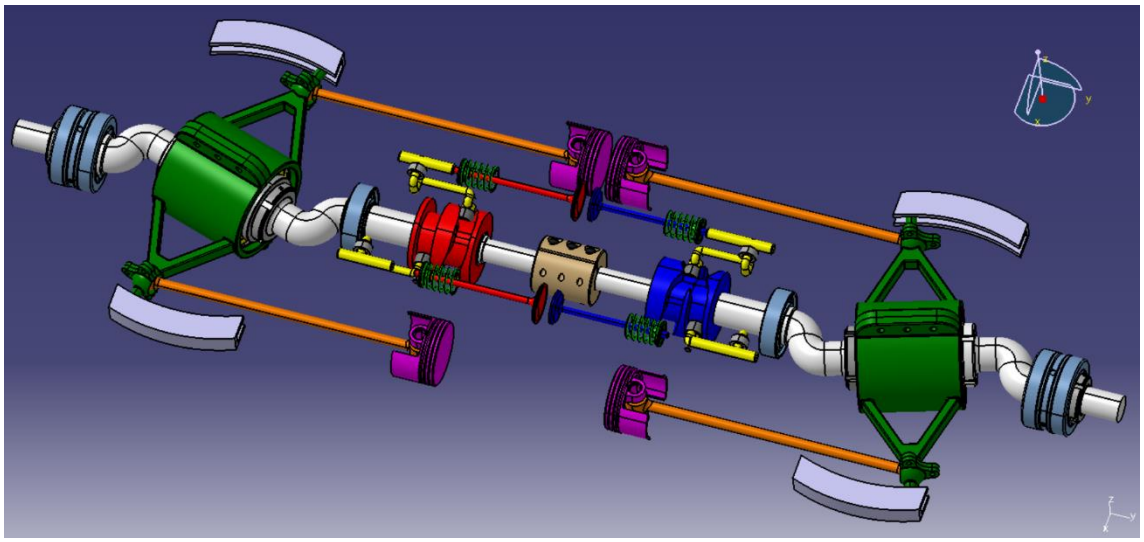

Figure 4.47 - Engine assembly without cylinder and intake valve nut in CATIA V5

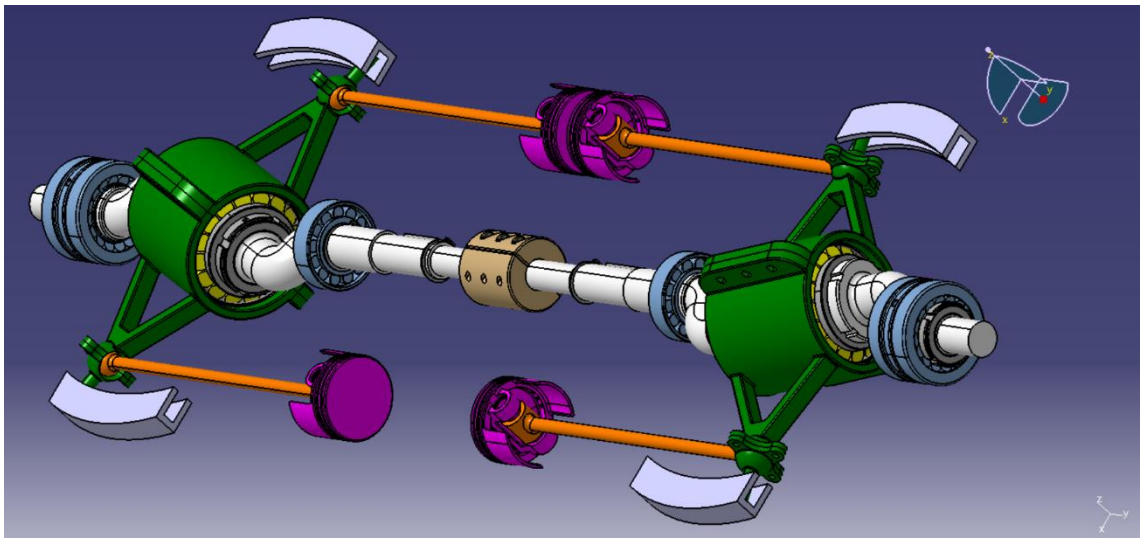

Figure 4.48 - Engine assembly without distribution system in CATIA V5

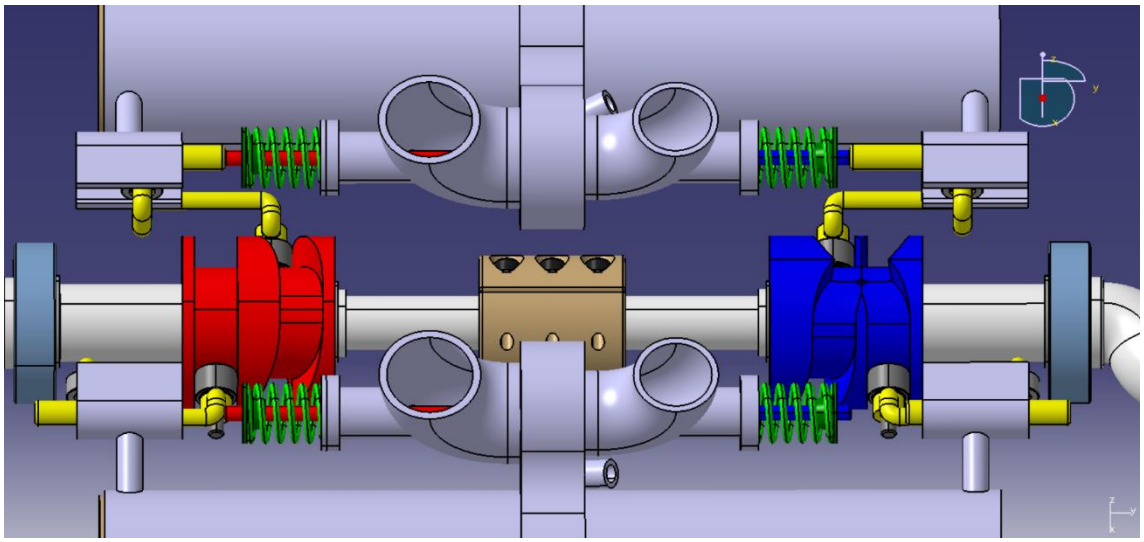

Figure 4.49 - Distribution mechanism system assembly in CATIA V5

4.9 Missing Detail Design

The assembly and simulation of the engine motion in CATIA V5 performed as expected. In real life, though, there is a detail that is missing and was not solved. This is the mechanism that ensures that the cam follower remains in the correct path when it reaches the crossing section of the cylindrical/barrel cam, otherwise it can easily jam.

Initially, the solution to secure the cam follower to its correct path was to add a second cam follower. While the first cam follower was travelling thought the crossing section of the groove profile of the cylindrical cam, the second cam follower behind it would prevent jamming through a rigid joint with the first cam follower. This solution could work if the groove profile was uniform and did not reverse. Because the groove profile is not uniform and reverses, it is mandatory to allow rotation in the concentrical axis of the arm follower of the *Figure 4.42* where the cam follower is placed, otherwise, the mechanism is impossible to work. But if rotation is allowed, then the second cam follower does not guarantee that the first cam follower stays in the correct path.

If the crossing section length is increased to allow both cam followers to be positioned at the same time in the linear zone of that section (the exact zone that intersects to each other at $45º$ degrees) before the first cam follower starts the intersection, then the cam follower would behave like traveling in a line. This way, perhaps the cam follower remains in the correct path but only by testing is possible to verify it.

However, that solution seems impossible because that linear zone would have to measure more than the double of the outer diameter of the cam follower to fit both. That would mean a very high increase in the length of the groove l_{groove}, which in turn

would result in the increase of the cam follower speed and the reduction in the cam follower bearing life which for the results of this paper is already in 516 hours and the minimum is 500 hours. So, a larger cam follower would be necessary, but larger cam followers have significantly less maximum allowable speed. Per example, the "FCR-19", which is the next biggest cam follower after "FCR-16" with $19mm$ of outer diameter has only a maximum allowable speed of $12000rpm$ *[62]*. For the l_{groove} of this paper, the "FCR-16" which has a maximum allowable speed of $16000rpm$ must travel at $9470rpm$. This proves that if the l_{groove} is increased, there are no available cam followers to meet the specifications required. With the l_{groove} of this paper which is $380.8mm$ the linear zone of the crossing section only measures approximately $1.73mm$ which is very small compared to more than the double of the cam follower outer diameter required.

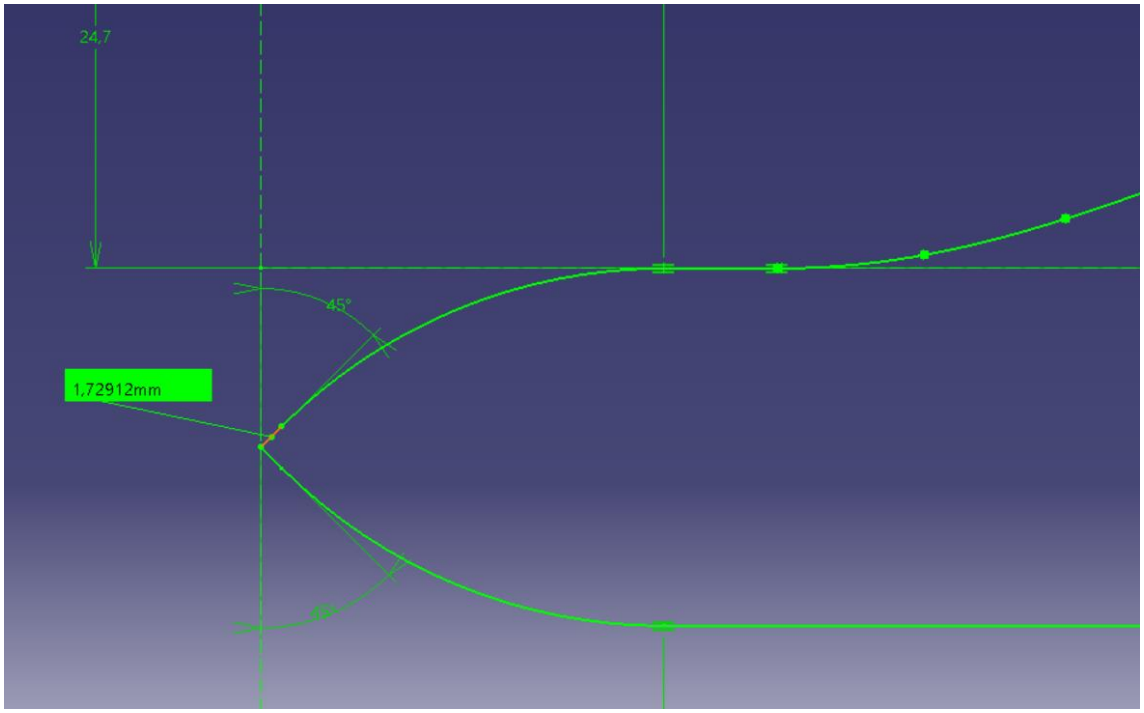

Figure 4.50 - Linear zone of the crossing section of the groove profile

Despite the problem described above, a simulation of the motion using two cam followers was created to verify the motion. A new piece painted in purple in the *Figures 4.51* and *4.52* was designed to connect the arm follower and the two cam followers. The simulation demonstrated a problem not previously noticed that invalidates the motion. The cam followers rotate and crash against the walls of the cylindrical cam when they are not aligned, meaning when not in static zones. When one cam follower rises a curve, it rotates in the center of the new piece.

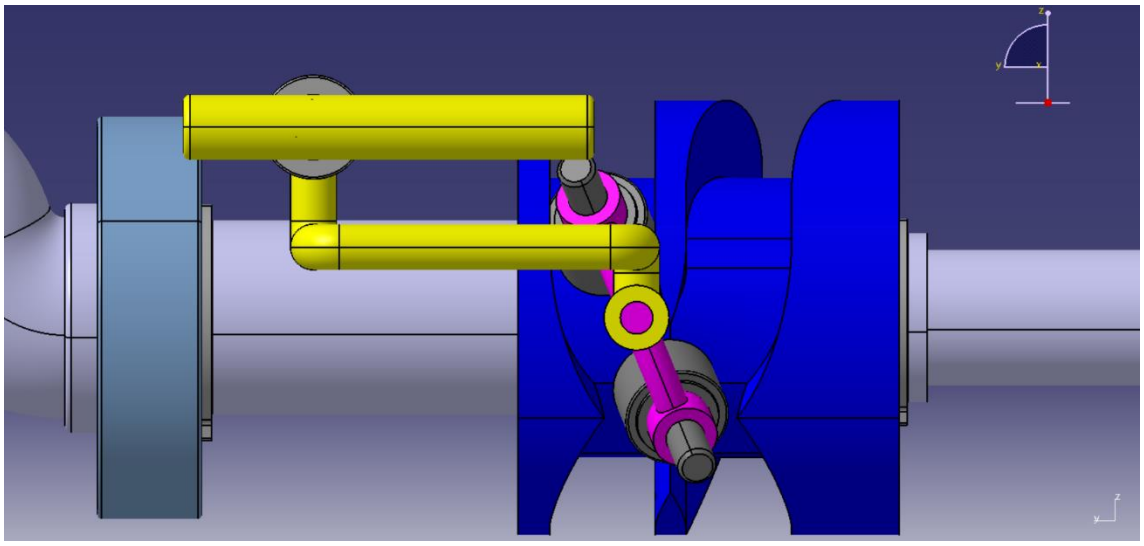

Figure 4.51 – Problem demonstrated in CATIA V5 (plane yz)

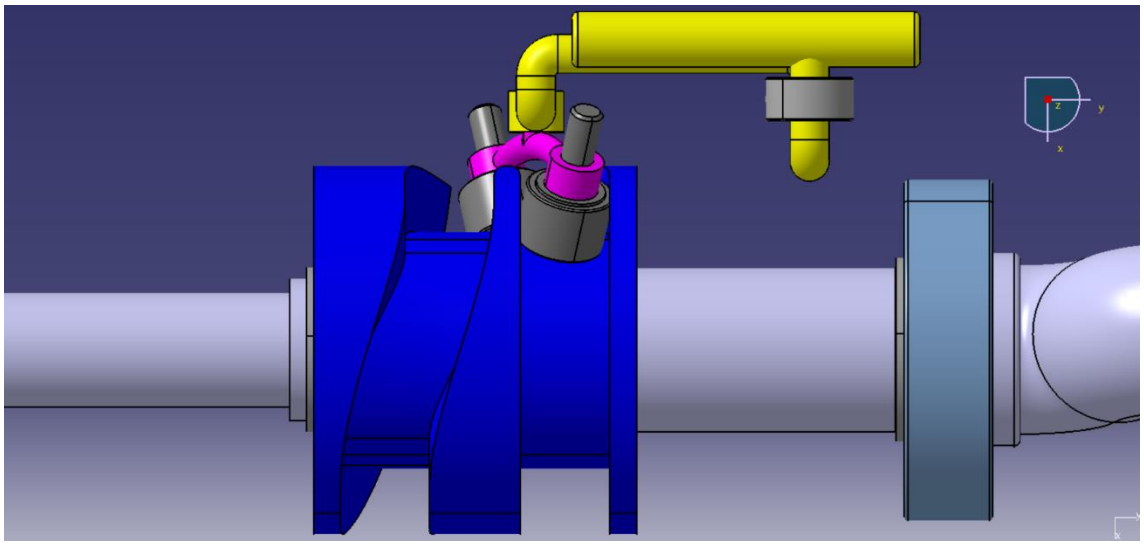

Figure 4.52 - Problem demonstrated in CATIA V5 (plane xy)

Two other possible solutions are presented in book *[61]*. The first is to add an oval shape or a sharp corner to the cam follower. This solution is used in self-reversing screws such as the screw of the *Figure 3.15* which is commonly used for winding machines (*Figure 4.53b*).

The other solution mentioned in the book is to add a mechanism that makes possible to close and open each groove like a switch to make a single groove while the cam follower travels through the intersection. In the book a design is presented of that mechanism despite not being in a cylindrical cam (*Figure 4.53a*).

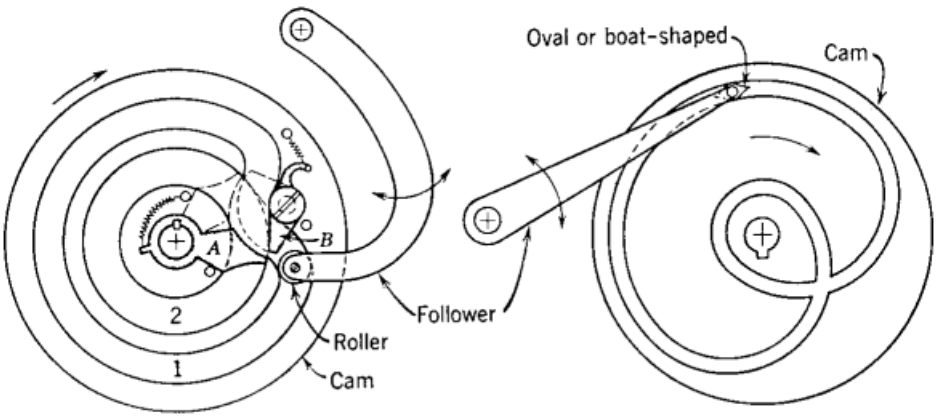

(a) Cam disk with switches A and B operated by roller.

(b) Grooved-cam disk with a boat-shaped follower.

Figure 4.53 - Solutions for two revolutions per cycle cams [61]

Chapter 5

5 Conclusion

5.1. Achievements

This work had the objective of designing and sizing a four-stroke axial engine.

The components of the motion crankshaft/wobble plate/connecting rod/piston were successfully made with the virtual movement in CATIA V5 behaving as expected. The engine was designed to use a $60mm$ piston diameter with a $75mm$ stroke. Two tapered rolling bearings connect the wobble plate to the crankshaft while a double tapered rolling bearing a cylindrical rolling bearing are used as support of the crankshaft to the engine block. To carry the bearings to their placement, the crankshaft was divided into two halves allowing the bearings to pass through the middle of both halves. The crankshaft was successfully sized having into account the need to pass the bearings through. Posteriorly, a structural analysis was conducted successfully to analyse the stress and deflection of the crankshaft to support the loads acting on it.

The valvetrain components encountered in any conventional engine such as the valves and spring were designed and sized successfully according to the initial parameters selected for the engine. The other components of the mechanism capable of actuate each valve once per two revolutions were also successfully designed but it has a flaw as explained in the *Section 4.9.* That mechanism is crucial for the correct motion of the valvetrain. While the mechanism does not work in real life, its motion in CATIA V5 was successfully simulated and thus it is possible to watch the full engine motion in action.

The last component to be dimensioned and sized was the cylinder and combustion chamber.

5.2. Future work

As mentioned previously, the virtual engine assembly and simulation work as planned but in real life a key part of the mechanism is missing which is needed to guarantee that the cam follower remains in the correct path. Devising and designing a mechanism capable of doing that is the future main work priority to complete this engine design. Once that goal is achieved, cooling and lubrication must be implemented

in the engine and then it can be tested first by 3D printing and then possible building a prototype.

There are also other details such the unnecessary long valves of this engine. If possible, it may be worth shortening slightly the valves stem as the valves are too long for what this engine requires which causes other parts to be unnecessarily longer and heavier such as, mainly, the crankshaft and the cylinder. This process does not seem complex, because shortening the stem only means possibly making a new groove and a new tip which can be done with easily available mechanical tools.

6 Bibliography

[1] “AchatesPower,” [Online]. Available: https://achatespower.com/.

[2] “DukeEngines Pure Power,” [Online]. Available: https://www.dukeengines.com/.

[3] J. Kalke and M. Opaliński, “Experimental test stand for development of an opposed-piston engine and initial results,” July 2017.

[4] “Covaxe,” [Online]. Available: https://covaxe.com/.

[5] J. Kalke, M. Opaliński and M. Szczeciński, “Opposed-Piston Engines: The Future of Internal Combustion Engines?”.

[6] R. Stone, Introduction to Internal Combustion Engines: Third Edition.

[7] C. F. Taylor, The Internal-Combustion Engine in Theory and Practice: Volume I, 1985.

[8] J. B. Heywood, Internal Combustion Engine Fundamentals.

[9] J. Martins, Motores de Combustão Interna: Segunda Edição.

[10] J.-P. Pirault and M. Flint, Opposed-Piston Engines: Evolution, Use, and Future Applications, 2010.

[11] Z. Yu and T. W. Lee, “Kinematic Structural and Funcional Analysis of Wobble-Plate Engines,” June 1986.

[12] P. Mazuro, “Reciprocating Engines with Cylindrical Axis Paralell to the Drive Shaft - Theory and Practice,” 2006.

[13] P. Mazuro and B. Makarewicz, “The Potential of Wobble Plate Opposed Piston Axial Engines for Increased Efficiency,” October 2020.

[14] “Axial Internal-Combustion Engines,” 15 February 2022. [Online]. Available: http://www.douglas-self.com/MUSEUM/POWER/unusualICeng/axial-ICeng/axial-IC.htm.

[15] J. C. McLanahan, “Barrel Aircraft Engines: Historical Anomaly or Stymied Innovation?,” September 1998.

[16] M. Latarche, Pounder´s Marine Diesel Engines and Gas Turbines: Tenth Edition, 2021.

[17] H. E. Smallbone, “Multiple Cylinder Engine”. US Patent 821,546, 22 May 1906.

[18] G. D. Angle, Airplane Engine Encyclopedia.

[19] W. G. Macomber, “Rotary Engine”. US Patent 1,042,018, 22 October 1912.

[20] H. L. F. Trebert, “Internal Combustion Engine”. US Patent 1,215,434, 13 February 1917.

[21] “Salmson,” [Online]. Available: https://en.wikipedia.org/wiki/Salmson.

[22] J. O. Almen, “Engine”. US Patent 1,255,973, 12 February 1918.

[23] C. B. Redrup, “Valve Mechanism of Internal Combustion Engines”. US Patent 2,042,730, 2 June 1936.

[24] C. B. Redrup, “Wobble or Swash Plate Engine”. US Patent 2,182,213, 5 December 1939.

[25] H. Alfaro, “Internal Combustion Engine”. US Patent 2,080,846, 18 May 1937.

[26] “The Revolver Cam Engine Previously known as the Dynacam engine,” [Online]. Available: https://www.youtube.com/watch?v=ScS-QCWHfb8.

[27] “Stroke-to-Bore Ratio: A Key to Engine Efficiency,” April 2012. [Online]. Available: https://achatespower.com/stroke-to-bore/.

[28] “Volkswagen Type 3,” [Online]. Available: https://en.wikipedia.org/wiki/Volkswagen_Type_3.

[29] AliExpress, “Motorcycle 60mm Piston Ring 13mm Pin Kit For YinXiang YX 150 160 CC,” [Online]. Available: https://www.aliexpress.com/item/4001310380284.html?spm=a2g0o.productlist.main.51.3bed1012kHzAFQ&algo_pvid=705afff7-2834-4651-975b-98c9634f4d98&algo_exp_id=705afff7-2834-4651-975b-98c9634f4d98-25&pdp_npi=3%40dis%21EUR%2120.75%2113.69%21%21%21%21%21%4021224.

[30] D. Giacosa, Motores Endotermicos: 3ª Edicion.

[31] “Certified AvGas Enignes,” [Online]. Available: http://continental.aero/engines/gasoline-engines.aspx.

[32] Lycoming, Operator´s Manual Lycoming: O-540, IO-540 Series, 2006.

[33] D. E. Winternone and A. Turan, Advanced Thermodynamics for Engineers: Second Edition, 2015.

[34] F. Brójo, *Propulsão de Aeronaves I,* 2020-2021.

[35] “HURRICANE,” [Online]. Available: https://www.hurricanerods.com/products/Hurricane-4340-5.394-H-Beam-Connecting-Rods-Chevy-Journals.html#.W6CpCM4zaUk.

[36] Copper Development Association, Cast Copper Alloy Sleeve Bearings.

[37] L. L. Myagkov, K. Mahkamov, N. D. Chainov and I. Makhkamova, “Advanced and Conventional Internal Combustion Engine Materials,” 2014.

[38] J. L. Lumley, Engines An Introduction, 1999.

[39] A. Singh, Fundamentals of Machine Design, 2017.

[40] R. Khurmi and J. Gupta, A Textbook of Machine Design: Fourteenth Edition, 2005.

[41] Kipp, “K0734 Ball joints DIN 71802,” [Online]. Available: https://www.kipp.com/gb/en/Products/Operating-parts-standard-elements/Joints/Angle-joints.html?search_keywords=DIN+71802.

[42] NSK, Motion & Control, Rolling Bearings, 2005.

[43] SKF, “SKF Bearing Select,” [Online]. Available: https://skfbearingselect.com/#/bearing-selection-start.

[44] R. G. Budynas and J. K. Nisbett, Shigley´s Mechanical Engineering Design: Ninth Edition, 2011.

[45] SKF, “Axial location of bearings,” [Online]. Available: https://www.skf.com/my/products/plain-bearings/spherical-plain-bearings-rod-ends/principles/design-of-bearing-arrangements/axial-location.

[46] E. L. L. Cabral, “Capítulo 4 - Preliminares Matemáticos: Transformação de Coordenadas,” in *Análise de Robôs*.

[47] R. C. Juvinall and K. M. Marshek, Fundamentals of Machine Component Design: Fifth Edition, 2012.

[48] AZO Materials, “AISI 4340 Alloy Steel (UNS G43400),” 13 September 2012. [Online]. Available: https://www.azom.com/article.aspx?ArticleID=6772.

[49] C. F. Taylor, The Internal-Combustion Enigne in Theory and Practice: Volume II, 1985.

[50] A. Vieira, *Tópico 03 - Veios Notas de Aulas, Órgãos de Máquinas,* 2020.

[51] J. P. Barbosa, Elementos de Máquinas, 2011.

[52] EESC USP, *Aula 08 - Uniões Eixos-Cubo.*

[53] A. Vieira, *Tópico 04 - Ligações cubo-veio Notas de Aulas, Órgãos de Máquinas,* 2020.

[54] S. McKelvie, “A Critique of the "Flathead" or Side-Valve Engine Design,” 12 July 2012. [Online]. Available: https://stevemckelvie.wordpress.com/2012/07/12/a-critique-of-the-flathead-or-side-valve-engine-design/.

[55] R. L. Norton, Design of Machinery: Fourth Edition, 2007.

[56] D. Industry, “Self-reversing screw - Bornemann Gewindetechnik GmbH & Co. KG,” [Online]. Available: https://www.directindustry.com/prod/bornemann-gewindetechnik-gmbh-co-kg/product-62200-2064687.html.

[57] Paruzzi, “Inlet valves 35.6 x 8 mm,” [Online]. Available: https://www.paruzzi.com/uk/type-3///1748.

[58] Paruzzi, “Outlet valves 32.0 x 8 mm,” [Online]. Available: https://www.paruzzi.com/uk/type-3///1749.

[59] T. Gilles, Automotive Engines, Diagnosis, Repair and Rebuilding: 6th Edition, 2011.

[60] E. Weingartner, “Do Different Valves Effect Flow Undercut vs Straight Stem, Back Cut vs No Back Cut,” 3 August 2022. [Online]. Available: https://www.youtube.com/watch?v=VHy6f7jYq0Q&t=577s.

[61] McGraw-Hill, Cam Design Handbook, 2004.

[62] M. &. C. NSK, Cam Followers and Roller Followers.

[63] THK, “Point of Selection,” in *Cam Follower*.

[64] K. Salonitis, M. Jolly, E. Pagone and M. Papanikolaou, “Life-Cycle and Energy Assessment of Automotive Component Manufacturing: The Dilemma Between Aluminum and Cast Iron,” July 2019.

[65] SKF, “31308 - Tapered roller bearings,” [Online]. Available: https://www.skf.com/uk/products/rolling-bearings/roller-bearings/tapered-roller-bearings/single-row-tapered-roller-bearings/productid-31308.

[66] SKF, “31306/DF - Tapered roller bearings,” [Online]. Available: https://www.skf.com/uk/products/rolling-bearings/roller-bearings/tapered-roller-bearings/matched-tapered-roller-bearings/productid-31306%2FDF.

[67] SKF, “N 206 ECP - Cylindrical roller bearings,” [Online]. Available: https://www.skf.com/uk/products/rolling-bearings/roller-bearings/cylindrical-roller-bearings/single-row-cylindrical-roller-bearings/productid-N%20206%20ECP.

[68] SKF, “KMK 8 - Lock nuts and locking devices,” [Online]. Available: https://www.skf.com/uk/products/rolling-bearings/accessories/lock-nuts/integral-locking/productid-KMK%208.

[69] SKF, “KMK 6 - Lock nuts and locking devices,” [Online]. Available: https://www.skf.com/uk/products/rolling-bearings/accessories/lock-nuts/integral-locking/productid-KMK%206.

[70] Norelem, “Circlips for shafts ?DIN 471,” [Online]. Available: https://norelem.es/en/Product-overview/Flexible-standard-component-system/07000/Nuts-screws-washers-securing-elements/Circlips-for-shafts-DIN-471/p/agid.4129.

[71] Bossard, “BN 272 - Screws and bolts with internal drive,” [Online]. Available: https://www.bossard.com/eshop/global-en/screws/screws-and-bolts-with-internal-drive/hex-socket-head-cap-screws-fully-threaded/p/272/?category=01.100.100.10&index=0&q=%3Arelevance.

[72] Bossard, “BN 713 - Flat washers without chamfer,” [Online]. Available: https://www.bossard.com/eshop/global-en/washers/washers-flat-without-chamfer/flat-washers-without-chamfer/p/713/?category=01.100.300.10&index=0&q=%3Arelevance.

[73] Ferrea Racing Components, High Power Valvetrain Components: 2022-23 Main Catalog.

[74] CNC-Motorsports, “Ferrea F6310 6000 Series,” [Online]. Available: https://cnc-motorsports.com/ferrea-f6310-6000-series-competition-plus-intake-valves-1-460-ford-5-0l-dohc-32-valves-2010-2011.html.

[75] CNC-Motorsports, “Ferrea F6312 6000 Series,” [Online]. Available: https://cnc-motorsports.com/ferrea-f6312-6000-series-competition-plus-exhaust-valves-1-222-ford-5-0l-dohc-32-valves-2010-2011.html.

[76] J. Baechtel, “Ferrea Helps Explain Valve-flow Dynamics - EngineLabs,” [Online]. Available: https://www.enginelabs.com/tech-stories/ferrea-helps-explains-valve-flow-dynamics/.

[77] The Spring Store, “Spring Calculator,” [Online]. Available: https://www.thespringstore.com/spring-calculator.html.

[78] NSK, Motion & Control, “Metric - NSK Rolling Bearing,” [Online]. Available: https://nsk-jp.partcommunity.com/3d-cad-models/sso/metric-nsk-rolling-bearing?info=nsk_rb%2Froller_bearings%2Fneedle_bearings%2Fcam_followers%2Fmetric_asmtab.prj&cwid=3198.

[79] Norelem, “Parallel keys ?DIN 6885 A,” [Online]. Available: https://norelem.es/en/Product-overview/Flexible-standard-component-system/03000/Dowels-parallel-keys-dowel-pin-pullers/Parallel-keys-DIN-6885-A/p/agid.2776?q=%3A%3AMM4%3A00000000000000005%2523%25235%3AMM4%3A00000000000000006%2523%25236%3AMM15%3A00000000.

[80] SKF, “RSTO 5 TN - Support rollers (Yoke-type track rollers),” [Online]. Available: https://www.skf.com/uk/products/rolling-bearings/track-rollers/support-rollers/productid-RSTO%205%20TN.